PERFORMANCE EVALUATION OF INVERTED PAVEMENT STRUCTURES

A Thesis
Presented to
The Academic Faculty

by

Sean Donovan

In Partial Fulfillment
of the Requirements for the Degree
Master of Science in the
School of Civil and Environmental Engineering

Georgia Institute of Technology
December 2022

PERFORMANCE EVALUATION OF INVERTED PAVEMENT STRUCTURES

Approved by:

Dr. J. David Frost, Advisor
School of Civil and Environmental Engineering
Georgia Institute of Technology

Dr. Sheng Dai
School of Civil and Environmental Engineering
Georgia Institute of Technology

Dr. Yi-Chang (James) Tsai
School of Civil and Environmental Engineering
Georgia Institute of Technology

Date Approved: December 1, 2022

Dedicated with love to my wife, Brittney

ACKNOWLEDGEMENTS

This thesis would not be complete without a team of supporters. I would like to extend a hearty “thank you” to Dr. David Frost for trusting me to make this study my own and for connecting me to ideas and people that will change my future and pavement engineering. I would also like to thank those who sacrificed their time to enable this work. Their contributions formed the “base course” of this research- there would be nothing to report without them. To Dr. James Tsai, Zhongyu Yang, and Ryan Salameh: your many years of work made our surveys easier than any other I’ve done. To the fine folks at the Morgan Quarry: thank you for welcoming us and for humoring me. To GDOT’s Phillip Snider: thank you for your time and expertise.

I would also like to thank those that have indirectly contributed to this study. To Brittney: you’ve rode shotgun on countless adventures and more than your share of household moves. You’ve motivated me with your own success and encouraged me when I needed it. If anyone wants to meet a woman who can truly “do it all,” they should meet my wife. Thank you for your love and partnership. I am also eternally grateful to my parents, Michele and Chip, for supporting my curiosity and pushing me to fulfill my potential. Thank you to John Anderson for inspiring the next generation of engineers dedicated to service. Finally, thank you to the USAF Engineers that ignited my passion for pavements. When I received my BS from Georgia Tech in 2017, I had no plans to return, but the Air Force had other ideas. Harold Muñiz, Brian Bowler and all the other pavement engineers that humored my questions and Dirt Boyz that let me tag along: thank you for your inspiration. This one is for you, and I hope to return the favor by paying it forward.

ENGINEERS… LEAD THE WAY!

TABLE OF CONTENTS

LIST OF TABLES

LIST OF FIGURES

LIST OF ABBREVIATIONS

AADT	Annual average daily traffic
AASHO	American Association of State Highway Officials
AASHTO	American Association of State Highway and Transportation Officials
AC	Asphalt concrete
APT	Accelerated pavement testing
CBR	California Bearing Ratio
D_0	Maximum surface deflection
DoD	Department of Defense
ESAL	Equivalent single axle load
FEM	Finite element method
FHWA	Federal Highway Administration
FWD	Falling weight deflectometer
GAB	Graded aggregate base
GDOT	Georgia Department of Transportation
IBP	Inverted base pavement
IRI	International roughness index
LEEP	Layered elastic evaluation of pavements
LET	Linear elastic theory
MEPDG	Mechanistic-Empirical Pavement Design Guide
PACES	Pavement condition evaluation system
PCASE	Pavement-Transportation Computer Assisted Structural Engineering

PSI	Pavement serviceability index
RMSE	Root mean square error
UFC	Unified Facilities Criteria
WES	Waterways Experiment Station

SUMMARY

Pavements are an integral part of modern transportation infrastructure. Growing pavement networks, diminishing resources, and climate change create a need for higher performing, more economical, and more sustainable pavement designs. Inverted base pavements ("inverted pavement" or IBP) is the term for a flexible pavement design philosophy different from conventional designs used in the United States. Inverted pavements maximize the performance of their constituent materials by taking advantage of their inherent properties. In IBP, the asphalt concrete surface layer is underlain by an unbound aggregate base layer, followed by a bound layer of stabilized aggregate subbase. This arrangement provides greater confining stress to the base course, resulting in a stiffer, more resilient structure. The improved performance of inverted pavement can reduce the thickness of the entire structure as well as the surface layer when compared to conventional pavement structures. Inverted base pavements may provide a solution to poor-performing, expensive, and unsustainable pavements.

The first goal of this thesis is to explore the long-term performance of inverted pavements in the United States. While they have a longer history of use in other countries, inverted pavements have not been widely accepted in the United States. After a review of relevant literature, a field evaluation was conducted on two test sections of inverted pavement in Georgia. Falling weight deflectometer (FWD) measurements and a surface distress survey were conducted on the sections at 21 and 13 years of age, respectively. Results showed that the test sections performed better than conventional pavements. FWD data revealed that inverted sections exhibited greater structural stiffness

and resistance to deformation over the life of the roadways. Material properties backcalculated from FWD data provided useful parameters for the modeling effort conducted in this study. The survey of surface distresses showed that inverted pavement sections accumulate less permanent deformation and load-related cracking, indicating superior load distribution and fatigue resistance.

The second goal of this research was to examine the suitability of IBP for aircraft traffic. Few previous studies have explored this application. A modeling effort was undertaken using a mechanistic-empirical pavement analysis software to evaluate inverted and conventional pavement under simulated airplane loading. The simulated test sections were designed using material properties and layer dimensions from the literature, the field study in this thesis, and the software default values. The results predicted IBP could bear a significantly greater amount of traffic in every climate tested, when compared to conventional sections designed for the same loading. Furthermore, many inverted designs outperformed conventional pavements despite having thinner cross sections and thinner asphalt concrete layers. This indicates that inverted pavements may provide a cheaper, more sustainable solution for airfield pavements without a decline in performance.

These results demonstrate that inverted pavements have a place in the future transportation networks of the United States. Further research is required to provide greater insight into the structures' response to loading, particularly in varying climates. Additionally, modeling efforts should be refined by considering the stress- and climate-dependent properties of pavement materials. Finally, full-sized field and lab efforts should be undertaken to explore the application of IBP as airfield pavements using

modern materials characterization and instrumentation. While a more complete understanding of inverted pavements is needed, this study has confirmed that inverted pavements can improve the performance, economy, and sustainability of our transportation networks.

1. INTRODUCTION

1.1 MOTIVATION

Paved surfaces form a vast transportation network vital to modern society. Due to constant traffic and weathering, pavement condition must be monitored and managed to ensure safe travel surfaces. The Federal Highway Administration (FHWA) reported in 2019 that of the nearly three million miles of paved public roads in the United States, 78% of urban roads and 88% of rural roads are flexible pavements (FHWA 2019). Over 156,000 miles of those public roads are in a condition worse than "acceptable" when measured using the International Roughness Index (FHWA 2020a). Additionally, the 2021 American Society of Civil Engineers Report Card listed 43% of public roadways in "poor" or "mediocre" condition (ASCE 2021). The problem is not limited to pavements used by automobiles: The 2021 National Transportation Statistics report noted that 21% of the 3,310 airports under the National Plan of Integrated Airport Systems had runways in "fair" or "poor" condition, indicating some level of pavement surface distress (USDOT 2021). Another insightful statistic involves rutting, a depression of the pavement surface caused by structural failure of the holistic pavement structure. In 2020, the FHWA noted that 20% of Federal-Aid Highways and 22% of National Highway System roads displayed rutting (FHWA 2020b; FHWA 2020c). The pavement condition problem is an expensive one: In 2017, 177 billion dollars were spent on roads and bridges in the United States, and rising global temperatures are estimated to add approximately 19 billion dollars to pavement costs each year by 2040 (ASCE 2021). Therefore, there is a need for more sustainable pavement structures with higher performance and lower life-cycle cost.

Inverted base pavement (IBP), also called “inverted pavement,” is an alternative to conventional pavement design that can offer improved performance, economy, and sustainability. Whereas conventional flexible pavement decreases in layer stiffness with depth, inverted pavement consists of a stiffer asphalt concrete (AC) surface over a less stiff unbound aggregate base layer, resting on a stiff stabilized subbase layer (typically cement-stabilized aggregate) (Barksdale 1984). The “sandwiching” of the unstabilized base layer by two stiff layers allows for increased compaction and confinement of the base layer, improving its mechanical performance (Barksdale 1984; Cortes 2010). Additionally, IBP structures allow for less load-bearing responsibility on the part of the AC, potentially allowing inverted designs to use less AC. Studies suggest these alternative structures may perform just as well as conventional pavement, but with a thinner cross section; or better than conventional pavement, with an equal cross section thickness (Grau 1973; Cortes 2010). Additionally, because AC is typically the most expensive construction material in pavement structures, designs that allow for less AC may reduce the construction cost of pavement. Finally, inverted pavement may offer sustainability benefits: AC is formed by the mixture of aggregate with an asphalt binder, a by-product of petroleum refining. Petroleum refining releases greenhouse gases into the atmosphere, contributing to global warming. A pavement structure with less AC may therefore positively contribute to efforts to reduce global warming. Additionally, the construction of pavement results in greenhouse gas emissions due to construction equipment and the transportation of materials. Pavement with a longer service life may result in less emissions by limiting the amount of construction and maintenance activities necessary.

The first goal of this study is to investigate the long-term performance of IBP in the United States. While inverted pavement is routinely used in other countries, it has not been widely accepted in the United States (Terrell 2002). Original field test sections were built in New Mexico (Johnson 1960), Virginia (McGhee 1971), and Louisiana (Rasoulian et al. 2001). While they performed well, these tests either did not use optimal material and thickness designs or did not provide for a direct comparison of unstabilized conventional and inverted pavement. Two more test sections were constructed on roadways in Georgia in 2001 and 2009 (Cortes 2010). Evaluation thus far confirms they have outperformed conventional pavement, but the time span of assessment has been limited. The most recent test sections placed in service in New Mexico, Virginia, North Carolina, and Tennessee have yet to provide performance data over a full pavement lifespan (R. Young, personal communication, 2022; Vaughan 2018; Jiang et al. 2022). Lab-scale tests focused on new lab sections have supported the use of IBP (Grau 1973, Barksdale 1984, Costigan 1984, Tutumluer & Barksdale 1995). The varying lab apparatuses, however, have not perfectly simulated the field conditions and wheel traffic that real pavements are exposed to. Furthermore, some of these lab tests have used sub-optimal inverted designs. More recently, Qamhia et al. (2018) conducted accelerated pavement testing that confirmed the conclusions made by original evaluations of the Georgia test sections. Much of the most recent inverted pavement research, including Terrell (2002), Cortes (2010), Papadopoulos (2014), Sha et al. (2020), Wang & Dong (2020), and Jiang et al. (2022) has included modeling and lab testing of samples from test sections in order to characterize the performance of the individual constituent layers of IBP. While they provided useful insight into mechanical behavior, these studies did not

provide a direct comparison of the holistic performance of conventional and inverted pavement under realistic traffic damage accumulation, nor did they consider the effects of moisture and temperature upon the pavement materials.

This study examines the two Georgia test sections: one built in Morgan County, Georgia in 2001 and one built in LaGrange, Georgia in 2009. The surface distress and falling weight deflectometer (FWD) data collected in this research provide insight into the performance of 21- and 13-year-old pavements with realistic traffic and environmental history. Furthermore, the Morgan County test section includes a control section of conventional pavement on the same travel path as the IBP, allowing for a direct comparison of the two designs. These efforts should therefore offer an improved understanding of the long-term performance of IBP in the United States.

The second goal of this study is to examine the performance of IBP in airplane traffic applications. Airfields tend to have higher standards for pavement than roadways: Due to heavier vehicle weights and higher tire pressures, airplanes exert much higher stress on pavement than cars and trucks. Surface distress tolerance is also typically less for airplanes than for automobiles - a small surface irregularity that may be acceptable for a car can result in serious disruption for an aircraft. Additionally, if pavement disintegrates into small pieces, these pieces can be sucked into a jet engine intake, causing catastrophic damage to the airplane.

Few field, lab, or modeling studies have been conducted to understand more about the performance of inverted pavement under airplane loading. Grau (1973) tested inverted designs under aircraft loading with full-scale lab tests. In this experiment, conventional pavement out-performed inverted pavement with the same cross section

thickness. The material used for the subbase of the IBP, however, was weaker than modern cement-stabilized subbases, and therefore not representative of the best-case design for inverted pavements. In 1984, Costigan also measured the performance of lab-scale inverted pavement test sections under aircraft loading. The structures, however, were designed for contingency use, meant to last much fewer passes than a permanent pavement would. This only provided a limited comparison between IBP and conventional pavement for airfield applications. No further examples of lab testing, modeling, or field use of inverted pavement for airplane traffic could be found. There is thus a significant absence of knowledge about the performance of inverted pavement under aircraft loading. This thesis aims to remedy that gap by using the mechanical properties measured from IBP test sections in Georgia to model the long-term performance of inverted pavement under aircraft traffic using a mechanistic-empirical pavement evaluation software.

2. INVERTED PAVEMENT DESIGN AND PERFORMANCE

2.1 CONVENTIONAL PAVEMENT DESIGN

Procedures for pavement design tend to be specified by the organization (federal, state, or otherwise) that owns the pavement. Most conventional pavement in the United States is designed by means of a mechanistic-empirical framework. Most government agencies have adopted these principles from the American Association of State Highway and Transportation Officials (AASHTO) 1993 Guide for Design of Pavement Structures and/or AASHTO's 2020 Mechanistic-Empirical Pavement Design Guide (MEPDG). The Department of Defense (DoD) developed its own mechanistic-empirical pavement design criteria, encoded in Unified Facilities Criteria (UFC) 3-250-01, Pavement Design for Roads and Parking Areas, and UFC 3-260-02, Pavement Design for Airfields (DoD 2001a; DoD 2016). A mechanistic-empirical pavement design process is founded on the two principles by which it is named: It is "mechanistic" because it uses an understanding of mechanics to build a response model. A mechanistic model utilizes fundamental material properties to calculate a response to a design case. For instance, the strain in a layer (the response) can be computed if the stiffness of the material (the fundamental material property) and applied stress are known. An empirical model uses data from experiments with similar conditions to predict performance from the calculated responses. For example, the AASHTO Guide for Design of Pavement Structures (1993) predicts pavement performance based on data from the 1960 American Association of State Highway Officials (AASHO) Road Test. The AASHO Road Test was a program of full-scale road test sections that measured pavement responses such as deflections and

strains and correlated those responses to performance criteria such as pavement serviceability index (PSI) (AASHTO 1993).

The design procedures advocated by these guides have similar basic goals. Failure criteria are based on both structural and functional performance (AASHTO 1993). Structural performance is a measure of pavement's load-carrying capability, whereas functional performance is a measure of ride quality- how smooth and level of a surface the pavement provides for traffic (AASHTO 1993). For instance, the DoD's failure criteria for flexible pavement are focused on two primary modes of distress: cracking and rutting. Performance needs are met by limiting tensile strain in the AC layer, which is empirically correlated to cracking, and limiting vertical strain in the subgrade, which is empirically correlated to rutting (Van Steenburg 2021).

There is an implicit assumption in conventional pavement design philosophy that dictates the arrangement of the cross section. The aforementioned guides all assume that layer stiffness should correspond to the stress in that layer, i.e., the stiffest layers in a pavement structure belong closest to the surface where the stress is highest (Tutumluer 2013). Conventional pavement is therefore designed with layers increasing in stiffness from the subgrade to the surface. While this philosophy has served well throughout the years, it may not be the most efficient use of material properties in the pavement structure.

2.2 INVERTED PAVEMENT DESIGN

Inverted pavement attempts to meet the same performance criteria as conventional pavement via an alternative layer arrangement. It is "inverted" because it does not follow

the conventional trend of stiffness decreasing with depth from the surface. Modern conventional pavement typically consists of one or more layers of asphalt concrete (AC) atop unbound layers. IBP instead consists of an AC surface on top of an unbound aggregate base layer, which rests on a stiff bound subbase layer (typically cement-stabilized or cement-treated aggregate). Figure 2.1 from Papadopoulos (2014) demonstrates the difference between the typical composition of conventional pavement and IBP and the different stiffness profiles of each.

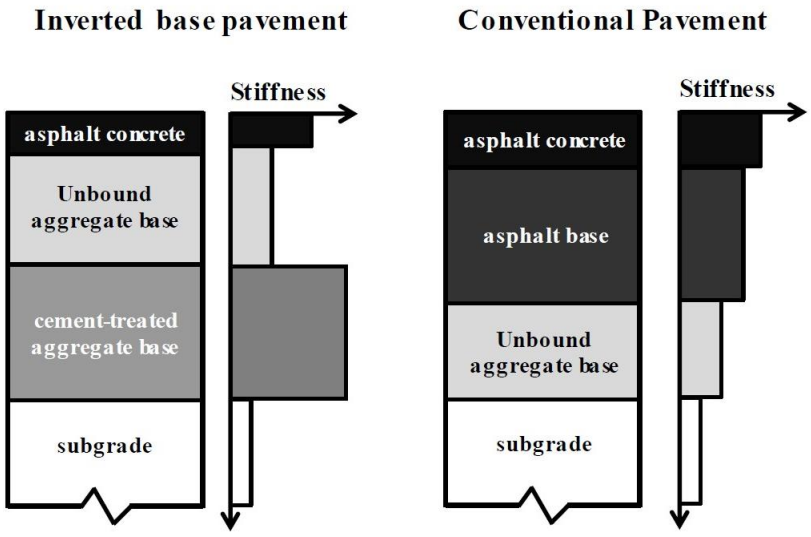

Figure 2.1 Inverted and conventional pavement composition. Figure from Papadopoulos (2014)

The inverted configuration maximizes the load-carrying contribution of each material. In particular, the unbound aggregate base provides greater capability in IBP than conventional pavement. With a thinner AC layer than conventional pavement, the unbound aggregate base is closer to the point of load application at the surface, where stress is higher. This takes advantage of the stress-dependent stiffness of unbound soil;

with higher confining stress in the base layer, the aggregate develops a higher modulus, resulting in less deformation (Tutumluer 2013). Furthermore, the stiff subbase layer relocates the neutral axis of bending from within the base course to below the interface between the base course and the cement-treated subbase (Tutumluer 2013). This causes the surface and base layers to perform primarily in compression when loaded (Tutumluer 2013). This is significant because AC is weak in tension, and unbound, non-cohesive materials such as those used in the base layer have minimal inherent tensile strength. Figure 2.2 illustrates the contrast in the location of the neutral axis between conventional and inverted pavement.

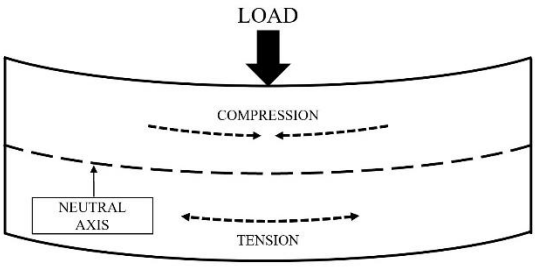

(a) Idealized beam

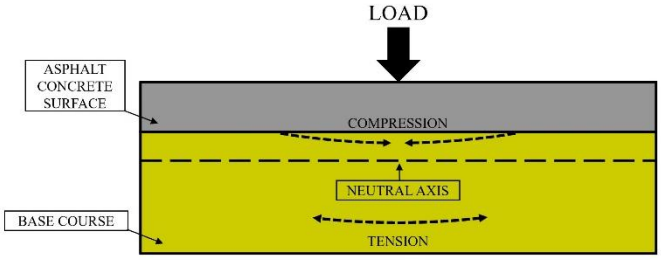

(b) Conventional pavement

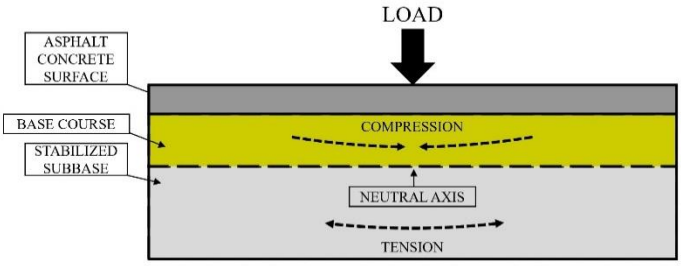

(c) Inverted pavement

Figure 2.2 Neutral axis of bending in (a) idealized beam, (b) conventional pavement, and (c) inverted pavement

Inverted pavement additionally maximizes the performance of the unbound base layer by achieving increased compaction compared to unbound layers in conventional pavement (Barksdale 1984). This is accomplished because of the strong support platform provided by the stiff cement-treated subbase (Cortes 2010). The density of the base layer can be further increased by utilizing a compaction technique called "slushing", commonly used in IBP construction in South Africa. During this process, the base course is flooded with water and subsequently compacted, allowing excess fines to be removed as they are suspended in the water. This creates a "material with significantly higher shear strength" (Jooste et al. 2005).

IBP may also improve the performance of the asphalt surface layer by decreasing the tensile stress in that layer (Papadopoulos 2014). Papadopoulos found that in inverted pavement with a thin layer of AC, the AC can perform under loading as a membrane instead of a beam. This transition in behavior reduces the maximum tensile stress in the surface layer, which is a source of load-related cracking and distress. It is unclear, however, if this results in holistically improved performance, as the membrane effect may instead induce shear in the asphalt surface (Papadopoulos 2014).

2.3 INVERTED PAVEMENT TEST SECTIONS

Inverted pavement has been widely used in South Africa since the 1950s as the design of choice for pavements under heavy truck traffic (Horne et al. 1997; Terrell 2002). While it has a long, successful service record in that country, it has not yet been accepted for widespread use in the United States.

The first American research into inverted structural configurations was an experimental project conducted by the New Mexico State Highway Department. In 1954 two test sections of IBP were constructed on a highway in Road Forks, NM, and four were constructed on a highway between Tesuque and Pojoaque, NM (Johnson 1960). Each site also had control sections of conventional pavement and additional experimental sections of pavement with stabilized base layers. The Road Forks site experiences a cold, dry climate, and the Tesuque-Pojoaque site is dry year-round with cold winters and hot summers (see Appendix A for relevant climate data). After exposure to "heavy traffic" for one year, surface distresses were inspected (Johnson 1960). Johnson (1960) found that at the Road Forks site, there was "no difference" in rutting between the inverted sections and the others, and longitudinal cracking was present in one of the inverted sections. He hypothesized, however, that the cracking was not due to structural differences but to differing site conditions, as that section was located adjacent to a lake and was built upon highly plastic subgrade. At the Tesuque-Pojoaque site, no rutting was present in any sections and cracks were only present in the sections with stabilized bases (Johnson, 1960). While this experiment provided a useful comparison between conventional and inverted pavement in realistic traffic and climate conditions, the lack of precise records of traffic loading provides limited understanding. Additionally, no follow-up inspections were documented to further demonstrate the long-term performance of IBP. This first study did, however, indicate that inverted pavement may provide similar performance to conventional designs.

In 1958, several test sections were constructed on in-service roadways in Charlotte County, Virginia (McGhee 1971). These sites tend to have warm, wet weather

(see Appendix A for relevant climate data). The inverted sections, located on Route 360 and Route 7360, consisted of AC surfaces over select borrow material, which was placed on cement-stabilized subgrade (McGhee 1971). While exhibiting the characteristic "sandwich" configuration of inverted pavement, the materials used were atypical. For some inverted test sections, McGhee reported the California Bearing Ratio (CBR) of the unbound base course to be 20. CBR has historically been used as a measure of soil stiffness and resistance to permanent deformation; per the FHWA, typical pavement base courses have a CBR in the range of 60-80 (Christopher et al. 2006). Additionally, the strength of the bound layer is questionable - modern inverted pavement use cement-treated crushed stone or gravel, but these test sections treated the natural subgrade with cement. McGhee (1971) reported the CBR of the untreated natural subgrade to be 20, potentially indicating a weaker subbase than in current IBP.

A regular testing program was conducted on these two Virginia test sections from 1958 to 1971, which included deflection testing, roughness tests, and visual inspections. McGhee (1971) notes that in 1962, the inverted sections at Route 360 had less deflection than conventional sections. At Route 7360, however, the inverted section showed the greatest amount of cracking and highest deflections compared to the control sections with fully stabilized cross sections. The inverted sections with an unbound base course of crushed stone instead of borrow material with a CBR of 20 did perform better than those with the borrow material (McGhee 1971). The results of this testing program should be considered somewhat inconclusive, as there were no unstabilized conventional designs for comparison. Furthermore, the inverted designs tested were not optimal. In addition to the material concerns noted, the geometry of these test sections, with thick surface and

base courses, likely did not allow for an optimal location of the neutral axis and the stress-dependent stiffness of unbound materials that results. Lastly, data collected after 1962, when the test sections had only been in service for four years, were not available.

Grau led a study at the US Army Engineer Waterways Experiment Station (WES), published in 1973, that examined the performance of stabilized layers in pavement structures subject to aircraft loading. Test sections were built outdoors in the warm, wet climate of Vicksburg, Mississippi (see Appendix A for relevant climate data). Two inverted test sections consisted of a surface course of 3 inches of AC, a base course of 6 inches of crushed stone, and a 15-inch bound subbase of 3.5% lime-stabilized lean clay or 10% cement-stabilized lean clay (Grau 1973). The control test sections had comparable surface layers with 21-inch base courses of either crushed stone or cement-stabilized clayey gravelly sand (Grau 1973). Mixed aircraft traffic was simulated with a loading cart that applied loads ranging from a 50-kip single wheel to a 360-kip 12-wheel assembly (Grau 1973). Traffic was applied until failure; defined as surface upheaval greater than 1 inch or surface cracking to the extent that the pavement was no longer waterproof (Grau 1973). Conventional sections far outperformed the IBP: The fully stabilized conventional section did not fail after 10,000 passes and the other conventional section failed after 5,000 passes (Grau 1973). The inverted section with a cement-stabilized subbase failed after 1,432 passes, and the IBP with lime-stabilized subbase failed after 198 passes (Grau 1973). The sections that failed all failed due to excessive cracking in the AC (Grau 1973). This study provided a significant example of conventional pavement exceeding the performance of inverted pavement under aircraft loading, but it should not be considered a final verdict. The “waterproof” failure criterion

used is not based on a mechanistic understanding of pavement structural performance. Failure in the surface layer is not necessarily indicative of poor performance of the entire pavement system, but may indicate poor quality AC. Additionally, the stabilized subbases of the inverted sections were weak compared to modern inverted designs: Not only was lean clay used in place of the more common crushed stone or gravel, but Grau (1973) also reported the CBR of the lime-stabilized subbase to be less than 100, and that of the cement-stabilized material to be approximately 300. Using the MEPDG's conversion from CBR to resilient modulus, the resilient moduli of these two materials are approximately 47,000 psi and 300,000 psi, respectively (AASHTO 2020). The MEPDG reports the resilient modulus of modern cement-stabilized aggregate is typically in the range of 500,000 to 1,000,000 psi (AASHTO 2020). A weak subbase would result in the neutral axis of the composite structure residing closer to the surface than optimal, putting some of the unbound base in tension during loading. Since these materials have minimal inherent tensile strength, this could explain the poor performance of the inverted sections. While this study provides valuable understanding of IBP performance under airplane loading, the inverted sections tested by Grau were likely lacking the structural support that is characteristic of modern IBP.

Costigan (1984) also documented the performance of inverted pavement under simulated airplane traffic. Test sections were constructed in 1982 in a hangar at the WES in Vicksburg, MS. The exact climate control conditions of the experimental setup were not recorded. The inverted pavement test sections consisted of 1 inch of AC atop 4 inches of crushed stone, which rested upon a 12-inch subbase of cement-stabilized sand (Costigan 1984). The dimensions of the IBP layers are notable, as the AC is thinner than

in previous experiments, and the ratio of subbase, base, and surface layer thicknesses are similar to those suggested by later optimization studies. The section most comparable to a conventional design consisted of 1 inch of AC upon 11 inches of cement-stabilized sand (Costigan 1984). Traffic applications of a simulated F-4 aircraft were applied via a loading cart fitted with an F-4 tire, applying 27 kips in one channelized lane (Costigan 1984). Loads were applied up to 1,000 passes or until failure; defined as rutting deeper than 3 inches or a punching failure through the surface layer (Costigan 1984). A falling-weight deflectometer (FWD) was also used to measure the maximum deflection from weights of 9 and 15 kips dropped upon an 11.8-inch diameter plate, providing an assessment of the overall stiffness of each pavement structure (Costigan 1984).

The test section of inverted pavement performed better than the "conventional" test section with stabilized base in every measure: The IBP was trafficked to 1,000 passes, with no cracking noted, 0.5 inches of rutting, and a maximum deflection of 41 mils (41 thousandths of an inch) from a 15-kip application of the FWD (Costigan 1984). The test section with a stabilized base course exhibited longitudinal cracks at 341 passes, ruts of 0.25 to 0.5-inch depth at 500 passes, and ruts of 2.5-inch depth at 663 passes, at which point ladder cracking permeated the traffic lane and testing was terminated (Costigan 1984). A 15-kip application of the FWD was conducted on this section at 500 passes, resulting in a maximum deflection of 67 mils (Costigan 1984). This study therefore showed that IBP can outperform other pavement designs under aircraft traffic if it has a thicker total cross section, but it should be noted that these designs were intended for low-volume contingency traffic, not permanent use. Additionally, no direct

comparison to high-quality conventional pavement (typically consisting of a thick AC surface over well-graded gravel or crushed stone base course) was provided.

Barksdale (1984) led the next notable investigation into the performance of inverted pavement. Several test sections of conventional and inverted pavement were constructed in a "laboratory facility under closely controlled environmental conditions" (Barksdale 1984). Test sections consisted of five conventional sections with varying base course gradations, five sections with full-depth AC, and two inverted sections. The IBP sections had thin AC (3.5 inches) but with 8 inches of crushed stone base and 6 inches of bound subbase, they were 2 inches thicker in total than the thickest conventional design (Barksdale 1984). Barksdale (1984) also noted that the density of the crushed stone base was higher in the inverted sections than in the conventional ones. Loading was applied via a cyclic pneumatic loading system, which applied a 6.5-kip uniform circular loading (9.1 inches in diameter, approximately 100 psi contact pressure) at 70-90 applications per minute (Barksdale 1984). A standard axle load is considered to be 9 kips (FHWA 2017a). The location of load application for a given test section was varied throughout testing to avoid localized punching failure (Barksdale 1984). Barksdale (1984) applied loads for up to 2 million repetitions until failure; defined as rutting greater than 0.5 inches in depth or the initiation of "Class 2" cracking (cracking classes were not defined). Horizontal strain was measured at the bottom of the AC and vertical strain was measured at the top of the subgrade (Barksdale 1984).

Both IBP designs withstood more repetitions until failure than the conventional sections (Barksdale 1984). The inverted pavement exhibited less vertical stress in the subgrade and less surface deflection (Tutumluer and Barksdale 1995). Where the IBP

sections failed in a combination of rutting and fatigue (cracking), most other sections failed in rutting (Barksdale 1984), which typically indicates a failure of the holistic structure to support loads. The vertical strain measured in the subgrade was less for inverted sections than conventional, further endorsing the capability of the IBP structure (Tutumluer & Barksdale 1995). Furthermore, the horizontal tensile strain measured in the AC was similar for conventional and inverted sections with similar AC layer thickness (Tutumluer & Barksdale 1995). This indicates that while the AC deformed equally and distributed similar amounts of stress, the superior subsurface layers of the inverted pavement better prevented failure. This study therefore provided significant support for further optimizing inverted pavement designs, albeit under ideal temperature and moisture conditions.

A test section of inverted pavement was constructed on Louisiana Highway 97 (LA 97, a low-volume rural highway) in 1991 to investigate means of reducing reflective cracking in flexible pavement with cement-stabilized bases (Rasoulian et al. 2000). This location experiences a warm, wet climate (see Appendix A for relevant climate data). The inverted section consisted of 3.5 inches of AC surface, 4 inches of crushed stone base course, and 6 inches of in-place stabilized soil cement subbase (Rasoulian et al. 2000). The control section of conventional pavement was composed of 3.5 inches of AC over an 8.5-inch in-place stabilized soil cement base layer, resulting in a cross section 1.5 inches thinner than the IBP (Rasoulian et al. 2000). Similar sections were constructed at an outdoor accelerated pavement testing (APT) facility in 1995.

LA 97 was monitored and tested several times from 1998 to 2001, during which it experienced average daily traffic of 2,000 vehicles (Rasoulian et al. 2000; Rasoulian et al.

2001). A distress survey in 1998 found that the control section had accumulated 0.89 linear feet of cracking per square foot of pavement compared to 0.014 linear feet per square foot in the inverted test section (Rasoulian et al. 2000). Continuous roughness and rutting measurements were conducted at the same time using a laser profiler, which found both sections had similar average rut depth and roughness (Rasoulian et al. 2000). These survey results were later corroborated in measurements conducted in 2001 (when the test section was 10 years of age) by Rasoulian et al. (2001). The APT sections were trafficked with a dual wheel load cart, and the number of equivalent single axle loads (ESALs) until failure was measured. Failure was defined in this study as rutting with a depth greater than 1 inch or crack density greater than 1.5 linear feet of cracking per square foot in 50% or greater of the section (Rasoulian et al. 2000). The IBP section received 4.7 times more ESALs at failure than the section consisting of just AC and soil cement (Rasoulian et al. 2000). Rasoulian et al. (2000) showed that in realistic loading and exposure conditions, IBP can perform equal to or better than conventional flexible pavement with stabilized base, if it has a marginally larger cross section. It also provided a performance assessment of inverted pavement at the greatest age to date (when originally published). Ultimately, this study provided valuable support for future investigations to maximize the efficiency of inverted pavements and examine the ability of more economical IBP cross sections to outperform conventional designs.

A quarry haul road in Morgan County, Georgia, provides an exceptional comparison of inverted and conventional pavement (Cortes 2010). The road was re-built in 2001, residing in a warm, wet climate (see Appendix A for relevant climate data). The test sections, depicted in Figure 2.3, included a 1,000-foot section of conventional

pavement and two different 400-foot sections of IBP (Terrell 2002). The first IBP section, named the "South African" section for the method used to compact the base layer, consisted of a 3-inch AC surface, 6 inches of Georgia Department of Transportation (GDOT) graded aggregate base (GAB) compacted using the South African "slushing" method, and 8 inches of 4-5% cement-stabilized GAB subbase (Terrell 2002). The second IBP section, dubbed the "Georgia" section, had the same dimensions and materials, except the base layer was compacted using standard compaction methods specified by GDOT instead of slushing (Terrell 2002). The conventional test section used for comparison consisted of 3 inches of AC at the surface, 8 inches of GAB as a base course, and 6 inches of "surge stone", a crushed stone with larger particles than GAB (Terrell 2002). Thus, the inverted and conventional sections had equal total thicknesses, allowing for a more direct comparison. One of the original goals of this study was to assess different means of aggregate compaction between the three test sections: The conventional base layer was assumed to be compacted to 100% of the modified Proctor maximum dry density, while the South African base course reached 99%-104% (measured using both sand cone and nuclear density gauge), and the Georgia base course reached 104%-107% (Terrell 2002). The unconfined compressive strength of the cement-stabilized subbase was recorded as 450 psi, and the material properties of the AC surface layers were not reported (Terrell 2002).

Figure 2.3 Morgan County, GA test sections. Image from Google (n.d. a)

Cortes (2010) noted that the roadway in Morgan County has experienced "uninterrupted high volume truck traffic since construction." A program of frequent testing and data collection has been undertaken since the test section was completed. Terrell (2002) collected material data during construction and conducted in-situ geophysical testing to characterize the unbound aggregate layers of each test section. He found that immediately after construction, the difference in stiffness of the South African and Georgia base layers was negligible, and the base course of the conventional section was stiffest. It was postulated that abnormal, prolonged compaction of the conventional subbase had provided a stiff platform for base course compaction, leading to superior base course stiffness (Terrell 2002).

Lewis et al. (2012) documented the performance of the Morgan County test sections from 2003 to 2011. In 2003 and 2006 inspections, rutting was found in the conventional section, with negligible rutting in both IBP sections (Lewis et al. 2012). At the same time, visual inspection found no distress in the inverted sections, but extensive cracking in the conventional section- particularly in the outbound lane, which

experienced more ESALs as loaded trucks exited the quarry (Lewis et al. 2012). FWD measurements were conducted in 2007 at target loads of 7, 9, 11, and 16 kips (Lewis et al. 2012). Figure 2.4 below, from Lewis et al. (2012), shows the maximum deflections measured from the 9-kip drop at each station along the test sections. The deflections of the conventional section far exceed those of the inverted sections, indicating greater structural capacity in the IBP. In a 2011 visual survey, Lewis et al. (2012) confirmed that the two inverted test sections continued to perform well without rutting or cracking. Of particular note, Lewis et al. (2012) reported greater deflections, rutting, and cracking in the first several-hundred feet of the roadway, where trucks were braking and turning to enter or exit the quarry.

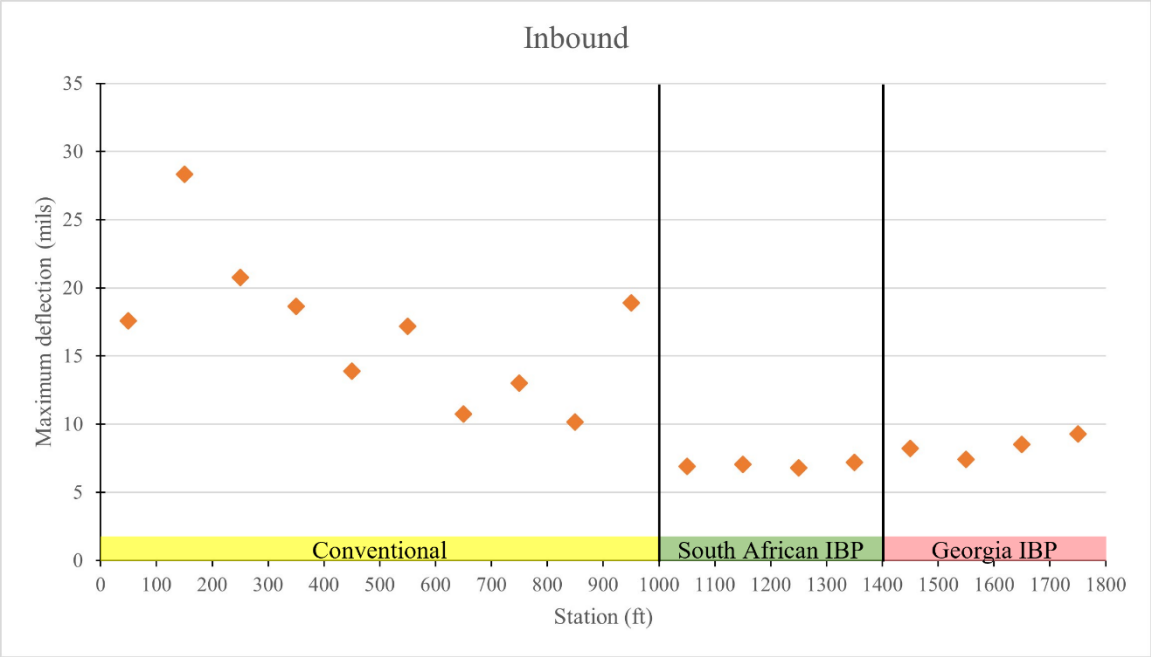

(a)

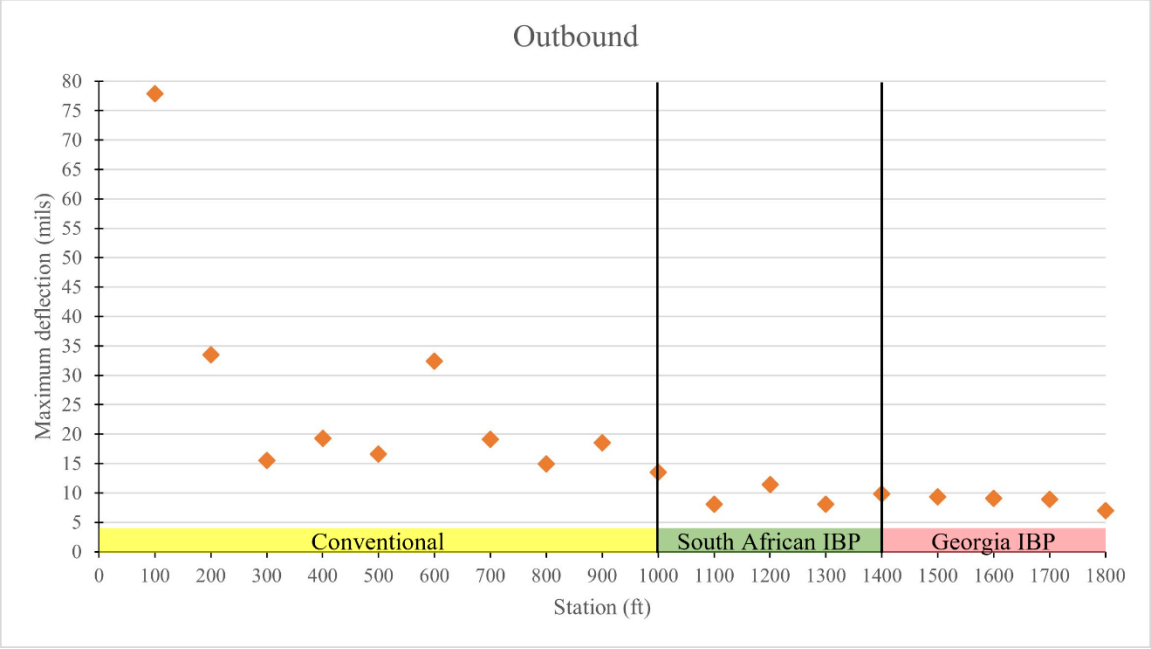

(b)

Figure 2.4 2007 maximum FWD deflections at Morgan County test sections for (a) inbound and (b) outbound lanes. Figure adapted from Lewis et al. (2012)

Frost (2017) continued to monitor the performance of the Morgan County test sections by documenting the results of surface profiling conducted via laser scanning in 2016, when the roadway had been in service for 15 years. The imaging data were processed to allow for measurement of cracking and rutting length, type, and severity. Distresses were then evaluated according to the GDOT pavement condition evaluation system (PACES), a rating of pavement condition based on surface distress. Frost (2017) found that the Georgia and South African inverted pavement sections, with average PACES ratings of 83.3 and 81.4, respectively, had outperformed the conventional section (average PACES rating of 75) at 15 years of age. Rutting was minimal along the entire road, but higher at the conventional section (Frost 2017). Load cracking was also more severe in the conventional section compared to the inverted section (Frost 2017). These distress measures demonstrate the superior load-bearing ability of the IBP structure compared to the conventional design. The Morgan County case study as a whole is the most convincing example to date that inverted pavements can outperform conventional pavements long-term, even with the same cross section thickness. Later work described in Chapters 3 and 4 of this thesis expands upon this body of knowledge to provide data on surface distress and subsurface performance of the Morgan County test section at an advanced age. The material properties measured in Chapter 3 will also be used for performance modeling of inverted pavements in Chapter 4.

The most recently constructed section of inverted pavement in Georgia was built in 2009 (Cortes 2010). The IBP was paved on 3,400 feet of Pegasus Parkway, a two-lane industrial parkway in LaGrange, Georgia shown in Figure 2.5 (Cortes 2010). LaGrange experiences a warm, wet climate (see Appendix A for relevant climate data), and the test

section was designed for 11,700 vehicles per day by the end of its service life, with trucks estimated to be 7% of those vehicles (Cortes 2010). Cortes (2010) monitored construction and characterized the materials and as-built dimensions: The structure consisted of 3.5 inches of AC atop 6 inches of GDOT GAB and 10 inches of subbase, consisting of GDOT GAB stabilized with 4% cement by weight (Cortes 2010). Cortes (2010) tested the AC using surface wave tests in the field and P-wave tests in the laboratory, reporting the constrained modulus to be in the range of 1,450 to 5,800 ksi and the Poisson's ratio to be 0.307. The compaction of the unbound aggregate base was not reported, but the unconfined compressive strength of the subbase was measured in the range of 435 to 725 psi (Cortes 2010).

Figure 2.5 LaGrange, GA test section. Image from Google (n.d. b)

Lewis et al. (2012) recorded the results of FWD tests conducted immediately after the construction of each layer in order to identify any potential problem areas that would

affect future pavement performance. No significant difference was found in most layers across the test section, except the subgrade had particularly high deflections from approximately Station 8+00 to Station 19+00. Frost (2017) included the LaGrange test section in his 2016 assessment of surface distresses using laser scanning profiling. The test section was evaluated according to the GDOT PACES metric; with an average rating of 94.7 after seven years in service, the LaGrange section was performing exceptionally well (Frost 2017). The GDOT-reported average PACES rating for a conventional pavement section at 10.6 years is 70 (Frost 2017). The predominant surface distress in 2016 was low-severity load cracking, which persisted on only 5.4% of the test section area. Moderate rutting was also noted in some areas, with no clear trend (Frost 2017). Frost (2017) also identified several areas where the test section was more distressed than other parts. Distresses were higher than average in the westbound lane at Station 30+00 to 34+00 and in the eastbound lane at Station 0+00 to 3+00. Frost (2017) hypothesized that the distress may be higher at these locations, where vehicles are entering the test section, because of discontinuity in support between the test section and the adjacent pavement structures, resulting in poor load transfer and greater impulse on the IBP section. Another area of increased surface distress was in the eastbound lane from Station 16+00 to Station 20+00, where Frost (2017) reported a horizontal curve at a downhill grade may result in greater braking and shear forces imparted on the structure. Cortes (2010) also reported weaker subgrade at Station 18+00 to 20+00 based on the results of dynamic cone penetrometer tests; this likely impacted the load-carrying capability and increased load cracking in this area, causing the decreased PACES rating noted by Frost (2017). While it lacks a control section for comparison to conventional pavement, this

assessment demonstrated excellent performance from inverted pavement at seven years in service. It also provides a helpful baseline for future assessments of the long-term performance of this IBP test section. This thesis will expand upon these efforts, as Chapter 3 will provide an evaluation of the pavement condition at 13 years of age and Chapter 4 will use results from FWD testing in a mechanistic-empirical model of inverted pavements.

Another recent IBP test section was placed in service in December 2015 on a quarry access road in Pineville, North Carolina (K. Vaughan, personal communication, 2022). The experimental setup was similar to the Morgan County, GA test section, with one section of inverted pavement and one section of conventional pavement as a control section. The Pineville IBP had similar layer dimensions to the Morgan County IBP, but the conventional structure consisted of 6 inches of AC and 10 inches of unbound aggregate base (Vaughan 2018). Another notable difference was that the Pineville inverted pavement design had targeted 2% cement content in its subbase and a 7-day unconfined compressive strength of 550 psi (Vaughan 2018). The actual 7-day unconfined compressive strength, however, was on the order of 1,500 psi; indicating the cement content and therefore the stiffness of the subbase was higher than intended (K. Vaughan, personal communication, 2022). The test section was built in a warm, wet climate (see Appendix A for relevant climate data) and is predicted to experience 1.5 to 2 million ESALs over its 20-year life (Vaughan 2018). FWD testing was conducted in September 2015, June 2016, December 2016, August 2017, and April 2018. Each test exhibited similar results; the average maximum deflection of the conventional section far exceeded that of the inverted section, indicating superior structural performance by the

IBP (Vaughan 2018). In the 2018 test, the average maximum deflection of the IBP was 7 mils, whereas that of the conventional was 15 mils. Additionally, Vaughan (2018) reported the average cost per square yard of the two sections to be $35.92 per SY for the IBP and $40.51 per SY for the conventional. Therefore, while the experience of the Pineville section is still limited, it provides another promising example that inverted pavement with approximately equal thickness to conventional pavement can not only better carry and distribute traffic loads, but also have lower construction costs.

Qamhia et al. (2018) reported on the construction and testing of two inverted pavement test sections at the outdoor APT facility at the Illinois Center of Transportation in Rantoul, IL. This site experiences a temperate climate with a significant freezing season (see Appendix A for relevant climate data). While primarily focused on investigating potential uses of quarry by-products, Qamhia et al. (2018) built two IBP test sections 20 feet in length and 12 feet wide, with an accompanying conventional section for control. The inverted sections had a 4-inch AC surface, 6 inches of dense-graded base course, and a 6-inch stabilized subbase for a total thickness of 16 inches (Qamhia et al. 2018). The first IBP section had a subbase consisting of quarry by-product stabilized with 3% cement, and the second had a subbase of quarry by-product stabilized with 10% fly ash (Qamhia et al. 2018). The inverted subbases were compacted to 92.5% and 96.6% relative compaction and exhibited a 7-day unconfined compressive strength of 270 psi and 250 psi, respectively (Qamhia et al. 2018). The base course of the first IBP section was compacted to 101.5% relative compaction, and the base course of the second IBP section was compacted to 109.2% relative compaction (Qamhia et al. 2018). The 16-inch control section consisted of a 4-inch AC surface layer atop 12 inches of base course

comparable in composition and relative compaction to the IBP sections (Qamhia et al. 2018). All test sections were placed upon a subgrade with a CBR of 6 (Qamhia et al. 2018).

FWD tests were conducted after construction, and Qamhia et al. (2018) recorded maximum surface deflections: The deflections were smallest in the inverted section with a cement-stabilized subbase (17 mils), followed by the fly ash-stabilized IBP (31 mils) and the conventional section (57 mils). Qamhia et al. (2018) then conducted APT using a unidirectional wheel load of 10 kips with 110 psi tire pressure at a constant speed of 5 mph. This loading was applied for 100,000 passes, until it was increased to 14 kips and 125 psi for 35,000 passes (Qamhia et al. 2018). Pressure cells on top of the subgrade measured vertical stress in the wheel path of the conventional test section and the cement-stabilized IBP section (Qamhia et al. 2018). Periodic surface profile measurements were conducted with a rutting depth failure threshold of 0.5 inches (Qamhia et al. 2018). The control section failed much earlier than the inverted section, with testing ceasing after 40,000 passes (Qamhia et al. 2018). The cement-stabilized inverted section did not reach failure, while the fly ash-stabilized IBP failed at approximately 130,000 passes (Qamhia et al. 2018). Qamhia et al. (2018) also noted "premature transverse fatigue and longitudinal wheel path cracking" in the conventional pavement, causing moisture intrusion and pumping that further distressed the section. The subgrade pressure cells reported vertical pressures in the control section three to five times that in the IBP (Qamhia et al. 2018). Finally, Qamhia et al. (2018) repeated FWD testing after APT loading, with similar results: maximum surface deflections were 17 mils for the cement-stabilized IBP, 30 mils for the fly ash-stabilized IBP, and 39 mils for the conventional

pavement. Upon forensic coring and exhumation, Qamhia et al. (2018) found that the thickness of the AC surface in some parts of the conventional section was up to 1.25 inches less than designed. They report that this construction error likely contributed to the expected structural advantage of the inverted pavement. At best, this study lends further support to the conclusions from Morgan County that IBP designs with similar thicknesses can outperform conventional pavements.

The most recently constructed section of inverted pavement in the United States was built in 2019 in Knoxville, Tennessee, as detailed by Jiang et al. (2022). The Knoxville test section is similar to the Pineville, NC site: It was also paved on a two-lane truck entrance road to a quarry and has one 16-inch section each of inverted and conventional pavement (Jiang et al. 2022). Notably, the surface layer of the inverted section is only 2.3 inches thick (Jiang et al. 2022), the thinnest AC layer of any in-use section of IBP. The inverted pavement also contains a 6-inch unbound aggregate base and an 8-inch subbase, consisting of Tennessee Department of Transportation “Grade D" base materials mixed with 4% cement by weight (Jiang et al. 2022). Similar to the Pineville and Morgan County sections, the Knoxville section experiences a warm, wet climate (see Appendix A for relevant climate data). Jiang et al. (2022) estimated the roadway will experience 330,000 ESALs over its lifetime. After two years in service, laser surface profiling and FWD tests were conducted to evaluate the performance of the test section. The surface distress assessment found an average rut depth of 10.7 mm per km in the IBP and 18.9 mm per km in the conventional pavement (Jiang et al. 2022). The average international roughness index (IRI) of the IBP was 1196.3 mm per km, and 1963.4 mm per km for the conventional section, indicating a slightly rougher surface exists in the

inverted section (Jiang et al. 2022). Lastly, Jiang et al. (2022) found no transverse cracking and similar levels of low-severity longitudinal cracking in both test sections, but far more medium-severity longitudinal cracking in the conventional section than the inverted section (4,049.2 mm per km, compared to 598.4 mm per km). The results of the FWD tests conducted by Jiang et al. (2022), however, may not provide as overwhelming evidence of the structural superiority of the inverted test section. The average maximum deflection under a 9-kip load was 5.9 mils for the conventional section and 6.2 mils for the IBP, indicating comparable stiffness. The average deflection at the most radially distant FWD geophone, an indication of the subgrade deflection and therefore a structure's ability to dissipate stress from loads, was 37 percent lower for the inverted pavement (Jiang et al. 2022). At three years of age at the time of testing, the results of the Knoxville test section should not be considered a final verdict but seem to indicate that like Morgan County and Pineville, the inverted pavement will perform better than the conventional section over time. Continued evaluation should be undertaken, as the situation allows for a useful comparison.

Two additional IBP test sections of note were constructed in Bull Run, VA and Raton, NM (R. Young, personal communication, 2022; Vaughan 2018). Both test sections consist of inverted designs similar to those of recent test sections reported here, with accompanying control sections of conventional pavement. No information on the performance of these sections has been published at the time of this writing. The Raton test section is notable, however, as the climate of that site is cold and dry, different from any inverted test section since the New Mexico test sections reported by Johnson (1960).

It will therefore likely provide useful insight into the behavior of IBP in climates with a more severe freezing season.

Figure 2.6 summarizes the cross-section dimensions of selected field and lab test sections of inverted pavement.

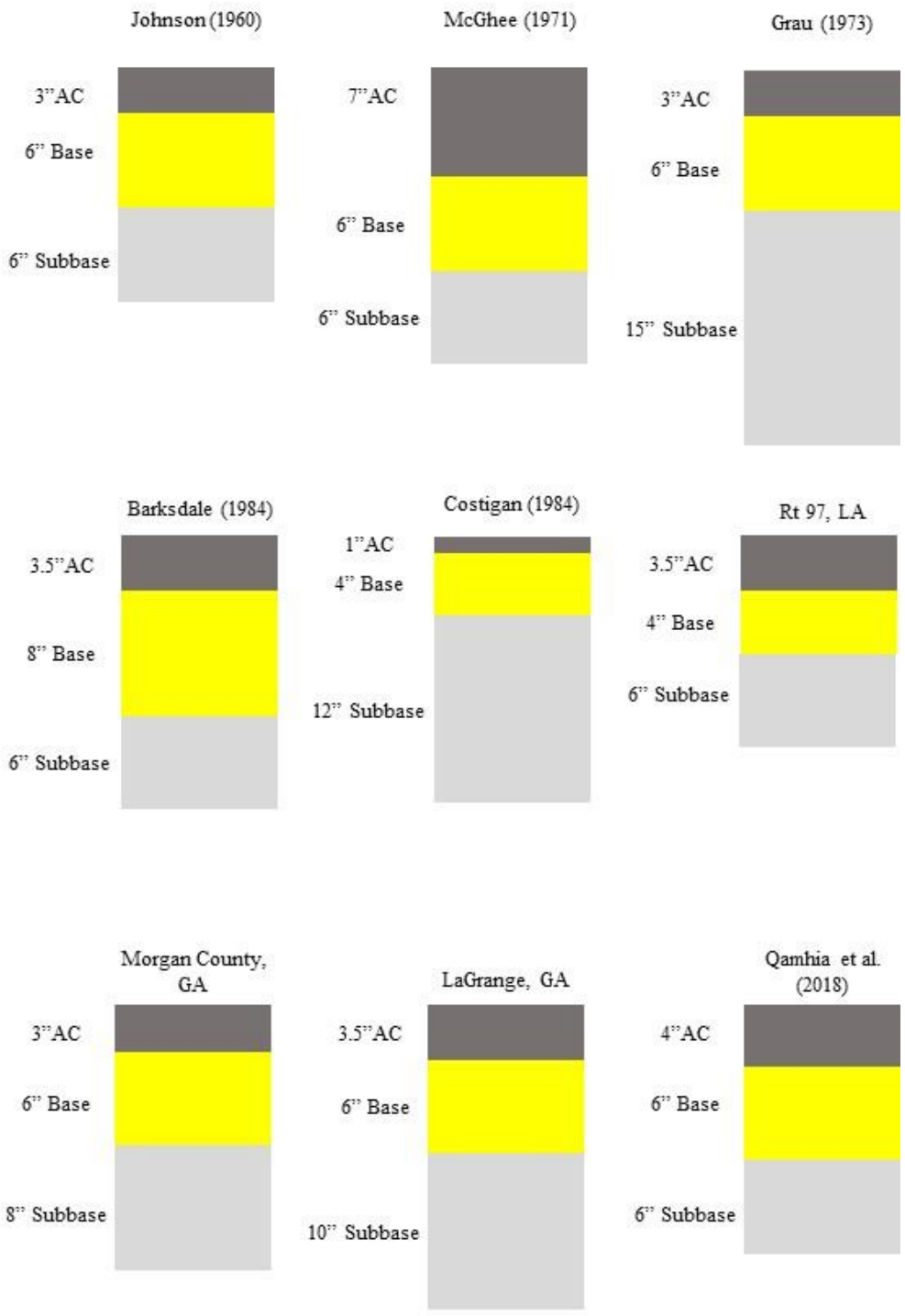

Figure 2.6 Cross sections of selected inverted pavement test sections

2.4 INVERTED PAVEMENT MODELING

Many recent efforts to evaluate the performance of inverted pavement have been conducted using numerical methods to avoid costly field and laboratory testing. Cortes (2010) was one of the first - he simulated the mechanical response of inverted pavement structures using a cross-isotropic, non-linear, elasto-plastic material model implemented in the finite element software ABAQUS. One IBP section was analyzed, consisting of 3.5 inches of AC, 6 inches of unbound aggregate base, and 10 inches of cement-stabilized subbase for a total section thickness of 19.5 inches. The dimensions and material parameters were based on data Cortes (2010) collected from the existing test section in LaGrange, GA. This inverted pavement was evaluated against three conventional sections: an 18-inch section of 6 inches of AC and 12 inches of base, a 22-inch section consisting of 10 inches of AC and 12 inches of base, and a 30-inch section of 18 inches of AC and 12 inches of aggregate base (Cortes 2010). Traffic loading was modeled as a static 80-psi load over a circular area with a radius of 6 inches. With a contact area of approximately 112 square inches and imparting a force of approximately 9,000 pounds, this loading was selected to simulate one side of the axle in an 18,000-pound ESAL (Cortes 2010). Cortes (2010) found the maximum vertical compressive stress in the subgrade was lower in the IBP section than in the conventional sections, indicating that inverted pavement is less likely to fail in rutting when compared to conventional designs with comparable or greater total thickness. This study set the stage for future inverted pavement modeling efforts, providing the necessary foundation to investigate different IBP dimension models.

Papadopoulos (2014) continued this line of research to examine the effects of various design parameters upon the performance of inverted pavement. Using a three-dimensional finite element model in ABAQUS, he explored the impacts of the thickness of the surface, base course, and subbase layers. Two inverted and eight conventional sections, each with unique layer dimensions, were tested with the same simulated static load used by Cortes (2010) as a simulated ESAL (Papadopoulos 2014). Papadopoulos (2014) found that decreasing the thickness of the surface layer of AC can result in that layer distributing stress as a membrane instead of a beam. An idealized beam distributes stress as shown previously in Figure 2.2 (a), with a zone of compression above the neutral axis and a zone of tension below the neutral axis. A membrane, however, experiences tensile stress on both the top and bottom of the layer. Papadopoulos's (2014) modeling showed that in some cases, the AC layers that behaved as a membrane experienced lower maximum tensile stress than the AC layers that behaved as a beam. According to the empirical damage accumulation functions used by the MEPDG (AASHTO 2020), tensile strain in the AC layer is correlated to damage accumulation (fatigue). Lower maximum tensile strain would therefore result in less load-related surface distress. If inverted pavements can make use of this transition from beam to membrane behavior, load cracking of flexible pavements may be decreased, possibly extending pavement service life. It is still not clear, however, if this effect ultimately improves performance of the surface layer: Papadopoulos (2014) found that the maximum tensile stress in the membrane-like layers was at the top of the layer, near the edge of the load. These layers also experienced tension at the bottom of the layer. This combination of tension at the top and bottom of the AC layer indicates shear, which may

result in a different form of load-related distress (Papadopoulos 2014). These shear distresses will likely be exacerbated by shear forces caused by acceleration and braking (Papadopoulos 2014).

Papadopoulos's modeling efforts also revealed two notable characteristics of the stress distribution of inverted pavements: Lower vertical stress was found in the aggregate base layers of conventional sections, indicating that the unbound base of inverted sections makes greater contributions towards carrying loads and distributing stress (Papadopoulos 2014). Additionally, tensile stresses were reduced in both the AC and cement-stabilized subbase when the thickness of the cement-stabilized subbase was increased (Papadopoulos & Santamarina 2014). This highlights the impact of the stiff subbase layer on the neutral axis and the subsequent performance of the holistic pavement structure, in addition to its role in dissipating stress before it reaches the subgrade.

Sha et al. (2020) conducted research with a similar purpose to Papadopoulos, focused on optimizing the structural design of inverted pavements with the help of a three-dimensional finite element model. Sha et al. (2020) constructed four IBP laboratory test sections with varying layer thicknesses and AC stiffness to validate the moduli and stress-strain response models for each material used in the model. The thickness of the asphalt concrete surface was specifically chosen to be either 2 inches or 4 inches, as Papadopoulos & Santamarina (2015) indicated that the transition from a beam to a membrane response occurs at a thickness of approximately 2 to 3 inches. The total thickness of the laboratory test sections ranged from approximately 17.7 to 21.7 inches (Sha et al. 2020). Furthermore, a single partial-depth transverse crack was sawn in the

cement-treated subbase of each test section to simulate damage accumulation in that layer (Sha et al. 2020). The physical testing program was twofold: First, FWD tests evaluated the stiffness of each layer (Sha et al. 2020). The test sections then received traffic loading from a heavy vehicle simulator; while the tire configuration was not noted, Sha et al. (2020) reported the test sections received 300,000 applications of an approximately 11-kip load traveling at approximately 6 miles per hour. Information collected from the strain gauges during traffic loading was used to inform the AC response model, and FWD tests were conducted once again to calibrate a model for modulus degradation (Sha et al. 2020).

The numerical model used by Sha et al. (2020) to examine the performance and optimize the design of inverted pavements simulated 6.5-foot by 5-foot test sections in a three-dimensional finite element model. An approximately 100 psi load was applied over a 36-square-inch rectangular area, imparting approximately 3.6 kips. Sha et al. (2020) evaluated each section using two critical responses: the maximum principal strain at the bottom of the AC layer and the maximum shear strain at a constant depth below the surface, which was either within or at the bottom edge of the AC layer, depending on the layer thickness. 28 different sections of inverted pavement with unique combinations of layer thicknesses and stiffnesses were tested by Sha et al. (2020). They found that the designs that exhibited the lowest critical strains, indicating superior resistance to fatigue deformation, had thinner and stiffer layers of AC (approximately 2 inches) and base course (approximately 4 inches) combined with thick layers of cement-stabilized subbase (approximately 16 inches) of moderate stiffness. Sha et al. (2020) also reported that

increasing the stiffness of the cement-stabilized subbase beyond typical levels had minimal impact upon the two strain responses analyzed.

The most recent modeling studies have corroborated results from the research previously mentioned. Wang & Dong (2020) investigated the mechanical responses of inverted pavement, full-depth asphalt concrete pavement, and flexible pavement with cement-stabilized base using Bitumen Stress Analysis in Roads software. The inverted section analyzed, however, differed significantly from the recommendations of Papadopoulos (2014) and Sha et al. (2020). It consisted of a 26-inch cross section with 9 inches of AC, 5 inches of base course, and 12 inches of cement-treated subbase. Wang & Dong (2020) found the maximum tensile stress of this section occurred within the base course layer, indicating that the neutral axis of bending was in the pessimal position to take advantage of the material properties of each layer. The test sections modeled by Wang & Dong (2020) were then constructed on a roadway in Changsha, China. Benkelman beam deflection tests were conducted; the stabilized section of conventional pavement had the lowest average deflection, and the inverted section had an average deflection marginally larger, but only 45% of the average deflection of the full-depth asphalt pavement (Wang & Dong 2020). Therefore, while the modeling and field testing efforts of Wang & Dong did not indicate superior performance by inverted pavement, their results should not be considered an assessment of IBP at its best.

Finally, Jiang et al. (2022) conducted three-dimensional finite element modeling in concert with their testing of the Knoxville, TN inverted test section. They used a stress-dependent response model for unbound layers and applied a dynamic load to simulated test sections with the same dimensions as those built in Knoxville (Jiang et al.

2022). Their modeling resulted in similar conclusions to Cortes (2010) and Papadopoulos (2014): Namely, inverted pavement with total thickness equal to conventional sections demonstrated lower tensile stress in the AC layer and compressive strain in the subgrade, indicating IBP would outperform the conventional pavement in fatigue and rutting (Jiang et al. 2022).

There are notable limitations to the inverted pavement modeling efforts conducted thus far: First, the static loading used by nearly all models does not account for the rotation of principal stresses that occurs when a horizontally traveling wheel applies loads to pavement. The inherently anisotropic unbound aggregate base layer deforms differently in real life than predicted by the models which used a horizontally stationary load. Second, these studies do not consider the fatigue behavior of the constituent materials of inverted pavement. Asphalt concrete, unbound aggregate, and cement-stabilized aggregate all accumulate plastic deformation differently. While certain responses measured in the aforementioned research may indicate the degree to which each layer accumulates damage, no model actually predicted the damage accumulated. Modern pavement models predict and evaluate performance by estimating the amount of damage a simulated pavement would accumulate using a function that correlates mechanical responses to the damages they create. Finally, the effects of environmental exposure were largely ignored in previous modeling studies: Asphalt concrete is a viscoelastic material; its stiffness varies with temperature. Additionally, unbound aggregate responds very differently to loading when it contains moisture, displaying unique responses if it is saturated, unsaturated, or containing frost. Previous modeling efforts did not address the effects of temperature and moisture on its response models.

These last two gaps will be broached in Chapter 4 of this thesis, as the modeling software used in Chapter 4 utilizes an empirical transfer function to predict the accumulation of pavement distresses based on mechanistic calculations of strain in the pavement structure; that calculation is varied according to climatic effects.

2.5 CONCLUSIONS

Efforts to evaluate inverted pavement dating back to the mid-twentieth century have used both test sections and numerical modeling to conclude that inverted pavement of equal total thickness can outperform conventional pavement in terms of resistance to rutting and fatigue. The first goal of this thesis is to examine the long-term performance of IBP in the United States. While numerous examples of the performance of inverted pavements have been provided in this chapter, the field data that measured IBP at its most advanced age is from an inverted pavement section at 15 years of age (Morgan County), which only consisted of a surface distress assessment and did not include investigation of the structural performance of each layer in the structure. The Department of Defense (2016) recommends flexible pavement should be designed for a life of 25 years; other agencies specify similar lifespans. There has not yet been a comprehensive evaluation of an inverted pavement at or near the end of its life. This thesis will broach that gap by evaluating an inverted pavement section at an advanced age. Furthermore, inverted pavements have been historically compared to conventional pavements of comparable thickness. Vaughan (2018) reported that in these cases, inverted pavement can be constructed at a lower cost, but no study has attempted to maximize the economy of inverted pavements while meeting the required performance. Finally, field sections and

modeling efforts have provided limited insight into the performance of IBP in varying climates. Most field sections have been constructed in similarly warm, wet climates (see Appendix A), and modeling studies have mostly ignored climatic effects on pavement performance. This study will aim to provide further understanding by modeling IBP with more economical cross sections while considering the impacts of temperature and moisture.

The second objective of this research is to investigate the suitability of inverted pavement designs for airfields. There is no known use of IBP on actively trafficked airports, and Grau (1973) and Costigan (1984) are the only researchers to apply simulated aircraft loading to inverted test sections. While those two studies have provided some insight, the test sections evaluated did not have optimal dimensions or materials, according to the latest recommendations for IBP provided by Papadopoulos and Sha. Modeling studies to date have only used loads and contact stresses comparable to automobile traffic. Most used loads on the order of 9 kips and contact stresses on the order of 100 psi. A C-17 cargo aircraft applies approximately 269 kips and 142 psi, while an F-15E fighter aircraft applies approximately 81 kips and 305 psi (IIT Corp 2015). Chapter 4 of this thesis will therefore focus its modeling on inverted sections designed for aircraft loading according to state-of-the-art IBP design recommendations and evaluate their performance under simulated airplane loading.

3. EVALUATION OF INVERTED PAVEMENT TEST SECTIONS

3.1 METHODOLOGY

The two test sections of inverted base pavement (IBP) in Georgia previously mentioned were further evaluated in this research. This section details the testing programs conducted at both the Morgan County and LaGrange sites.

3.1.1 FALLING WEIGHT DEFLECTOMETER

The falling weight deflectometer (FWD) is a tool used to measure the structural condition of pavement and characterize the stiffness of its layers. The FWD applies a known load in the form of a falling weight, and surface deflection is measured using several geophones at known radial distances from the point of load application. The surface deflection at the point of load application, commonly referred to as the D_0, is the maximum deflection measured by the FWD (FHWA 2017a). It can be used to holistically evaluate the stiffness and load-carrying capability of a pavement structure: With the load kept constant, a stiffer structure will deform less than a less stiff structure. The plot of radial deflections, known as the deflection basin, helps interpret the stiffness of individual pavement layers using a process known as "moduli backcalculation" (FHWA 2017a). An idealized deflection basin is shown in Figure 3.1.

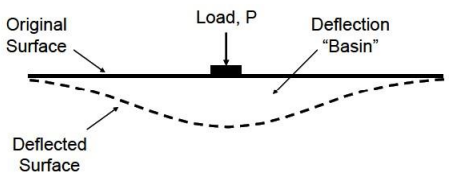

Figure 3.1 Idealized FWD deflection basin. Figure from FHWA (2017a)

The basic process of estimating layer moduli using FWD data (often referred to as "backcalculation") is as follows: First, the number and thickness of layers in the pavement structures are either assumed or determined from construction history or in-situ testing (FHWA 2017a). Next, a stress distribution pattern through each layer is arbitrarily assumed, as shown in Figure 3.2. This key assumption allows analysis to consider surface deflection at a given radial distance to be caused only by the deflection of the layers under loading stress at that radial distance (FHWA 2017a). For instance, in the idealized FWD in Figure 3.2, the surface deflections measured by sensors 2 and 3 are considered to result from the deflection of the subgrade only, since that is the only layer under stress at that radial distance. Similarly, the surface deflection measured by sensor 1 is considered to result from the deflection of both the base course and the subgrade, and the surface deflection measured by sensor 0 is considered to include the deflection of every layer in the structure.

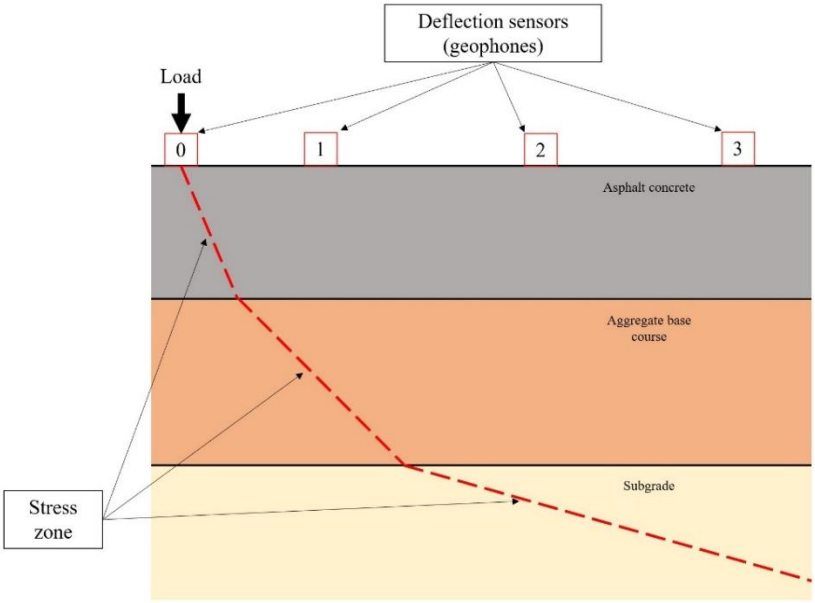

Figure 3.2 FWD stress distribution

The layer moduli are then estimated using an iterative process of forward calculation and error reduction that starts with the subgrade modulus: the moduli of all layers are assumed using initial or "seed" moduli, then the deflection of the subgrade layer and the resulting surface deflections are calculated for radial distances where surface deflection is based solely on subgrade deflection- this is the forward calculation (FHWA 2017a). The forward-calculated (estimated) surface deflections are compared with the measured surface deflections of the sensors considered to be within only the subgrade's zone of influence. The subgrade modulus is then varied, and the forward calculation is repeated until the forward-calculated surface deflections match the measured deflections (FHWA 2017a). Once a subgrade modulus is backcalculated, the process is repeated for the layer above the subgrade using the backcalculated subgrade modulus. This iterative process is repeated upwards for each layer until a modulus has been estimated for each layer (FHWA 2017a).

The main differences in the various backcalculation software programs available are the forward calculation method (how deflections are predicted based on the assumed moduli) and the error-reduction algorithm used to adjust moduli to reduce the difference between predicted and measured deflections (FHWA 2017a). There are also several important sources of error to note that do not result from operator or equipment error: First, the presence of a stiff layer such as bedrock or groundwater at depths less than approximately 39 feet can result in the moduli of upper pavement layers being incorrectly predicted (FHWA 2017a). This is because most forward calculation models assume the subgrade to be a semi-infinite halfspace, but bedrock or a groundwater table provides a sharp line of contrast within the subgrade (FHWA 2017a). Second, the moduli of

pavement materials are highly dependent upon temperature and moisture conditions (FHWA 2017a). Asphalt concrete (AC) is a viscoelastic material; its stiffness decreases with increasing temperature. The stiffness of soil and other unbound materials varies with moisture, and it exhibits different behavior if unsaturated or saturated. The conditions of the materials at the time of testing therefore have considerable impact upon the estimated moduli. Finally, many forward calculation models assume each layer to be homogenous. If discontinuities are present in a layer, such as cracks in the AC surface, they will violate the assumption of homogeneity, resulting in a difference between the response of the model versus the test subject (FHWA 2017a).

The FWD testing in this research was conducted at both the Morgan County, GA and LaGrange, GA test sections by the Georgia Department of Transportation (GDOT) Office of Materials and Testing - Pavement Management Unit. They used a Dynatest FastFWD with a load plate with a standard diameter of 300 millimeters (approximately 11.8 inches) and geophones at radial distances of 0, 8, 12, 18, 24, 36, 48, 60, and 72 inches. Testing was intended to be conducted at every 100-foot station, but not every test was performed exactly at that location. If surface distress was present at the planned testing location, the FWD was moved several feet to a location without cracks. As recommended by the FHWA (2017a), two seating drops of 6 kips were performed at each testing location to reduce erroneous movement of deflection sensors on rough pavement. Four drops were then conducted at each location with target loads of 6, 9, 12, and 14 kips. Deflections were measured with the accompanying geophones, while surface and air temperatures were measured with thermometers integrated into the FWD apparatus.

The location of each drop was measured using a Global Positioning System housed in the truck that towed the FWD.

Backcalculation of layer moduli was conducted using ELMOD 6.1.89 software produced by Dynatest. This program allows for varying methods of forward calculation and backcalculation: In this research, both the finite element method (FEM) and linear elastic theory (LET) methods of forward calculation were used. Both methods calculate responses using a static loading model. FEM allows for nonlinear analysis of stress-dependent materials but does not allow for an analysis that includes a stiff layer (Dynatest 2019). LET assumes layers are homogeneous and produce linear elastic responses to stress. The LET method also allows for the inclusion of a stiff layer in analysis (Dynatest 2019). An important limitation of the LET method, however, is its inability to account for nonlinear stress-dependent materials. When loaded by the FWD, materials such as natural soil and crushed stone will experience different principal stresses at different radial distances from the load. The stiffness of these materials will therefore vary with radial distance. The LET option, however, assumes the stiffness of materials is not stress-dependent and therefore will not vary with radial distance. There is therefore inherent bias in these backcalculation methods, which likely under-predicts the moduli of unbound layers far from the surface (where principal stresses are low) and over-predicts the moduli of unbound layers very near to the surface (where principal stresses are high).

Similar backcalculation procedures were used for all of the pavement tested in this study, with key differences noted below. The Poisson's ratio of each material was assumed for each material based on the recommendations of the FHWA (2017b): 0.35 for both AC and unbound materials, and 0.25 for cement-stabilized aggregate. Seed moduli

were not required to be input by the methods used in ELMOD, and they were not used as backcalculation programs converge to different solutions (modulus estimates) for different seed moduli (FHWA 2017a). A parametric study was conducted to assess which options within ELMOD reduce the error between the calculated and measured deflections, and therefore provide the most accurate modulus estimates. Error was measured as is typical in FWD analysis, via percent root mean square error (RMSE) (FHWA 2017b) according to Equation 1:

$$Percent\ RMSE = 100 \times \sqrt{\frac{1}{N}\sum_{i=1}^{N}\left(\frac{c_i - m_i}{m_i}\right)^2} \quad (1)$$

where N is the number of deflection sensors, c_i is the calculated deflection at sensor i, and m_i is the measured deflection at that sensor. For each alternative considered, the average percent RMSE was calculated as the arithmetic mean of the percent RMSE for each drop in a given test section. The alternative with the lowest average percent RMSE was selected in each case. Both the inbound and outbound lanes of the Morgan County test section were used as the test case to determine which of the following basic ELMOD options should be used in analysis.

ELMOD offers several options for the algorithm used to reduce error and converge upon the most accurate estimated modulus: the absolute difference between calculated and measured deflections can be minimized, the percent difference can be minimized, or an alternating method (Dynatest 2019). The alternating method first conducts backcalculation while minimizing the absolute differences, then backcalculates again using the resulting parameters (moduli, nonlinearity coefficients, and depth to stiff

layer) but minimizes the percent differences, and then repeats the backcalculation a third time while minimizing the absolute difference. It was found that the alternating method resulted in the lowest average percent RMSE. When utilizing the FEM forward calculation method, ELMOD also allows users to choose between modeling each material as linear or nonlinear. Modeling all materials as nonlinear provided the lowest average percent RMSE when using the FEM method.

With these basic options determined, both test sections were analyzed with greater granularity. The Morgan County site was analyzed according to the design of each section: the conventional, South African inverted, and Georgia inverted sections were evaluated separately. For the LaGrange test section, potential problem areas were identified in each test section by the surface distress results from Frost (2017). In the westbound lane, the section from station 12+00 to 25+00 was evaluated as a control section due to the low amount of distress noted by Frost (2017), whereas the westbound section from station 30+00 to 33+00 was evaluated separately due to the higher distress reported. Similarly, the eastbound sections of station 1+00 to 3+00 and 16+00 to 20+00 had more surface distress and the section from 26+00 to 33+00 had less, and thus were analyzed separately (Frost 2017). These sections from both sites were all evaluated for three criteria: the forward calculation method (FEM vs LET), inclusion of a stiff layer (or not) in analysis (which requires the use of LET forward calculation), and fixing an AC modulus to account for irregularities caused by surface distress. The exact combination of these three options used for each section will be noted later in this chapter along with the estimated layer moduli.

3.1.2 SURFACE DISTRESS

Measurement and analysis of pavement surface distress is a common method used to assess the condition and performance of a pavement structure. Many agencies responsible for pavement management have developed their own methods and criteria for evaluation. The Georgia Department of Transportation (GDOT) utilizes a method referred to as the pavement condition evaluation system (PACES), defined in Tsai et al. (2021). PACES uses a systematic inspection method to identify and rate surface distresses, resulting in an aggregated quantitative rating that indicates the prevalence and severity of the distresses present at the time of the survey (Tsai et al. 2021). The PACES manual establishes standard definitions for distresses and corresponding levels of severity. The rating is computed by aggregating the extent per segment length of each distress at each severity level. A corresponding deduction value is assigned for each distress extent and severity level, and these deduction values are subtracted from 100 to give the PACES rating (Tsai et al. 2021). Therefore, a PACES rating of 100 indicates a pavement without surface distress, and a lower value indicates a pavement with surface distress. The distress types identified by the PACES manual are rut depth, load cracking, block cracking, reflection cracking, patches and potholes, raveling, edge distress, bleeding/flushing, corrugations/pushing, and loss of section (Tsai et al. 2021). Tsai et al. (2021) prescribe methods for measurement and evaluation of severity for each distress type. The most prevalent distresses noted in this study were rutting, load cracking, and block cracking. Rutting is defined by the PACES manual as “longitudinal depressions that form under traffic in the wheelpaths and are greater than 20 feet long. Rutting is a permanent deformation of the wheelpaths caused by traffic loadings” (Tsai et al. 2021).

Load cracking refers to surface cracks caused by fatigue of the AC surface due to repeated loading (Tsai et al. 2021). It is only considered load cracking if it occurs in the wheelpaths (Tsai et al. 2021). Severity levels of load cracking are described by the illustrations in Figure 3.3. Block cracking, however, is caused by temperature cycling and shrinkage of AC- not by loading (Tsai et al. 2021). Typical block cracking is shown in Figure 3.4.

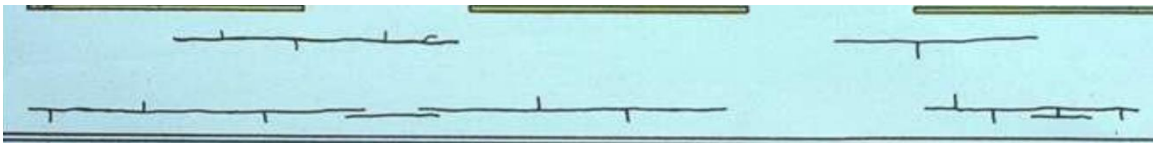

(a)

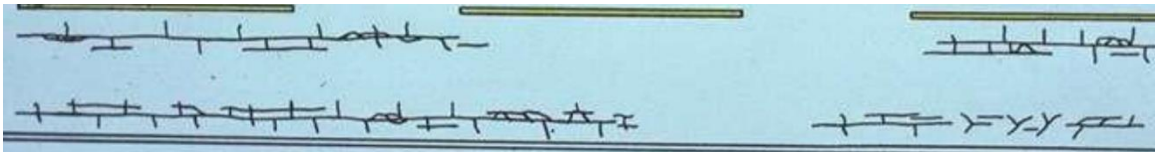

(b)

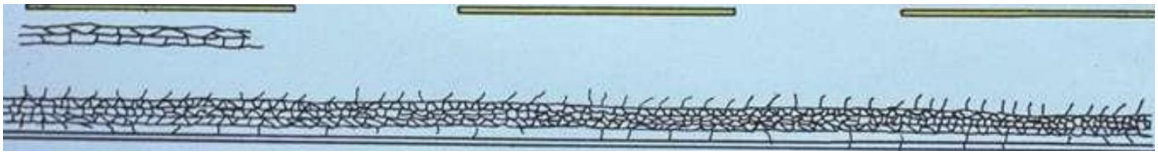

(c)

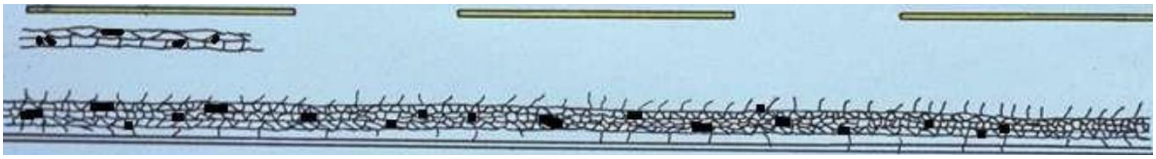

(d)

Figure 3.3 Load cracking severity levels (a) 1, (b) 2, (c) 3, and (d) 4.
Figures from Tsai et al. (2021)

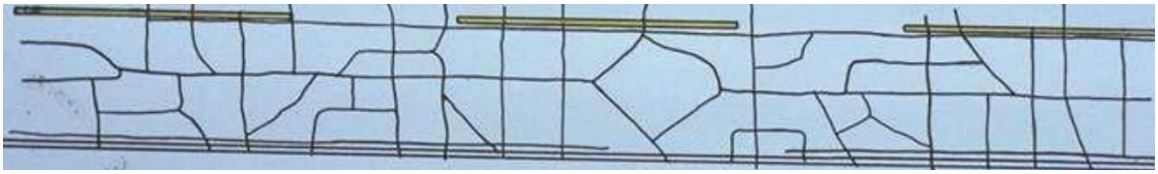

Figure 3.4 Block cracking. Figure from Tsai et al. (2021)

Data for the surface distress surveys discussed below were collected according to methods very similar to those described by Tsai et al. (2012) and Frost (2017). A laser imaging system mounted on a van was used to collect three-dimensional profiles of the pavement surface at driving speeds. These images allow for measurement of rutting depth and assessment of cracking. Laser imaging can be particularly helpful in detecting cracks that are not visible to the naked eye (Tsai et al. 2012). Cameras, global positioning equipment, and distance measurement equipment were also used to connect pavement profile images to the corresponding location on the test sections. Figure 3.5 shows the sensing vehicle used for the surveys. Six passes were conducted with the sensing vehicle. The images collected were inspected for each run, and the run with the fewest images missing data was used for measurement of rutting and cracking.

Figure 3.5 Surface distress survey equipment

The pavement profile images depicted 5-meter segments of the pavement. These images were input into a commercial pavement distress identification software, LcmsRoadInspect (Pavemetrics Systems 2022). The software measured rut depth in 1-

meter intervals. The rut depth was averaged for each wheel path in each image. Since the software could not accurately detect fine cracks that may have been outside its resolution or obscured by dust on the pavement, the range images without crack detection were used to visually assess the cracking according to the PACES manual. The predominant type and severity of cracking in each 5-meter image were recorded. Crack extent by severity, as well as maximum average rut depth, were aggregated for 100-foot segments to produce a PACES rating for each segment as described in Tsai et al. (2021). Sections 3.2.3 and 3.3.3 discuss the results of the distress survey for each test section. Figure 3.6 shows sample images for rutting and cracking evaluation.

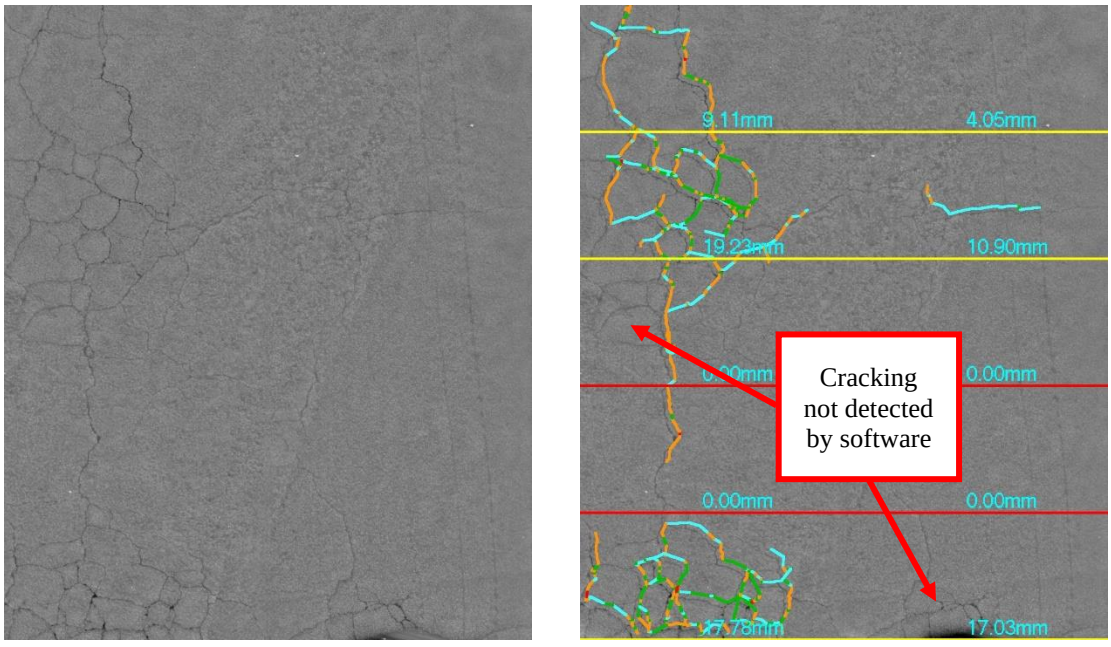

(a) (b)

Figure 3.6 Sample pavement profile images (a) before automatic distress detection and (b) after automatic crack detection

3.2 MORGAN COUNTY TEST SECTION

3.2.1 TEST SECTION HISTORY

The Morgan County test section was constructed at a quarry access road in Morgan County, GA in 2001 (Cortes 2010). The 1,800-foot roadway is composed of three different pavement designs: The first 1,000 feet of the test section (from Station 0+00 to 10+00) is the control section, designed in the manner of conventional flexible pavement (Terrell 2002). The conventional section has a 3-inch AC surface, 8 inches of GDOT graded aggregate base (GAB) as its base course, and 6 inches of "surge stone", a crushed stone with larger particle sizes than GAB, as its subbase (Terrell 2002). The next 400 feet (Station 10+00 to 14+00) of the Morgan County test section is an inverted pavement design known as "South African" inverted pavement, because the South African "slushing" method was used to compact its base layer (Terrell 2002). It consists of 3 inches of AC atop a 6-inch GDOT GAB base layer, resting on an 8-inch bound subbase composed of cement-stabilized GDOT GAB (Terrell 2002). The remaining 400 feet (Station 14+00 to 18+00) are known as the "Georgia" inverted pavement section, because the base course was compacted using standard GDOT methods instead of slushing (Terrell 2002). The Georgia IBP was constructed with the same layer dimensions as the South African IBP- the only difference was the method used to compact the base layer (Terrell 2002).

The climate in Morgan County, GA is warm and wet (see Appendix A for relevant climate data). Cortes (2010) noted that the test section has experienced an "uninterrupted high volume of truck traffic since construction." Traffic loads are typically normalized for comparison by converting the spectrum of measured axle weights to

equivalent 18,000-pound single axle loads (ESALs). The axle load spectrum of the Morgan County site was not measured, but an approximation of the number of ESALs sustained by the roadway can be produced using the sales tonnage measured by the quarry. The test section is the only roadway available to enter or exit the quarry, and every truck exiting the quarry with a load of material must be weighed at the scale house. Therefore, a very reasonable estimate of the traffic (number of passes) by truck type can be made using the total weight of material sold, the average load carried by truck type (single unit or multi-unit), and an estimate of the average traffic fraction by truck type. The number of passes by a single unit and a multi-unit truck are then multiplied by their respective ESAL design factor, given by GDOT (2022a), resulting in a good estimate of the number of ESALs caused by each pass. According to this method of approximation, the Morgan County test section has undergone approximately 230,000 ESALs during its lifetime. This figure should only be considered an estimate for context - the exact number of ESALs varies with the load and axle configuration of each individual truck. It should also be noted that the exact number of ESALs withstood by the outbound lane is greater than the inbound lane, as the axle loads of full trucks leaving the quarry are greater than those of empty trucks. Finally, this figure differs significantly from the estimate of ESALs reported by Lewis et al. (2012). They used a non-standard method to estimate ESALs: They divided the total sales tonnage by 18 kips, the standard load in one ESAL. This assumes that the load was evenly divided on all axles, which fails to account for the varying distribution of loads over multiple axles in a truck. If this method is used, the number of ESALs withstood by the Morgan County test section would be approximately 700,000.

Results are reported below in three different segments: Conventional, South African IBP, and Georgia IBP. Visual assessment during field testing confirmed the reports of Lewis et al. (2012) and Frost (2017) that the first several hundred feet of the conventional test section had experienced greater distress than the remaining portion of the section. This is due to the additional shear loading caused by trucks braking and turning as they enter or exit the roadway. The conventional test section is therefore split into two segments, where the first 300 feet of the conventional test section have been excluded from results in this chapter. Average values reported for the conventional test section include only those from Station 3+00 to 10+00 to provide an accurate comparison to the inverted sections.

3.2.2 FWD RESULTS & DISCUSSION

A program of FWD testing was conducted at the Morgan County test section as detailed in section 3.1.1. Maximum deflections for the 9-kip drop were recorded to measure the overall stiffness of each pavement design. Figure 3.7 plots these maximum deflections at each point measured and compares them with the maximum deflections measured in 2007, reported by Lewis et al. (2012). The average maximum deflection in the inbound lane was 20.38 mils for the conventional section (excluding the first 300 feet), 7.73 mils for the South African IBP section, and 7.12 mils for the Georgia IBP section. In the outbound lane, the average maximum deflection was 40.01 mils for the conventional section, 12.15 mils for the South African IBP, and 8.82 mils for the GA IBP. Average maximum deflections of inverted sections ranged from 22% to 35% of the average maximum deflection of the conventional section. The composite structure of the inverted sections was therefore stiffer than the conventional pavement. As might be

expected, the outbound lane had higher maximum deflections at nearly every station compared to the inbound lane. This is because the additional weight of the laden trucks caused greater fatigue damage. This difference in deflection between inbound and outbound lanes, however, was less for the IBP than the conventional pavement. Whereas the maximum deflection of the conventional section doubled in the outbound lane, the figure only grew by approximately 40% for the IBP section. Furthermore, maximum deflection increased from 2007 to 2022 by an average of 72% for the conventional pavement, but the increase for IBP designs ranged from negligible to 19%. This indicates that inverted pavement designs better resist the accumulation of structural damage and maintain their structural stiffness.

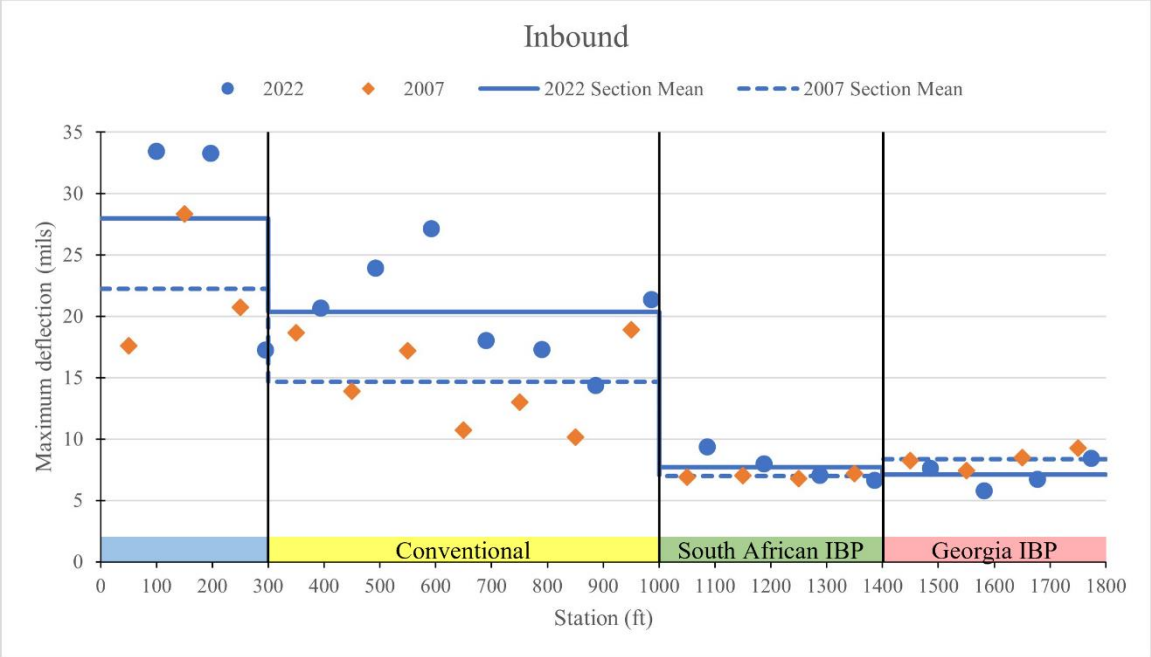

(a)

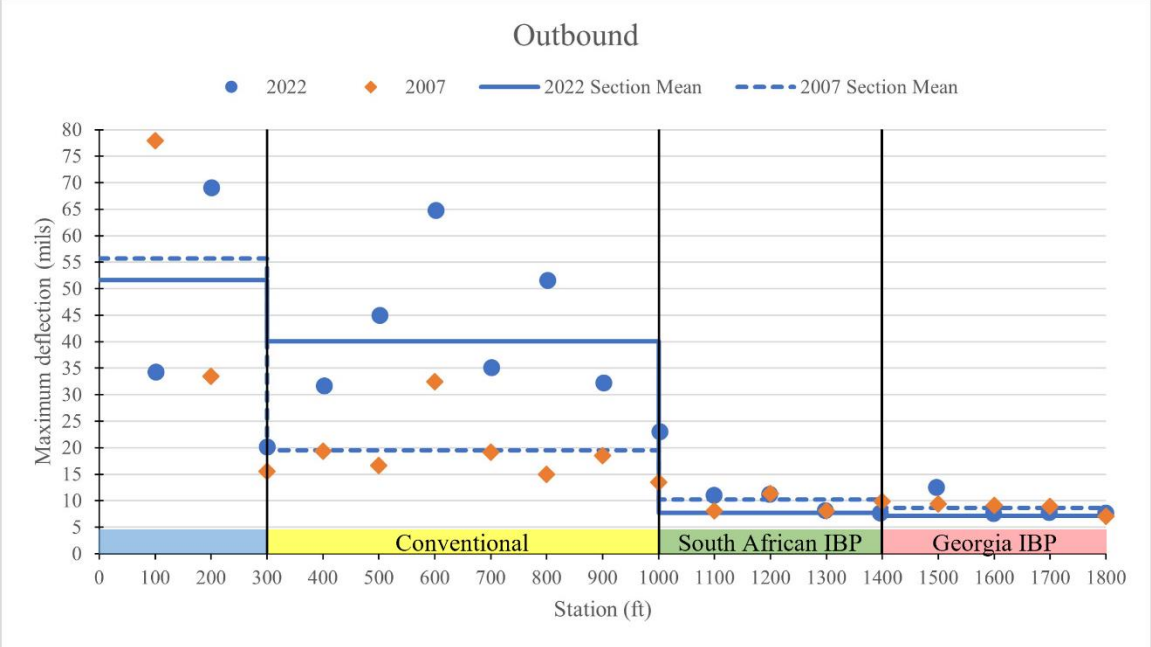

(b)

Figure 3.7 Maximum 9-kip FWD deflections at Morgan County test sections for (a) inbound and (b) outbound lanes. 2007 data from Lewis et al. (2012)

Backcalculation of layer moduli was conducted as noted in section 3.1.1. Varying options and methods in ELMOD were evaluated for each section on the basis of reducing the percent RMSE. Moduli were backcalculated for Morgan County site using the LET method in ELMOD with a stiff layer analysis and no fixed AC modulus. Moduli were estimated for the 9-kip and 14-kip drops at each station. 9 kips is a standard drop weight used in roadway analysis, and 14 kips (the heaviest drop conducted) is the closest load to aircraft traffic, a subject of interest in this study. Furthermore, varying drop weights allow for comparison of the stress-dependent moduli of unbound materials. Backcalculated moduli for each 9-kip drop are displayed in Figure 3.8.

Variability and outliers in the estimated layer moduli were accounted for by calculating the average moduli with outliers excluded. First, the average and standard deviation of each layer modulus were calculated for each section. The moduli that exceeded the average plus one standard deviation or were less than the average minus one standard deviation were considered outliers and excluded. The remaining moduli were then averaged and are reported in Table 3.1.

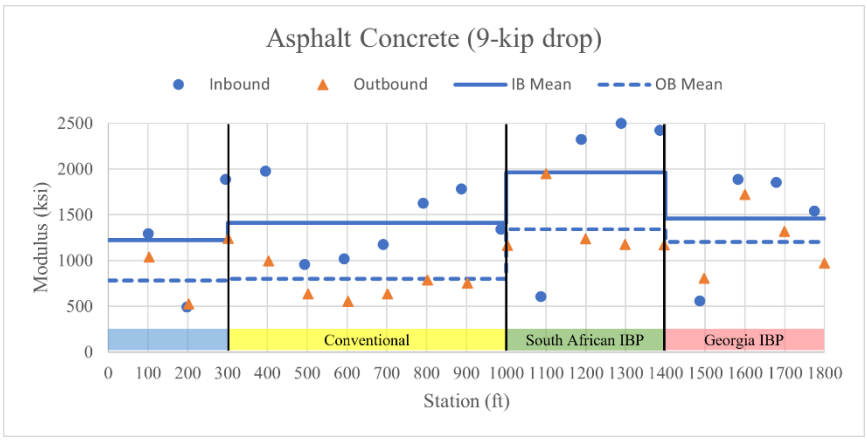

(a)

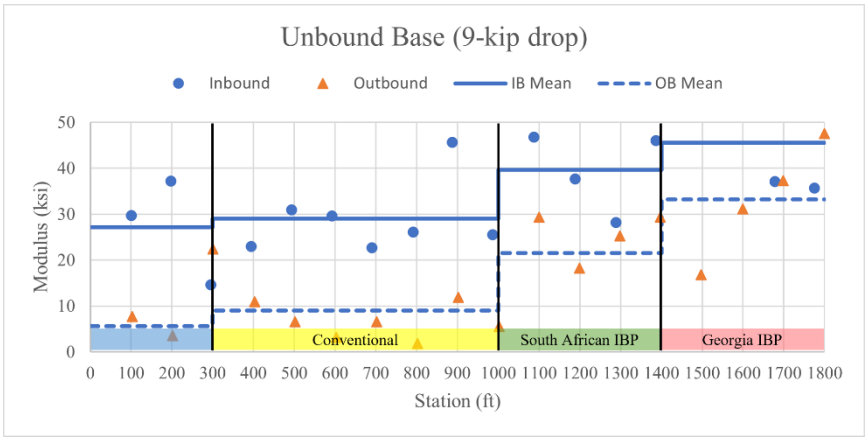

(b)

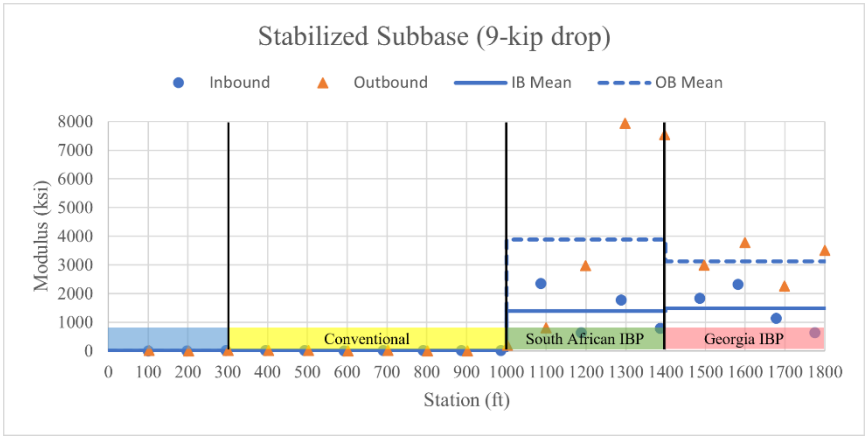

(c)

Figure 3.8 Moduli from 9-kip FWD deflections at Morgan County test sections for (a) asphalt concrete, (b) unbound base, and (c) stabilized subbase layers

Table 3.1 Morgan County backcalculated layer moduli

Target drop load: 9 kips								
Section	Outbound				Inbound			
	Avg modulus (ksi)			Avg % RMSE	Avg modulus (ksi)			Avg % RMSE
	AC	Base	Subbase		AC	Base	Subbase	
Conventional	761	8	4	6.06	1,481	26	6	2.11
South African IBP	1,186	26	3,769	2.91	2,413	44	1,067	4.56
Georgia IBP	1,031	34	3,421	4.48	1,759	42	1,487	4.36
Target drop load: 14 kips								
Section	Outbound				Inbound			
	Avg modulus (ksi)			Avg % RMSE	Avg modulus (ksi)			Avg % RMSE
	AC	Base	Subbase		AC	Base	Subbase	
Conventional	902	7	6	4.27	1,600	25	7	4.10
South African IBP	1,464	33	2,363	3.10	1,373	61	1,034	4.99
Georgia IBP	1,220	40	2,832	2.27	1,465	42	2314	4.91

The FHWA (2017b) suggested guidelines for RMSE based on backcalculation results from conventional pavements. They recommended that RMSE less than 1 percent provides "credible estimates," RMSE less than 2 percent is considered "reasonable," and RMSE greater than 3 percent is regarded as "questionable." Only some sections achieved acceptable average percent RMSE, and error varied considerably between drops. The thin (3-inch) AC layers may be the source of increased error: The FHWA (2017b) suggests that surface layers less than 3 inches thick will have "minimal influence on the surface deflection" due to their membrane-like deformation. Despite no change in inherent material stiffness, the thin AC layers do not deform in the manner predicted by the elastic response models used in forward calculation. This can result in elevated levels of error (FHWA 2017b). Moduli backcalculation resulted in a slightly lower average percent

RMSE for the inverted sections. It is hypothesized this is due to the lower level of surface distress noted in the IBP in 3.2.3, resulting in greater homogeneity and model conformance in those sections. As expected, some of the moduli of unbound base layers increased from the 9-kip drop to the 14-kip drop. This corresponds to the increase in stiffness resulting from increased principal stresses caused by a heavier load.

Another noticeable aspect of the backcalculated layer moduli from the Morgan County test section is the high AC modulus estimated at every section (approximately 1,400 ksi on average). The AC modulus of the IBP test sections tested by Sha et al. (2020) similarly ranged from 752 ksi to 1,276 ksi. The FHWA (2017b), however, reported that a typical initial (undamaged) modulus for AC is in the range of 300 to 600 ksi and a typical cracked AC modulus is in the range of 100 to 200 ksi. Some degree of cracking in the AC surface was noted in every section at Morgan County during testing. Furthermore, the maximum surface temperature during testing was 89 ºF and the average surface temperature during testing was 77 ºF. These two factors suggest that the backcalculated AC moduli would be less than a typical modulus for undamaged AC, but the moduli estimated here far exceed those reported by the FHWA. The FHWA (2017b) did note that "if the [asphalt concrete] layer is known to have severe alligator cracking and results in high backcalculated layer moduli, it is recommended that… the [AC] layer moduli be fixed at [100-200 ksi]." Fixing the AC modulus at 200 ksi during backcalculation, however, did not improve the percent RMSE or produce reasonable moduli estimates for other layers. The higher-than-expected AC moduli were not limited to the inverted sections, ruling out refraction along the stiff subbase and/or greater AC density as major sources of this error. The unreasonable estimate of the AC moduli is

likely due to the low thickness of the AC surface in every pavement structure at the Morgan County site. As previously noted, the deformation of thin AC layers is different from that predicted by forward calculation. This can result in unreasonably high backcalculated moduli (FHWA 2017b). This hypothesis corresponds to the data from Sha et al. (2020), who tested IBP sections with AC layers 2 inches and 4 inches thick. Further research, however, is recommended to ascertain a more reasonable estimate of the AC moduli of inverted pavements.

The moduli of the other layers in the Morgan County test section generally agree with standard values. The standard moduli range reported by the FHWA (2017b) is 10 to 150 ksi for unstabilized crushed stone or gravel and 300 to 3,000 ksi for cement-aggregate mixture. Furthermore, Sha et al. (2020) backcalculated unbound base moduli from 47 ksi to 52 ksi and stabilized subbase moduli from 1,823 ksi to 1,828 ksi. The backcalculated moduli from this study are comparable, with predictably higher moduli for the denser base layers of IBP sections. The higher base course moduli of inverted pavements further highlight the difference between conventional and inverted pavement: Despite comparable initial densities noted by Terrell (2002), the unbound layers of each design have accumulated damage differently. The IBP base layers have maintained greater stiffness, contributing to the structure's superior resistance to deformation.

3.2.3 SURFACE DISTRESS RESULTS & DISCUSSION

A survey and analysis of pavement surface distresses were performed on the Morgan County test section as described in 3.1.2. The only distresses noted were rutting, load cracking, and block cracking. Table 3.2 contains the average PACES rating for each test section (conventional, Georgia IBP, and South African IBP) and compares them to

the PACES ratings measured in 2016, as reported by Frost (2017). Figure 3.9 depicts the PACES rating at each 100-foot segment and compares them to the 2016 PACES ratings. Appendix B contains tabulated results of the survey for each 100-foot segment, as well as the calculated PACES ratings.

Table 3.2 Morgan County average PACES rating

Section	2022 PACES rating	2016 PACES rating (Frost 2017)	Difference
	Inbound		
Conventional	64	77	13
South African IBP	69	82	13
Georgia IBP	65	86	21
	Outbound		
Conventional	43	67	24
South African IBP	75	81	6
Georgia IBP	51	81	30

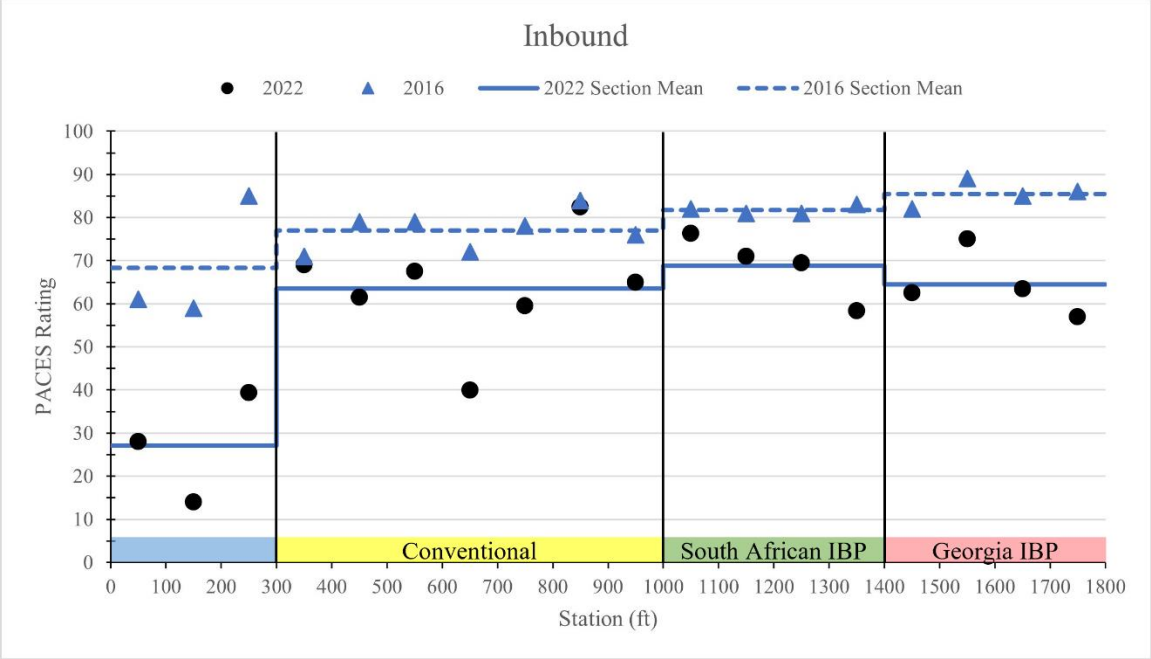

(a)

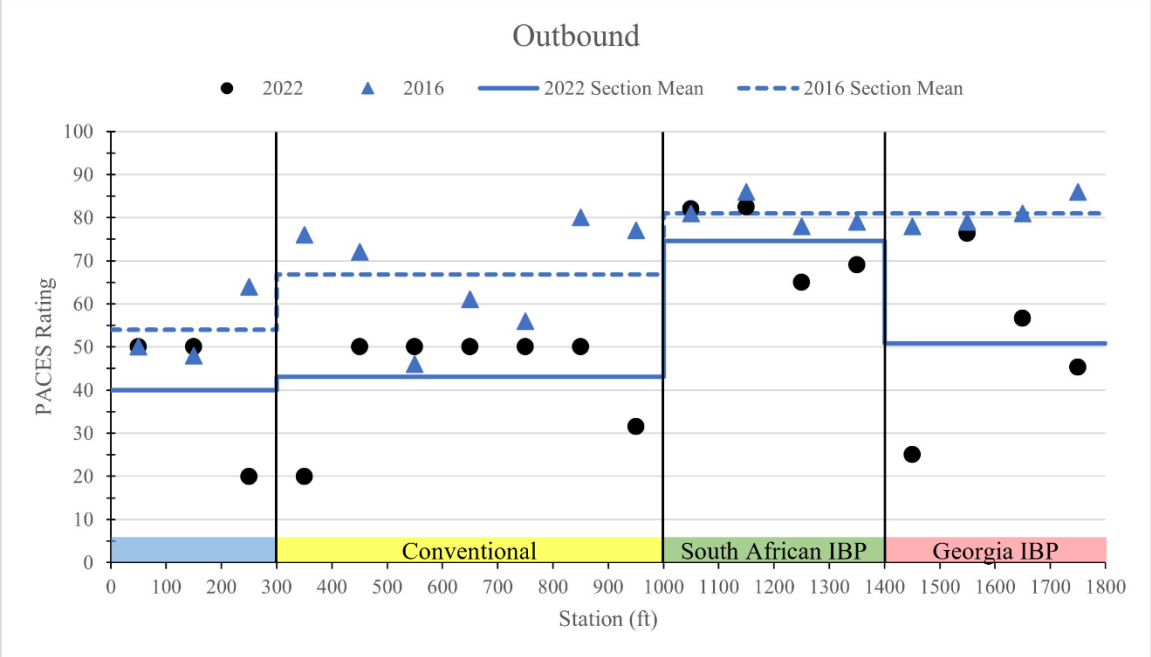

(b)

Figure 3.9 PACES rating by segment at Morgan County test sections for (a) inbound and (b) outbound lanes. 2016 data from Frost (2017)

The South African IBP section had the least amount of surface distress as indicated by its PACES rating. It also showed the smallest decrease in PACES rating from 2016, suggesting that it performed better and accumulated damage at a lesser rate during that six-year period. The Georgia IBP section had the next highest PACES rating, followed by the conventional section. This indicates that both inverted test sections outperformed the conventional section when measured at 21 years of age. The decrease in rating from 2016 was greatest for the Georgia IBP, followed by the conventional section, then the South African IBP. The greater rating and lesser decrease of the South African IBP indicates that the difference in compaction techniques may affect the long-term ability of the pavement structure to resist deformation and damage accumulation. The analysis below explores possible factors that may have contributed to the accelerated deterioration of the Georgia IBP section. Except for the South African inverted section, ratings were less in the outbound direction due to the increased loading of loaded trucks exiting the quarry. Finally, the decrease in rating from 2016 was greater for the outbound lane compared to the inbound lane. This implies that the loading in the inbound direction may be insufficient to provide an accurate comparison of the test sections.

The greatest rut depth of a segment was less than 0.5 inches. Table 3.3 reports the average rut depth of each test section in each wheelpath (left and right). Figure 3.10 graphs the rut depth in each wheelpath for each 100-foot segment. Figure 3.11 displays sample cross-section profiles produced from laser imaging in the outbound lane.

Table 3.3 Morgan County average rut depth

Section	2022		2016 from Frost (2017)	
	Average left rut depth (in)	Average right rut depth (in)	Average left rut depth (in)	Average right rut depth (in)
Inbound				
Conventional	0.002	0.008	0.000	0.000
South African IBP	0.000	0.190	0.000	0.000
Georgia IBP	0.002	0.003	0.000	0.016
Outbound				
Conventional	0.005	0.129	0.000	0.116
South African IBP	0.002	0.026	0.000	0.031
Georgia IBP	0.000	0.234	0.000	0.078

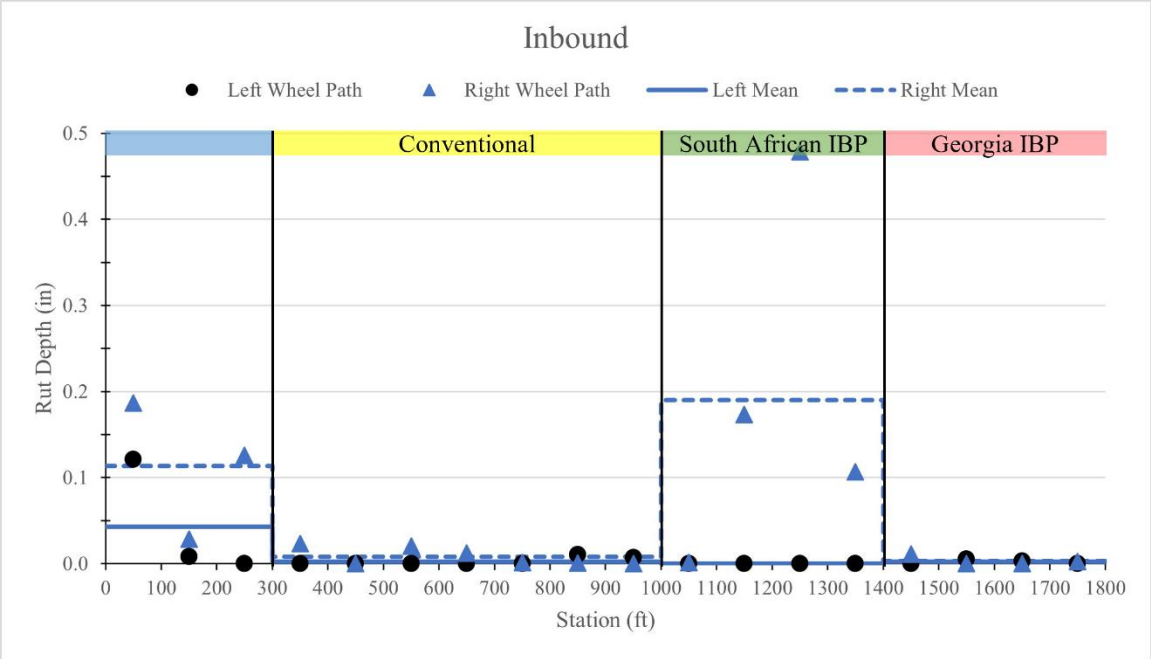

(a)

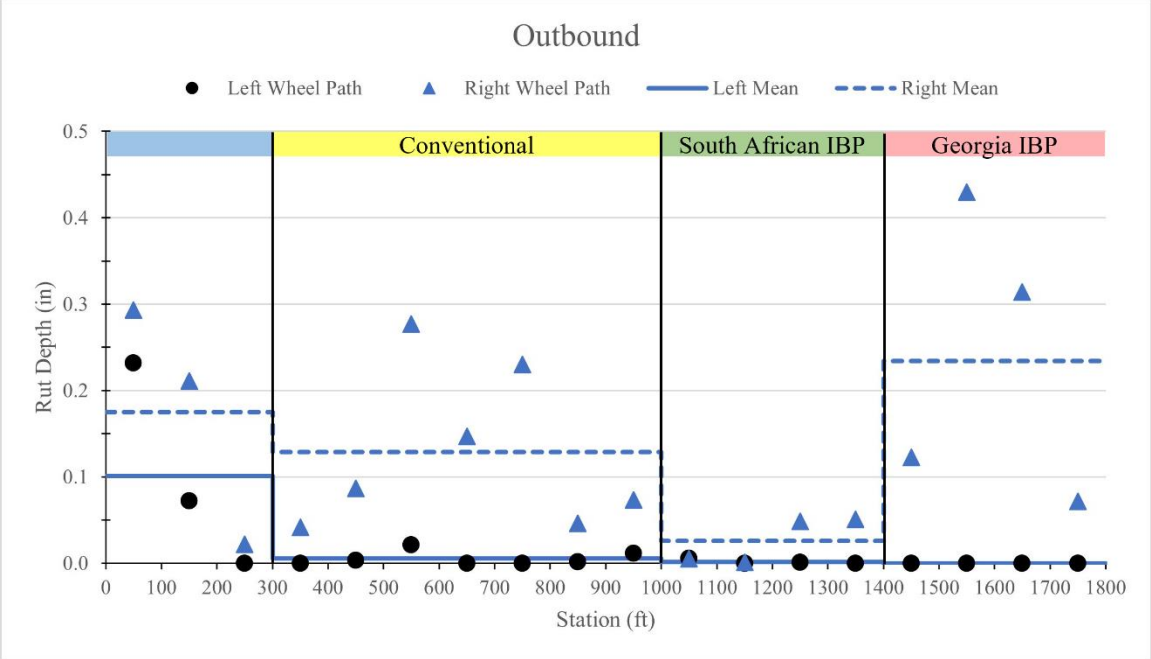

(b)

Figure 3.10 Rut depth by segment at Morgan County test sections for (a) inbound and (b) outbound lanes

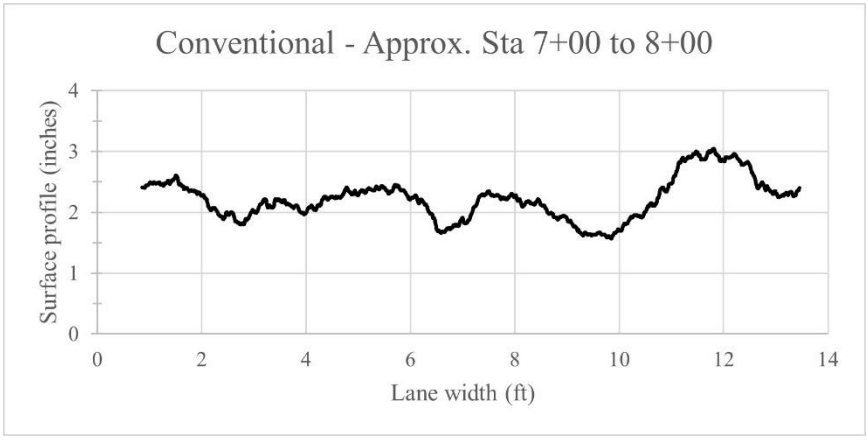

(a)

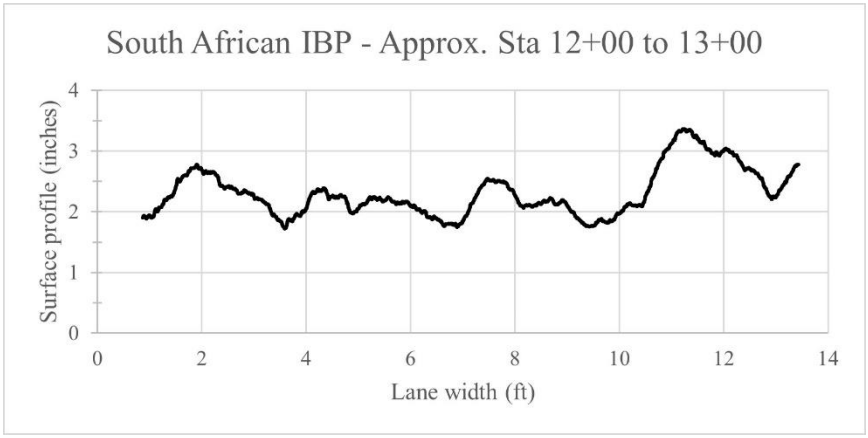

(b)

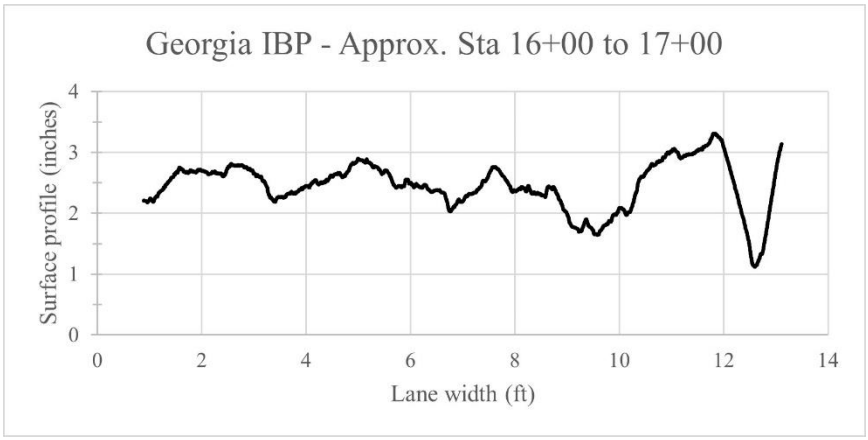

(c)

Figure 3.11 Sample surface profiles at Morgan County test sections in outbound lane for (a) conventional, (b) South African IBP, and (c) Georgia IBP sections

Close to zero rutting was measured in the left wheelpath of nearly the entire section. This is particularly notable in the outbound lane, where the right wheelpath exhibited a non-negligible amount of rutting. Right wheelpath rutting was particularly high near stations 0+00 to 3+00, likely contributing to low PACES ratings for these segments. Increased right wheelpath rutting throughout may be due to increased edge distress. Edge distress is defined by the PACES manual as cracking that occurs outside of the wheelpath, within one to two feet of the pavement edge (Tsai et al. 2021). It is often caused by poor compaction of pavement materials and/or water infiltration due to ponding at the edge of the paved lane. These factors lead to weakened unbound aggregate layers, perhaps contributing to greater rutting measured in the right wheelpath. It is also notable that the rutting in the outbound direction of the Georgia IBP section was more severe than the South African IBP. This likely contributed to the lesser PACES rating for the Georgia IBP in that direction. The opposite is true in the inbound direction. Minimal change in rut depth occurred between 2016 and 2022. Only the right wheelpath of the South African IBP in the inbound lane and the Georgia IBP in the outbound lane increased appreciably.

Cracking of some form was noted in every segment of the Morgan County test section. Figure 3.12 shows the extent, type, and severity of the cracking in each segment in the inbound direction. Figure 3.13 shows the same for the outbound direction. A higher severity level (i.e., Severity 4) indicates more severe distress. Figure 3.14 shows crack progression in a sample portion of the conventional test section.

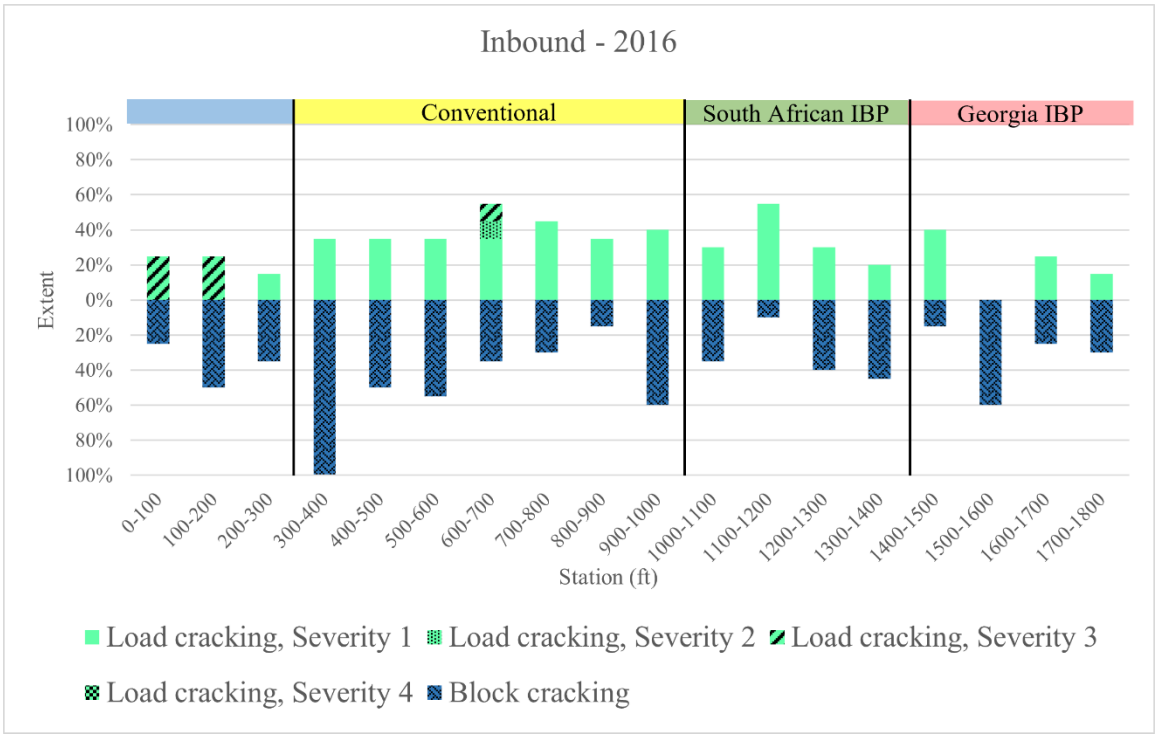

(a)

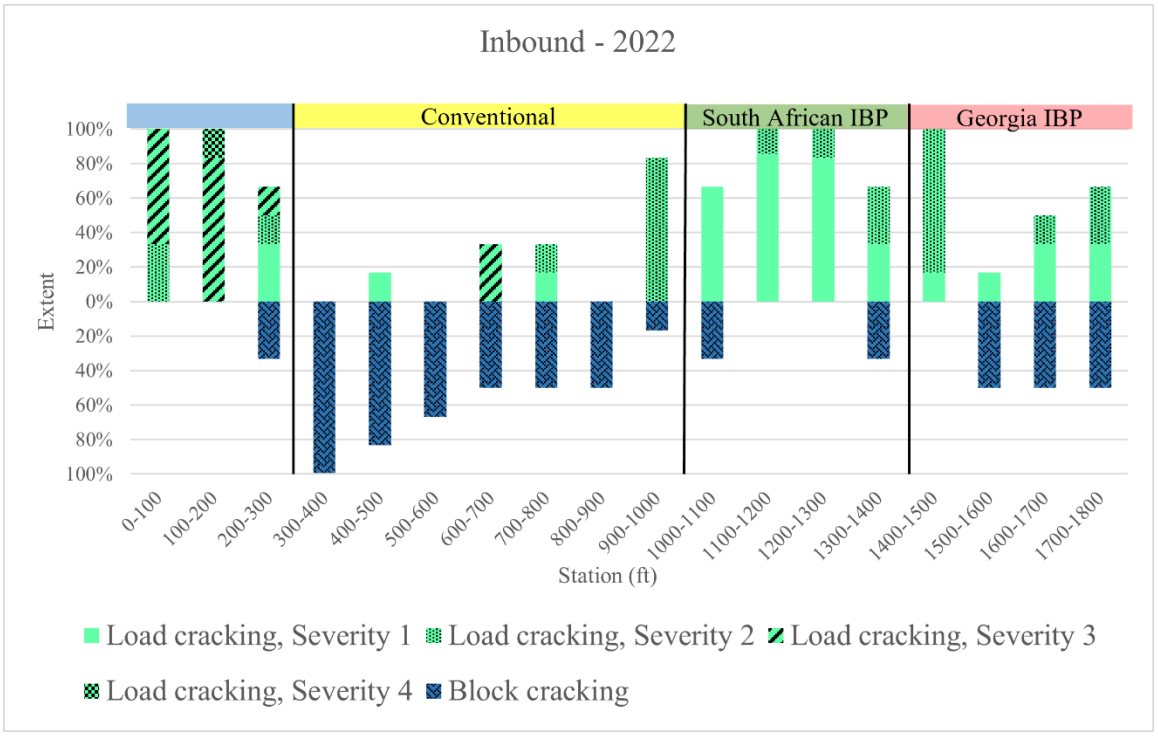

(b)

Figure 3.12 Crack type and severity at Morgan County test section inbound lane for (a) 2016 and (b) 2022. 2016 data from Frost (2017).

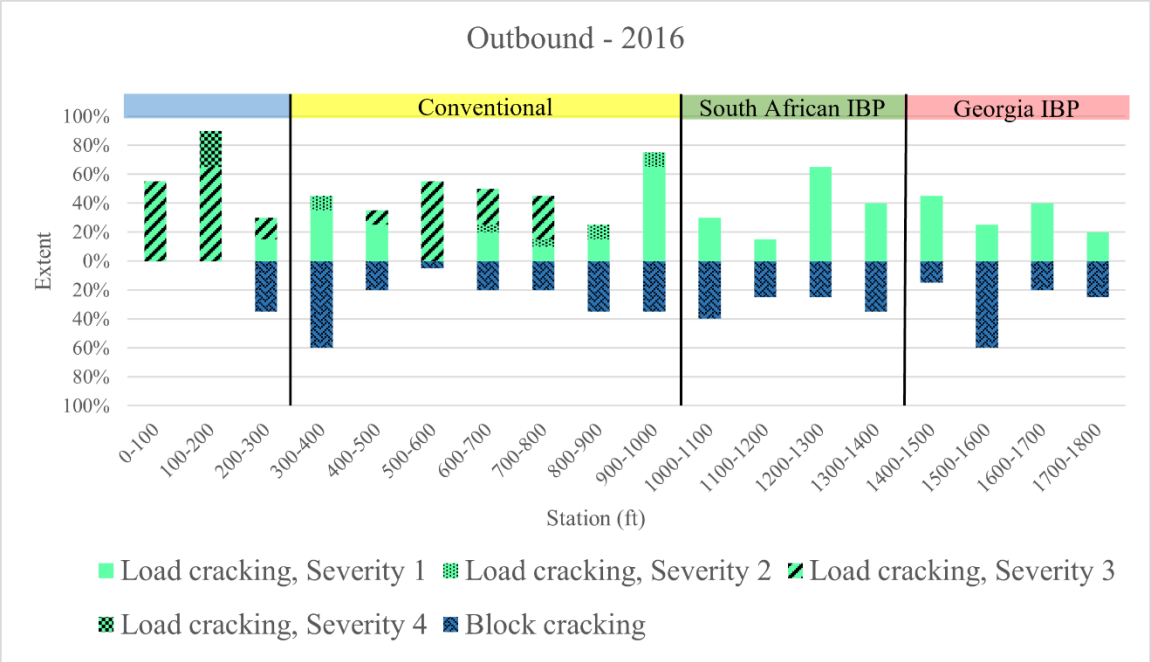

(a)

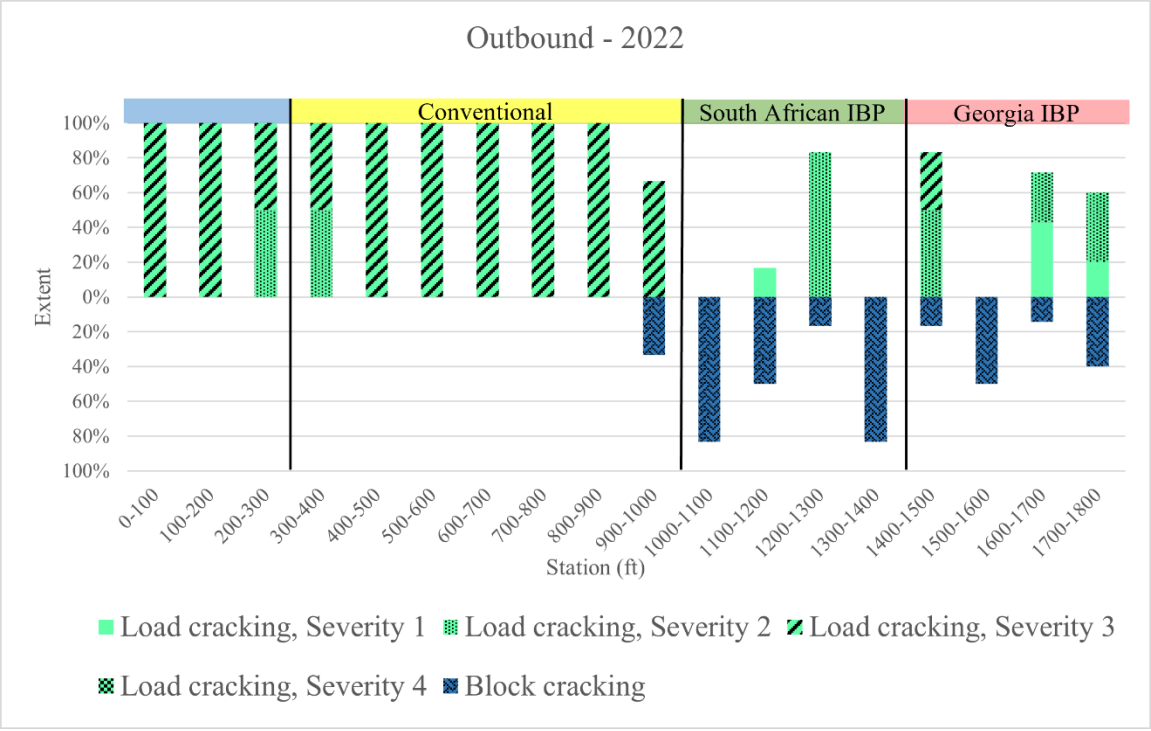

(b)

Figure 3.13 Crack type and severity at Morgan County test section outbound lane for (a) 2016 and (b) 2022. 2016 data from Frost (2017).

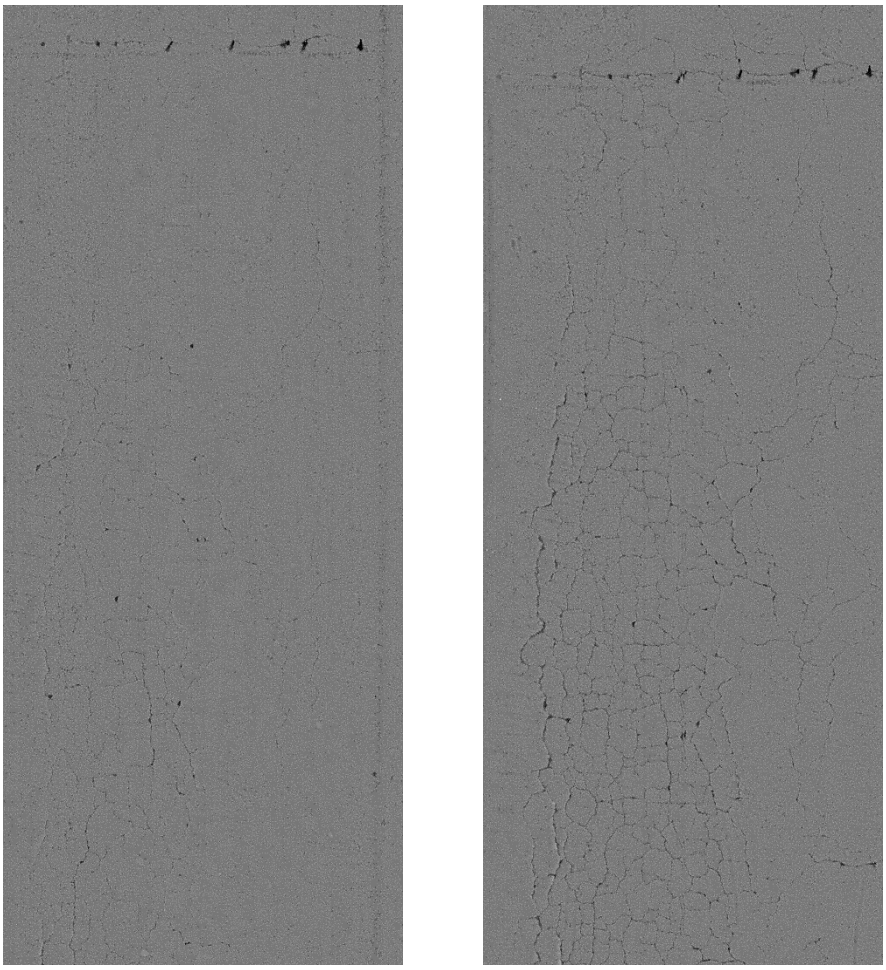

(a) (b)

Figure 3.14 Crack progression from (a) 2016 to (b) 2022 in outbound direction of conventional test section

In the inbound direction, the conventional section exhibited some high severity load cracking at the entrance, likely due to trucks turning onto the roadway at high speed, creating shear at the surface and damaging the AC. Otherwise, block cracking, which is caused by the thermal degradation of AC, was the predominant form of cracking in that section. The South African IBP showed low severity load cracking and some block cracking. The Georgia IBP section displayed a mix of low-to-medium severity load cracking, with some block cracking. In terms of load-related distress, the inverted

sections had similar extent of load cracking to the conventional section, but generally lower severity. Compared with the 2016 surface distress evaluation reported by Frost (2017), most of the inbound lane exhibited greater extent and severity of load cracking. The exception to this observation was the portion of the conventional test section from station 3+00 to station 10+00. In this segment, Frost (2017) noted a greater extent of load cracking than was observed in 2022, while a greater extent of block cracking was noted in 2022 than 2016.

In the outbound direction, the conventional section showed high severity load cracking nearly throughout, much greater than the extent and severity noted in 2016 by Frost (2017). The inverted sections showed a mix of medium severity load cracking and block cracking. The Georgia IBP section exhibited a greater extent and severity of load cracking than the South African IBP, contributing to its worse PACES rating. Additionally, the extent and severity of load cracking increased in the Georgia IBP, while no conclusive change occurred in the South African IBP. This may suggest that the South African method of "slushing" compaction can lead to a more durable inverted pavement structure over a long period of time. The inverted sections again outperformed the conventional section in the outbound direction. Load-related distresses were less prevalent and less severe in the IBP in 2022, and they accumulated less damage since 2016, indicating superior performance.

Evaluation of pavement surface distresses is not without its limitations. In this case, a more quantitative assessment of crack extent, type, and severity could not be conducted due to a lack of software resolution and dust on the roadway obscuring cracks. A visual rating was used instead, which is subjective by nature, as each evaluator will

interpret and execute the PACES manual slightly differently. These implicit biases are notable when comparing the 2016 assessment to the one conducted in this study. The human error is less impactful, however, when comparing sections evaluated by the same person. Overall, the current assessment of surface condition shows that the inverted pavement structures performed well during their life, with negligible rutting and minimal load-related cracking. Finally, the surface condition of the inverted pavement at Morgan County is better than that of a conventional section subject to the same conditions, indicating better holistic performance.

3.3 LAGRANGE TEST SECTION

3.3.1 TEST SECTION HISTORY

The LaGrange test section of inverted pavement was constructed on Pegasus Parkway in LaGrange, Georgia in 2009 (Cortes 2010). Pegasus Parkway is a two-lane industrial parkway that experiences a warm, wet climate (see Appendix A for relevant climate data). The eastern terminus of the test section is designated station 0+00, and the western end is designated station 34+00. The 3,400-foot test section is composed of just one IBP design: a 3.5-inch AC surface, 6 inches of GDOT GAB base course, and 10 inches of cement-stabilized base (Cortes 2010).

Traffic has not been measured directly on the test section, so the number of ESALs that have traveled on it must be approximated. Annual average daily traffic (AADT) data was collected by GDOT at a station on Pegasus Parkway, but approximately 1.5 miles westbound from the western end of the test section (GDOT 2022b). The percent traffic by truck type (single unit and combo-unit) was not collected

at this station, so another approximation was required. Percent traffic by truck type collected from two test stations in proximity to the test section with the same classification, “Minor Arterial (urban)”, were averaged to estimate the test section’s percent traffic by truck type (GDOT 2022b). AADT data was then converted to annual traffic, summed for the life of the test section, and multiplied by the estimated percent traffic by truck type, giving the truck traffic by type for the lifetime of the test section. These figures were multiplied by the ESAL design factors from GDOT (2022a), noted in section 3.2.1, to produce an estimate of ESALs. This method calculated that the LaGrange test section has withstood approximately 1.3 million ESALs.

3.3.2 FWD RESULTS & DISCUSSION

FWD testing was conducted at the LaGrange site as described in section 3.1.1. Maximum surface deflections for the 9-kip and 14-kip drops were recorded to evaluate the holistic structural stiffness of the inverted pavement design. Figure 3.15 plots these maximum deflections at each point measured, along with the mean maximum deflection and the mean maximum deflection plus and minus one standard deviation.

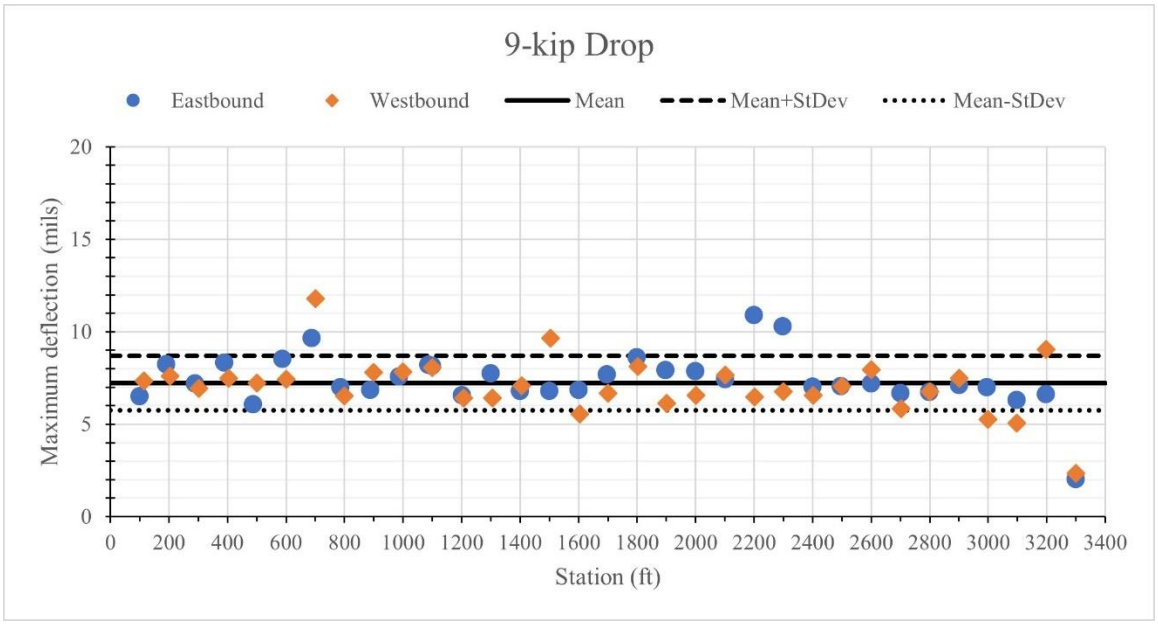

(a)

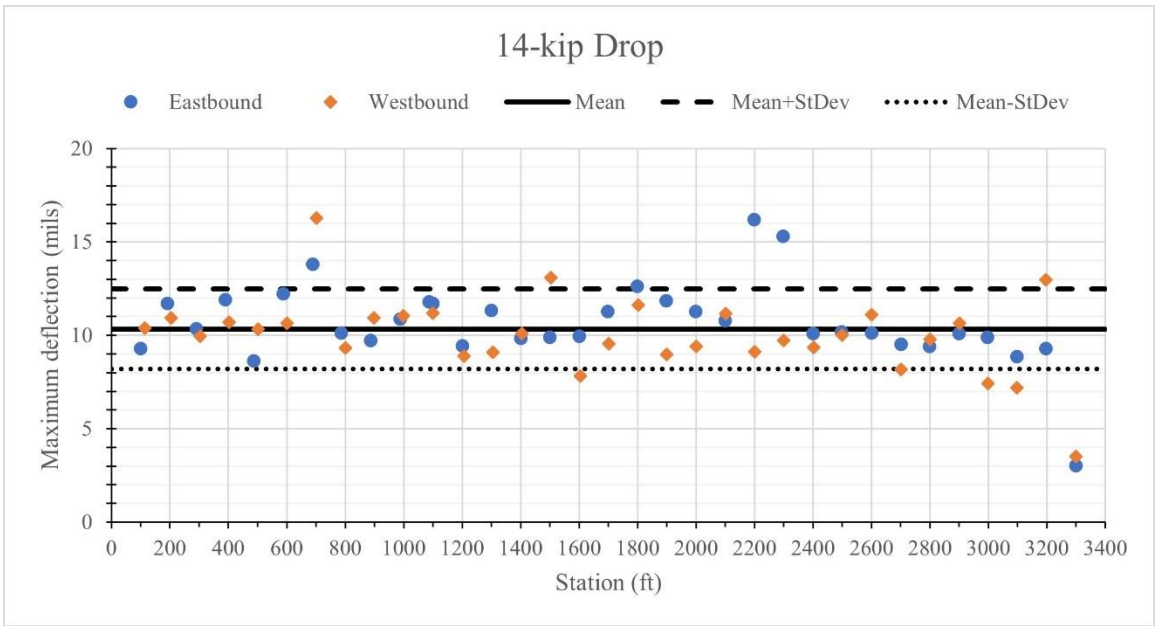

(b)

Figure 3.15 Maximum FWD deflections at LaGrange test section for (a) 9-kip and (b) 14-kip drops

FWD deflections indicate that the LaGrange test section is performing well (and mostly uniformly) throughout its length. The average maximum deflection is approximately 7.2 mils for the entire section, 7.1 mils in the westbound lane, and 7.4 mils in the eastbound lane. Lewis et al. (2012) recorded an average maximum deflection of 8.54 mils in their 2009 FWD testing. This indicates that the structural stiffness of the test section has not measurably declined in the 13 years since construction. The areas of concern noted by literature do not appear to have resulted in a less stiff structure when assessed by the maximum surface deflection: Cortes (2010) had noted weak subgrade at station 18+00 to 20+00 and Frost (2017) recorded a higher amount of surface distress in that area. While there is variability in that region, there is not a significant pattern of elevated maximum deflections. Furthermore, the area of suspected weak subgrade noted by Lewis et al. (2012) at approximately station 10+00 to 15+00 appears to have had minimal, if any, impact on the stiffness of the structure. Finally, maximum deflection at both ends of the test section, where Frost (2017) noted increased distress due to the change in pavement design and loading conditions, was comparable to the rest of the test section, but with increased variability in the deflections in the westbound lane at the western end (station 30+00 to 33+00). The only two areas of concern from this testing are at station 7+00 and 22+00 to 23+00, where there may be a pattern of increased deflection.

Moduli were backcalculated for the 9-kip and 14-kip drops at each station in the LaGrange test section using the LET method in ELMOD with a stiff layer analysis and no fixed AC modulus. This produced the lowest percent RMSE of all possible combinations. Variability was managed by calculating average moduli with outliers

excluded as noted in section 3.2.2. The average moduli for each layer of the LaGrange test section are reported in Table 3.4.

Table 3.4 LaGrange backcalculated layer moduli

Target drop load: 9 kips				
Section	**Avg modulus (ksi)**			**Avg % RMSE**
	AC	**Base**	**Subbase**	
Eastbound	1354	39	1810	1.83
Westbound	1078	46	2978	1.60
Target drop load: 14 kips				
Section	**Avg modulus (ksi)**			**Avg % RMSE**
	AC	**Base**	**Subbase**	
Eastbound	1294	49	1708	1.44
Westbound	1040	54	2686	1.23

The error in this backcalculation was minimal: percent RMSE for each lane and drop fell under the 2% threshold considered "reasonable" by the FHWA (2017b). Moduli of unbound layers also increased in the 14-kip drop compared to the 9-kip drop, as expected due to increased principal stress caused by the higher loads. Similar to the Morgan County moduli backcalculation, AC moduli predicted for the LaGrange test section were significantly higher than typical values cited by the FHWA (2017b), particularly for the temperatures experienced during testing. The surface temperatures during FWD testing ranged from 92 ºF to 117 ºF, suggesting lower AC moduli should be expected. Fixing the AC modulus during backcalculation, as suggested by the FHWA (2017b), did not improve the error in backcalculation or produce reasonable estimates of the moduli of other layers. Like the Morgan County section, the LaGrange IBP had a thin

(3.5-inch) AC surface, which responds differently to loads than predicted by the LET model used in forward calculation. This is the likely source of unrealistic AC moduli.

The moduli of the unbound base and stabilized subbase layers were well within the range of typical values reported by the FHWA (2017b), but there was a significant difference between the average moduli of the subbase layer in the eastbound lane versus the westbound lane. For both drops, the average subbase moduli estimated for the eastbound lane was approximately 60% of that of the westbound lane. There was high variability in all moduli backcalculated in both lanes, but the subbase moduli had the highest: both the subbase moduli in both lanes had a relative standard deviation of 44% for the 9-kip drop. Additionally, the relative standard deviation of moduli for the other layers was approximately 10% higher for the westbound lane. Despite this variability, the model converged upon reasonable solutions, as measured by the percent RMSE. The variability is therefore likely due to the site conditions at the time of testing, particularly the elevated temperatures. Surface temperature increased a total of 25 ºF during the several hours of FWD measurements. Such a temperature increase would result in varying AC stiffness throughout testing, changing deflection basins and introducing variability into moduli backcalculation.

3.3.3 SURFACE DISTRESS RESULTS & DISCUSSION

A survey of pavement surface distresses was performed on the LaGrange test section as described in section 3.1.2. Low severity load cracking, low severity block cracking, and rutting were the only forms of distress noted. Appendix B contains the results of the survey for each 100-foot segment. A PACES rating was calculated for each segment as detailed in section 3.1.2. Table 3.5 contains the average PACES rating for

each direction of the test section and compares it with the rating reported by Frost (2017) from the 2016 survey. Figure 3.16 shows the 2022 and 2016 ratings of each segment in each direction.

Table 3.5 LaGrange average PACES rating

Direction	2022 PACES rating	2016 PACES rating (Frost 2017)	Difference
Westbound	81	94	13
Eastbound	63	95	32

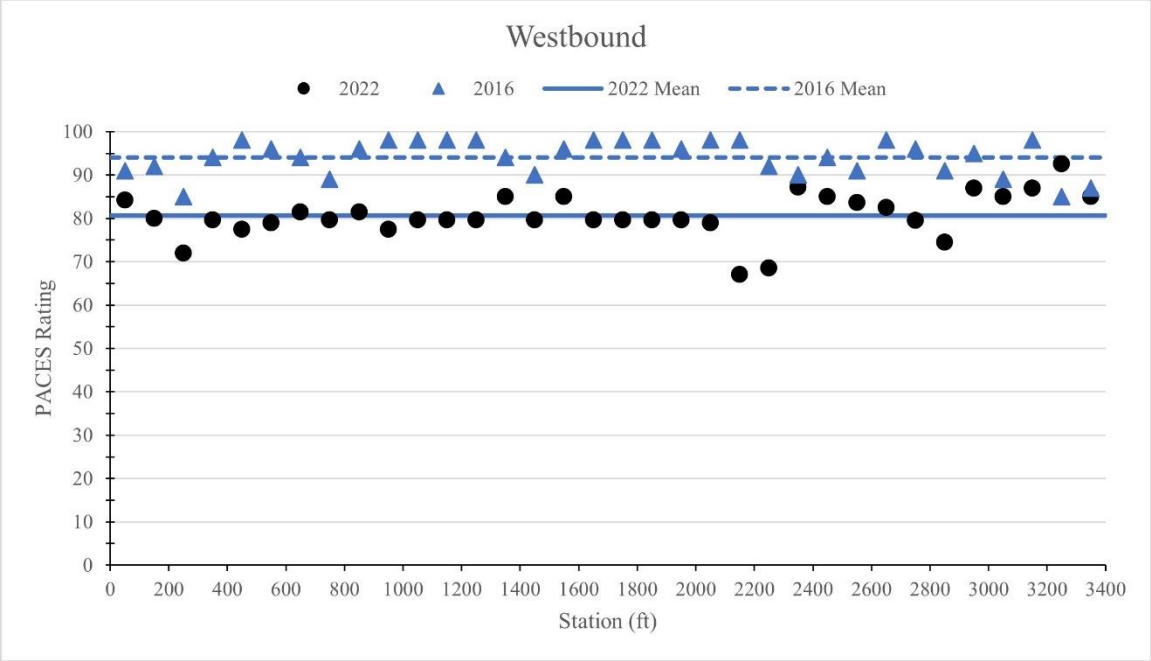

(a)

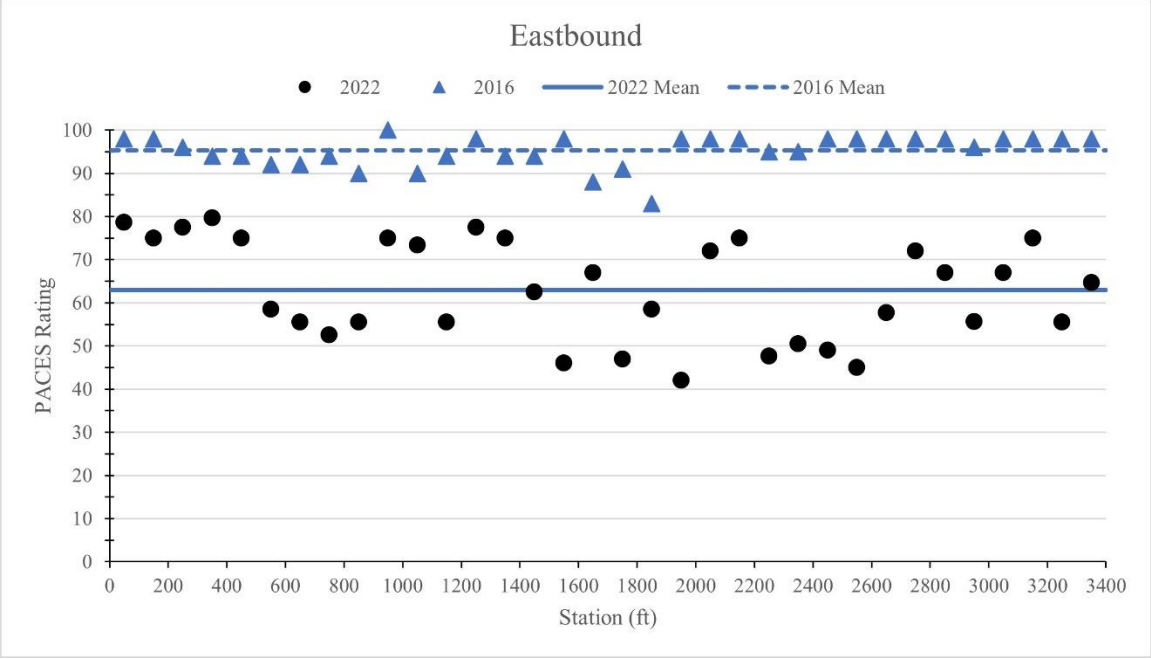

(b)

Figure 3.16 PACES rating by segment at LaGrange test section for (a) westbound and (b) eastbound lanes. 2016 data from Frost (2017)

The PACES rating of the westbound lane indicates the pavement surface is in good condition. There was a 13-point decrease since the last inspection. The only potential area of concern in the westbound lane is from station 21+00 to station 23+00, where the PACES rating is lower than the rest of the lane. The eastbound lane exhibited a PACES rating 18 points lower than the westbound lane, and 32 points lower than its 2016 rating. This rate of degradation is more severe than might be expected, even in conventional pavement (Y. Tsai, personal communication, 2022). It showed greater variability in rating, with a distinct "basin" of lower ratings from station 15+00 to station 20+00. The reason for the relatively poor performance of the eastbound lane will be explored further in this section, but further investigation is required to ascertain the root cause of the difference between lanes. Finally, the PACES rating did not indicate any greater surface distress present at the entrances and exits of the test section, as reported by Frost (2017) and suggested by the increased maximum FWD deflections in section 3.3.2.

There was little permanent deformation in the LaGrange test section, with the highest measured average rut depth for a 100-foot segment less than 0.375 inches. Table 3.6 records the average rut depth in each wheelpath of each lane, including data collected in this study and in 2016 by Frost (2017). Figure 3.17 shows the average rut depth in each wheelpath for each 100-foot segment. Figure 3.18 shows a sample surface profile of a transverse cross section in the eastbound lane of the LaGrange test section.

Table 3.6 LaGrange average rut depth

Direction	2022		2016	
	Average left rut depth (in)	Average right rut depth (in)	Average left rut depth (in)	Average right rut depth (in)
Westbound	0.13	0.09	0.18	0.06
Eastbound	0.15	0.06	0.13	0.08

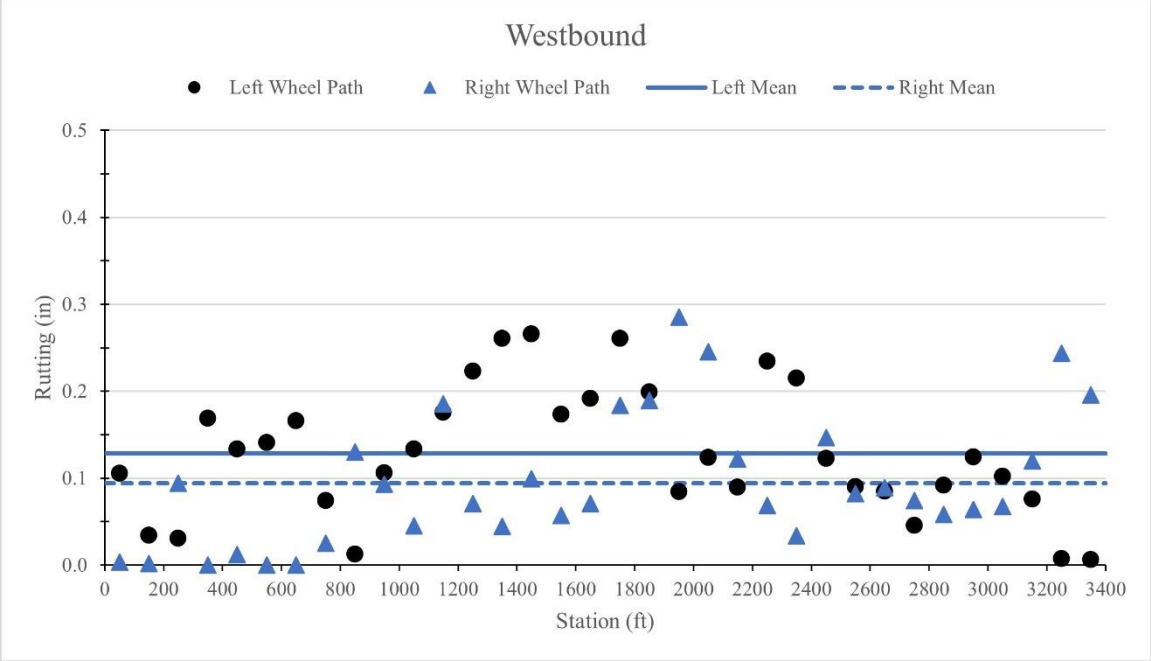

(a)

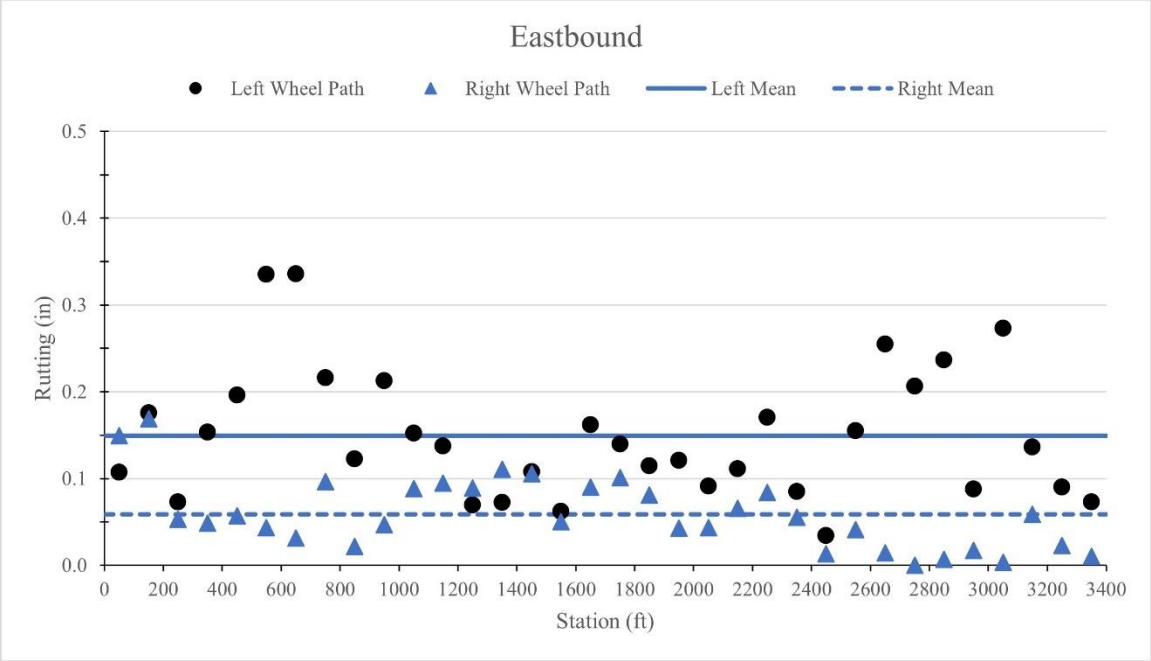

(b)

Figure 3.17 Rut depth by segment at LaGrange test section for (a) westbound and (b) eastbound lanes

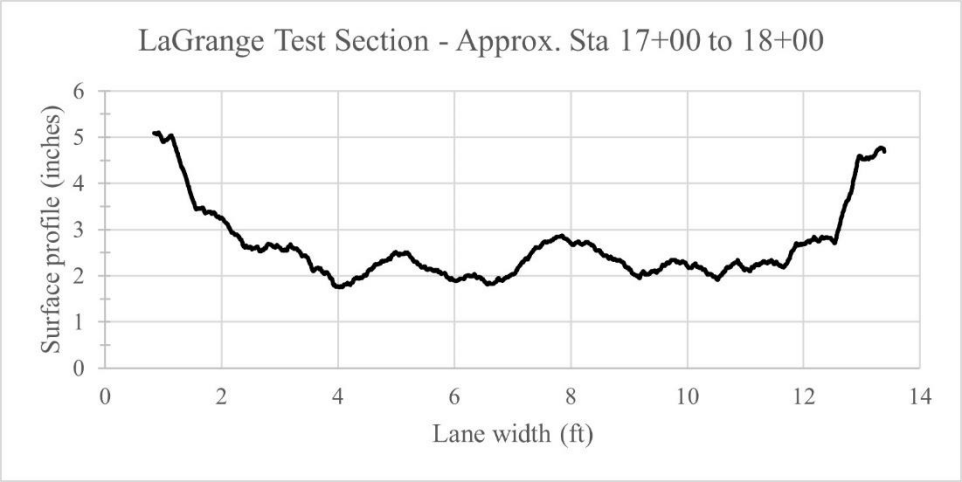

Figure 3.18 Sample surface profile at LaGrange test section in eastbound lane

Rut depth in the LaGrange test section was greater in the left wheelpath than the right wheelpath, which was also noted in the 2016 survey by Frost (2017). The reason for this discrepancy is unknown but may be due to differences in driving behavior or cross slope. Forensic investigations are recommended to explore this anomaly further. The westbound lane exhibited a "plateau" of increased rut depth from station 13+00 to station 23+00, which includes the region of weakened subgrade reported by Frost (2017) from station 18+00 to station 20+00. The eastbound lane had peaks in rut depth from station 5+00 to station 7+00 and from station 26+00 to station 31+00. Frost (2017) had also reported that the subgrade at station 7+00 and from station 25+00 to station 34+00 might be weaker than other segments of the roadway. The areas of increased rutting on the test section are therefore likely due to poor subgrade conditions or preparation, and not due to poor performance of the inverted pavement design. Finally, rutting increased only marginally since 2016. In some cases, the average rut depth marginally decreased. This is likely due to differences in data collection and/or processing.

Cracking in the LaGrange roadway was limited to low severity load cracking and low severity block cracking. Figure 3.19 presents the extent of these distresses for the westbound lane, and Figure 3.20 shows cracking in the eastbound lane.

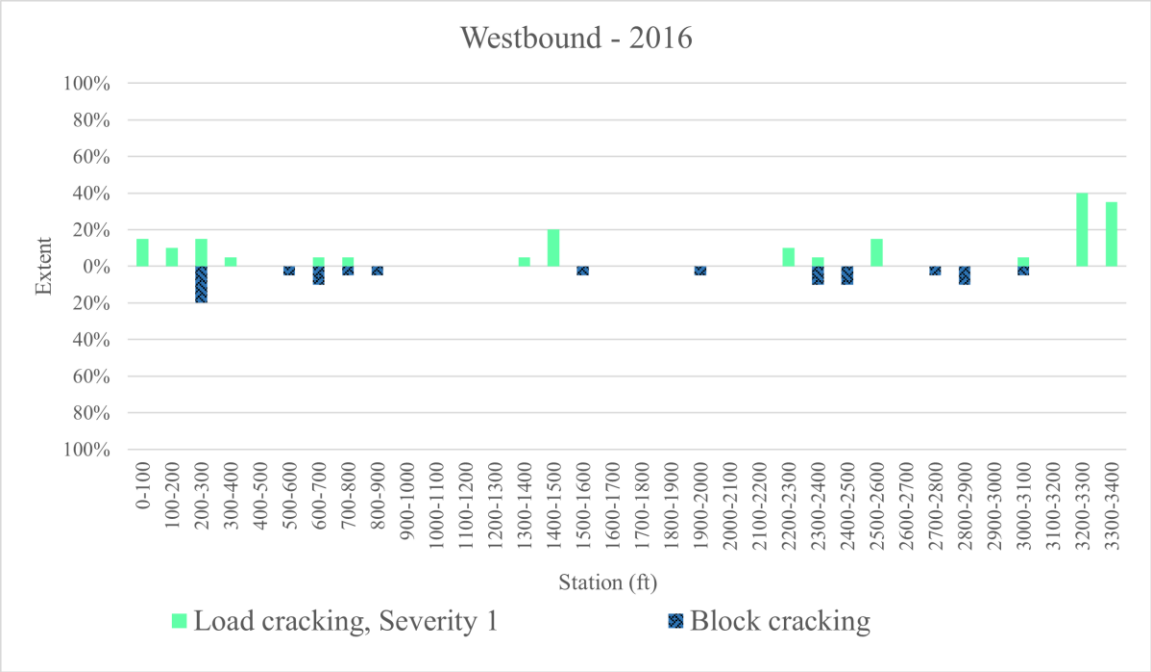

(a)

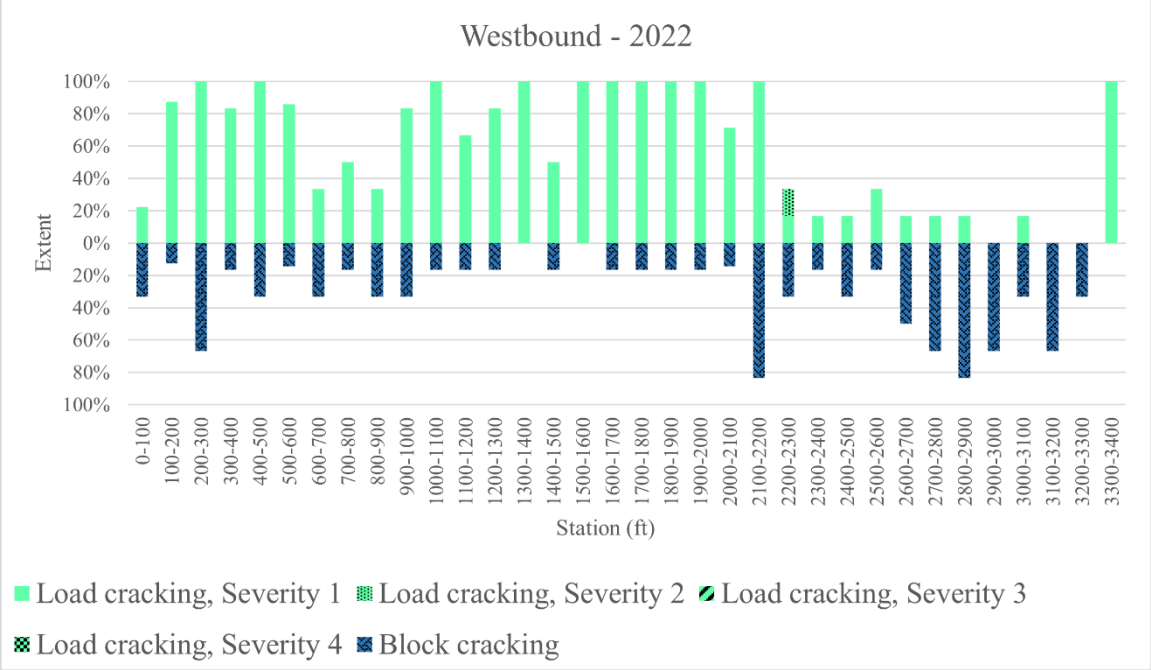

(b)

Figure 3.19 Crack type and severity at LaGrange test section in westbound lane for (a) 2016 and (b) 2022. 2016 data from Frost (2017)

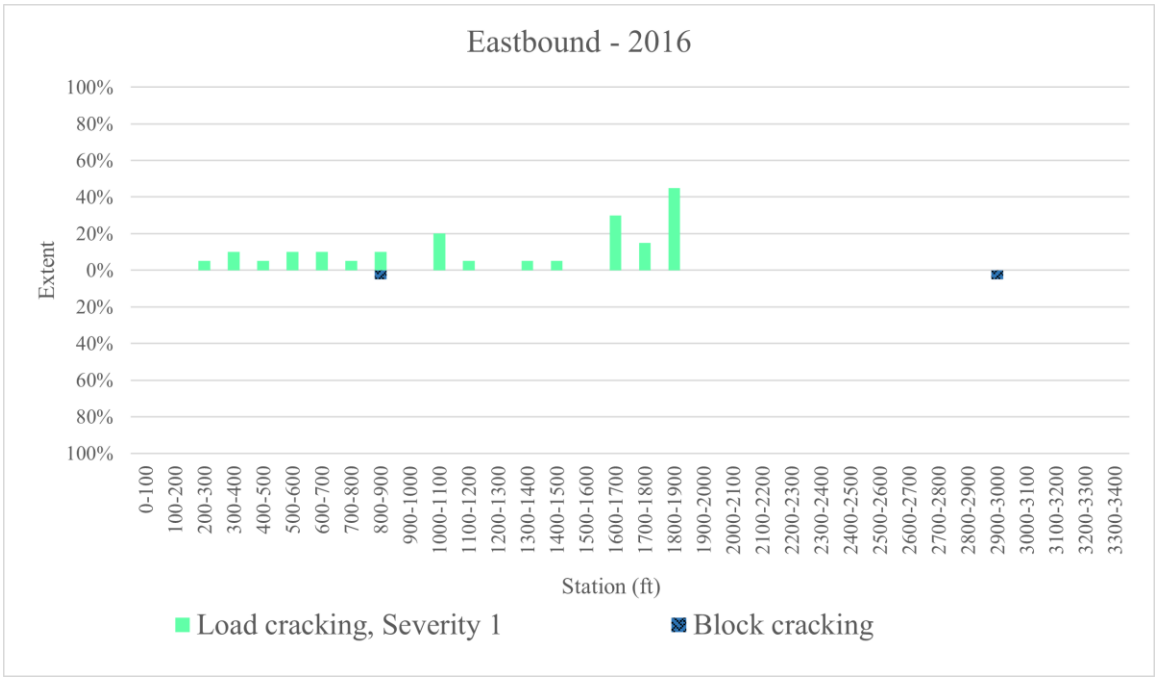

(a)

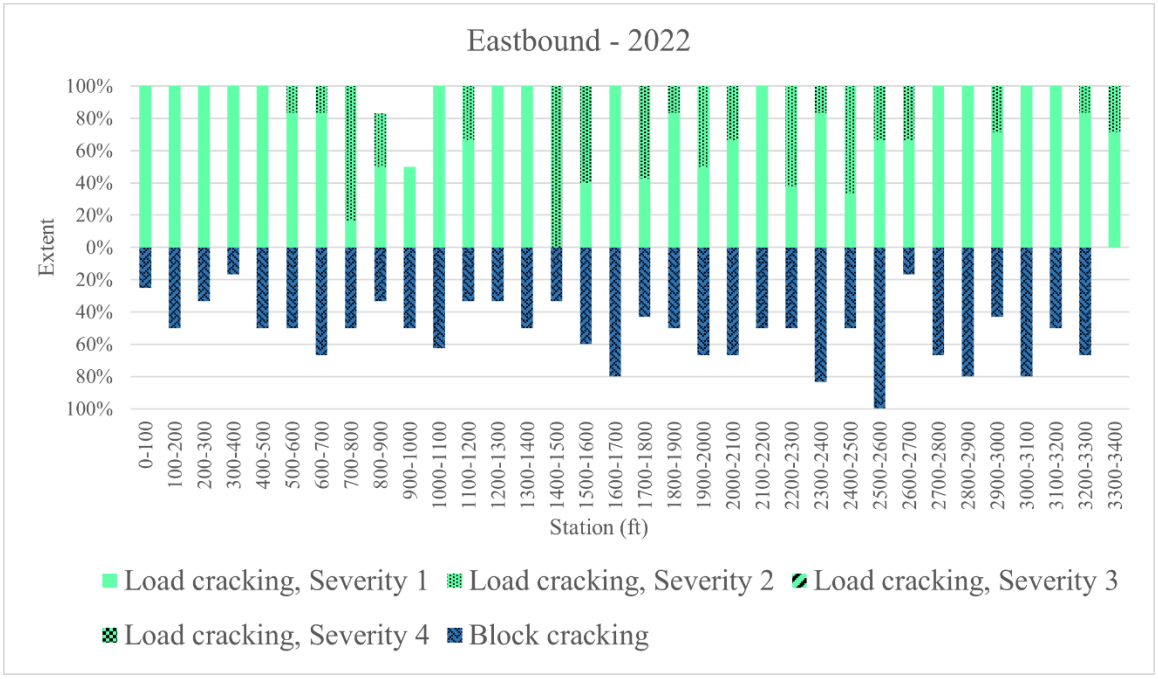

(b)

Figure 3.20 Crack type and severity at LaGrange test section in eastbound lane for (a) 2016 and (b) 2022. 2016 data from Frost (2017)

Low severity load cracking and low severity block cracking were present in nearly the entire roadway in 2022, compared with a minimal extent in 2016. The extent of block cracking was minimal throughout, except the westbound lane showed a greater extent of block cracking from station 26+00 to station 33+00, where load cracking was less prevalent. Notably, crack extent was minimal in the westbound direction from station 23+00 to station 25+00, where Frost (2017) reported an area of potentially more resilient subgrade. The eastbound lane had a similar extent of block cracking, with load cracking that was generally more widespread and severe. This was the main reason the PACES rating of the eastbound lane was significantly lower than that of the westbound lane. The reason for this general difference is unknown, but it could be due to a difference in the traffic in each direction. No measurement of ESALs was performed for this test section, but future testing should include such a measurement to illustrate any potential differences. Another potential source of greater load-related distress in the eastbound lane is the site topography. The test section cuts across a north-to-south slope for most of its length, with the eastbound lane constructed on the low part of the slope. While there is no record of cut/fill volumes, there could potentially be less fill material used in the subgrade of the uphill side of the test section (the westbound lane). If there is a difference in the resilient modulus and durability characteristics between the fill material and the in-situ subgrade, it could lead to a difference in performance between the two lanes. Finally, the large decrease in PACES rating in the eastbound lane might be due to the subjective nature of visual crack assessment. Evaluation of the crack type and severity was performed by different evaluators in 2016 and 2022, potentially leading to widely

differing results. Ultimately, however, further studies are required to investigate the difference between the eastbound and westbound lanes.

The eastbound section also exhibited two areas of more severe load cracking: The segment from station 7+00 to station 8+00 not only showed more severe load cracking, but it also exhibited greater FWD max deflection, as noted in section 3.3.2. This segment aligns with an area of weak subgrade and greater rut depth, indicating that poor subgrade is likely causing holistically poorer pavement performance in this section. There is a downhill horizontal curve noted by Frost (2017) in the eastbound direction from approximately station 16+00 to station 19+00. This change in the roadway alignment and cross section causes drivers to brake, which, when combined with the horizontal forces from turning, impart additional shear to the pavement surface. These additional loads are the likely source of elevated load cracking in this region and justify the relatively greater maximum FWD deflection values noted at station 18+00 in section 3.3.2.

In summary, a surface distress survey of the LaGrange test section of inverted pavement indicates the westbound pavement has performed well in the 13 years since its construction. The IBP structure has accumulated minimal permanent deformation, suggesting that its holistic ability to distribute traffic loads to the subgrade is satisfactory. Load-related cracking, while common throughout the roadway, is low in severity. This signals that the inverted pavement structure is supporting the surface layer and resisting fatigue well.

4. PERFORMANCE MODELING OF INVERTED PAVEMENT DESIGNS

The two goals of this study are to examine the long-term performance of inverted base pavement, also known as "inverted pavement" or IBP, and to investigate the suitability of IBP for use in airfields. This chapter details an effort to compare the lifecycle performance of inverted base pavement to conventional flexible pavement under aircraft traffic. Various simulated test sections of pavement were designed and evaluated using Pavement-Transportation Computer Assisted Structural Engineering (PCASE) software developed by the Department of Defense (DoD) and produced by IIT Corp. Section 4.1 describes how the materials and layer thicknesses of the simulated test sections were selected. Section 4.2 illustrates how PCASE's layered elastic design and evaluation modules work, and how they were used in this modeling study. Section 4.3 presents the results of the assessment.

4.1 DESIGN OF SIMULATED TEST SECTIONS

The design of the test sections evaluated in this modeling effort involved two basic steps: determining the material properties of pavement layers and determining the thickness of each layer. PCASE requires two material properties to be defined for each layer in a pavement structure: The first is modulus, i.e., backcalculated falling weight deflectometer (FWD) modulus, and the second is Poisson's ratio. These properties were determined from relevant literature and the field testing performed in Chapter 3 of this study. The default values in PCASE were used for the Poisson's ratio of each material.

These values agree for the most part with other literature such as the FHWA's FWD guidelines (2017b). Table 4.1 lists the PCASE default Poisson's ratios used in modeling as well as the Poisson's ratios recommended by the FHWA (2017b).

Table 4.1 Poisson's ratios from literature (PCASE Default was used in modeling)

Material	Poisson's ratio	
	PCASE Default (IIT Corp 2015)	**FHWA (2017b)**
Asphalt concrete	0.35	0.35
Base course	0.35	0.35
Cement-stabilized subbase	0.25	0.25-0.35
Cohesionless subgrade soils	0.4	0.35-0.4

The Poisson's ratio of the cement-stabilized subbase was selected to remain the default 0.25 instead of another number in the range suggested by the FHWA (2017b), because Cortes (2010) measured the Poisson's ratio of the cement-stabilized subbase at the LaGrange test section to be 0.251. The default Poisson's ratio of the subgrade remained 0.4, as this value assumes greater lateral deformation of the subgrade under vertical stress and is therefore conservative.

The modulus of each material was selected from either literature or the backcalculation effort noted in Chapter 3. Sets of moduli from the same source, referred to here as "material models", were grouped for compatibility. Three different material models were created: the default moduli from PCASE, moduli backcalculated by Sha et al. (2020), and moduli backcalculated by this study (referred to as the "GT" material model). These moduli are listed in Table 4.2.

Table 4.2 Moduli used in modeling

Material	Modulus (ksi)		
	PCASE Default (IIT Corp 2015)	Sha et al. (2020)	GT
Asphalt concrete	200	1,041	200
Base course	60	52	47
Cement-stabilized subbase	700	1,112	2,295
Cohesionless subgrade soils	15	15	15

The PCASE Default material model was used only when modeling a conventional pavement design, as literature has shown the material properties of IBP differ from the defaults given by PCASE. The other two material models, determined from field tests of IBP sections, were used to model both inverted and conventional test sections for sake of comparison. The Sha material model, however, provides an unlikely asphalt concrete (AC) modulus value for any pavement, as described in 3.2.2. Moduli in the Sha material model were calculated by averaging the backcalculated moduli of the test sections described in Sha et al. (2020). Moduli in the GT material model were determined by averaging moduli backcalculated from the 14-kip FWD drop on the LaGrange test section. The 14-kip moduli were selected as that was the closest FWD loading to aircraft loading. The moduli from the Morgan County test section were excluded from the average, as the average percent root mean square error of the backcalculation for that section was greater than two percent, considered “questionable” divergence by the FHWA (2017b). Additionally, the average AC modulus backcalculated by this study was not used for the GT material model, for the reasons specified in 3.2.2. The PCASE default AC modulus was substituted in its place. Finally, a consistent subgrade modulus

of 15 ksi was used for each material model, as this helps simulate the construction of these test sections at the same site, allowing the analysis to focus on the engineered structure.

Two different design philosophies were used to determine the layer thicknesses of the test sections evaluated in this chapter: The conventional sections used the PCASE layered elastic design module, which will be explained in detail in 4.2. The inverted sections used three ratios of layer dimensions from literature, with AC thicknesses of 1, 2, 3, and 5 inches. This is similar to the range of AC thicknesses tested in the modeling work of Papadopoulos & Santamarina (2015); they suggested an AC layer of 1-2 inches was optimal to take advantage of the transition to membrane-like deformation. The first dimension ratio used was the ratio that Papadopoulos & Santamarina (2015) found to produce optimal critical strains; in terms of AC thickness/base thickness/subbase thickness, the ratio was 1/6/10. This ratio uses a thick base layer and a very thick subbase compared to the others. The next dimension ratio came from Sha et al. (2020); it is the same ratio they used in their experiment: 1/2/4. The final dimension ratio, the "LaGrange" ratio, was the same ratio as the field dimensions of the LaGrange test section: 1/2/2.67. The LaGrange ratio had the comparably thinnest cement-stabilized subbase of any dimension ratio tested.

27 different combinations of material models and dimensions were tested. All material models were used to produce a conventional test section using the PCASE layered elastic design module. For the inverted sections, the two inverted material models were combined with every dimension ratio and every AC thickness. The full list of simulated test sections is contained in Appendix C.

4.2 LAYERED ELASTIC DESIGN AND EVALUATION METHODOLOGY

PCASE uses a mechanistic-empirical procedure to simulate pavement performance. It uses a layered-elastic model to calculate stresses and strains in pavement structures, and empirical transfer functions to consider the effects of traffic loading and climatic conditions on functional performance DoD (2001a).

The mechanical calculation performed by PCASE uses several assumptions that limit analysis: First, it assumes that pavement layers are composed of linear elastic materials (DoD 2001a). It also models traffic loading as a vertical uniform circular load (DoD 2001a). As mentioned in 2.4, any pavement modeling that considers a vertical load on linear elastic materials is inherently limited, as real pavement materials undergo principal stress rotation and seldom behave as linear elastic materials. Finally, PCASE assumes that aggregate layers are saturated with moisture (DoD 2001a). This is a conservative assumption for the materials that make up most pavement structures, which are primarily composed of coarse-grained particles and therefore behave in an undrained manner. It is not conservative, however, for materials where undrained conditions exist, e.g., in a clay subgrade.

A notable advantage to modeling in PCASE, however, is its consideration of the effects of climate on pavement performance. PCASE allows users to calculate a decreased AC modulus for increased temperatures- this option was not used in this study, which will be discussed later in this section (Van Steenburg 2021). PCASE also considers the effects of temperatures (both high and low) on the fatigue behavior of asphalt concrete (Van Steenburg 2021). Furthermore, it considers the effects of freezing temperatures (frost action and freeze/thaw degradation) and moisture (shear strength) on

soil and aggregate layers (Van Steenburg 2021). PCASE uses a climate database with data from weather stations around the world to group time periods where pavement materials behave similarly and evaluates pavement responses in each time period (Van Steenburg 2021).

PCASE software also contains a database of vehicle (including aircraft) loading characteristics, such as standard loads, gear/axle patterns, and tire pressures (IIT Corp 2015). It uses this information to calculate the maximum equivalent circular load a pavement structure receives from each pass of every vehicle selected by the user (DoD 2001a). It also considers vehicle speed and wander width to estimate the loading frequency (DoD 2001a).

The PCASE design module recommends layer thicknesses from user-specified material data (type, modulus, and Poisson's ratio) and required traffic life (number of passes of each type of vehicle). It first assumes layer thicknesses and computes the strain caused by an individual loading repetition of every vehicle in the user-specified traffic using Burmister's solution for multilayered elastic continua, considering the aforementioned climate effects DoD (2001a). PCASE then uses these strains as inputs for empirical relationships that correlate strain to failure criteria, outputting a number of allowable coverages (Van Steenburg 2021). The failure criteria for flexible pavement are tensile strain at the bottom of the surface layer (related to cracking) and vertical strain at the top of the subgrade (related to rutting) (Van Steenburg 2021). The software then compares the allowable coverages to the user-specified required coverages. PCASE iteratively generates layer thickness combinations until the allowable passes are greater than the required traffic, where layer thicknesses have been minimized (Van Steenburg

2021). All layer thicknesses can be calculated by PCASE, or specific thicknesses can be user-specified, and the software will then calculate the required thicknesses of the other layer(s). In the design of the conventional test sections for this study, all thicknesses were computed by PCASE to allow for comparison of the most economical cross sections. Additionally, software options to design for frost and drainage are available. The frost option specifies subgrade compaction depth and relative compaction based on calculated frost penetration depth (Van Steenburg 2021). The drainage option computes drainage layer thickness based on permeability, drainage path dimensions, and time to drain (Van Steenburg 2021). Both of these design options were ignored, as they are out of the scope of this study. The climate-related behavior of inverted pavements is a topic that warrants its own dedicated research effort.

While the PCASE layered elastic design module was used to design the simulated conventional sections, the evaluation module was used to evaluate the performance of every test section. The PCASE layered elastic evaluation module follows the same framework as the design module, but instead calculates allowable passes from given layer thicknesses and material properties. It also cites a failure mode, indicating which failure criterion the model estimates was exceeded: vertical strain in the subgrade (rutting) or horizontal tensile strain in the AC (cracking).

The simulated traffic used in this modeling study was selected from US Air Force standards specified by the DoD (2001a). Airfield traffic areas, which dictate vehicle speed and wander, and therefore loading frequency, are standardized according to function. Areas with low traffic volume or lower aircraft weight (due to aircraft lift) are grouped into traffic area “C,” the option selected in this effort (DoD 2001a). This area

includes secondary taxiways and the interior of runways between touchdown areas (DoD 2001a). This traffic area was selected because it is the most intensive use for flexible pavements allowed by current DoD policy (2001a). The use of AC surfaces is not permitted in areas with heavy, channelized traffic such as runway touchdowns or primary taxiways (DoD 2001a). It is also not allowed in areas used for parking and maintenance (DoD 2001a). This is due to prior poor lifecycle performance of flexible pavements in these areas due to the effects of fuel spillage and severe jet blast in addition to the shorter lifespan of flexible pavement under heavy loading compared to rigid pavement (DoD 2001a).

PCASE also offers standardized traffic patterns (number and type of vehicles) that are used by the DoD and US Air Force for analysis. These traffic patterns minimize vehicle spectra to standardized "design aircraft", allowing engineers to address uncertainty in which aircraft might use an airfield at any time. The "Air Force Medium" traffic pattern is typical for Air Force airfields and was selected for this research (DoD 2001a). This traffic pattern includes the design aircraft, passes, and standard loading characteristics specified in Table 4.3. Evaluation was limited to the C-17 and F-15E, as these are the most demanding vehicles in terms of passes and contact pressure.

Table 4.3 Air Force Medium traffic pattern (DoD 2001a; IIT Corp 2015)

Aircraft	Passes	Standard main gear load (lbs)	Standard main gear contact pressure (psi)
C-17	400,000	269,217	142
F-15E	100,000	35,235	305
B-52	400	253,760	265

PCASE requires users to select a location as the basis for its analysis of climatic effects on material properties. Several different climates were used for this evaluation; the base case used the Hartsfield Jackson International Airport in Atlanta, GA as its weather station, the high-temperature case used the Doha International Airport in Doha, Qatar as its weather station, and the low-temperature case used the Fort Richardson, Alaska weather station. As previously mentioned, the PCASE method of AC degradation for high temperature was not used. This method is based on an empirical relationship described by the DoD (2001b), where mean pavement temp and loading frequency are used to predict the AC modulus. This somewhat arbitrary, outdated method requires no input of material properties. In fact, even the DoD (2001b) admits that "predicted values may not always agree with actual field values." A review of the literature determined that the method recommended by Seo et al. (2013) was superior. They improved upon the method suggested by the Mechanistic-Empirical Pavement Design Guide (AASHTO 2020) and developed a relationship for estimating in-situ AC modulus based on loading frequency, asphalt viscosity, temperature, and aggregate blend. Seo et al. (2013) found their method compares favorably with in-situ FWD moduli compared to AASHTO's (2020) method. Degraded AC moduli were calculated for each material model in the high-temperature case using a reference temperature of 115 ºF, the design surface temperature for the Doha weather station given by PCASE (IIT Corp 2015). These moduli are shown in Table 4.4.

Table 4.4 Degraded asphalt concrete moduli for high-temperature case

Material model	AC modulus (ksi)	High-temperature AC modulus (ksi)
PCASE Default	200	28
Sha	1,041	106
GT	200	28

Finally, PCASE requires users to select several other options for analysis: First, the bonding condition between each layer can be specified as "fully bonded", "partially bonded", or "unbonded" (IIT Corp 2015). These refer to the horizontal freedom of movement between layers, and anything but "fully bonded" is typically used only for rigid pavement overlays (Van Steenburg 2021). "Fully bonded" was therefore selected in every case modeled here. The software also allows a selection between a loading frequency of 10 hertz, the default for runways, and 2 hertz, the default for all other traffic areas (IIT Corp 2015). 10 hertz was selected, as it is more severe.

4.3 MODELING RESULTS & DISCUSSION

Three simulated test sections of conventional pavements and 24 simulated test sections of inverted pavements were evaluated as described in 4.2. Appendix C contains the dimensions, material properties, and allowable passes calculated for the simulated test sections in every case (base case, high-temperature, and low-temperature). Table 4.5 presents the results of the conventional sections with allowable passes higher than those required in Table 4.3. Table 4.5 also shows the results of the IBP sections with an acceptable number of passes according to Table 4.3, with total cross sections thinner than the acceptable conventional sections.

Table 4.5 Modeling base case, selected results

Design	Material model	Dimension ratio	AC thickness (in)	Total thickness (in)	C-17 passes	C-17 failure mode	F-15E passes	F-15E failure mode
Inverted	GT	LaGrange (1/2/2.67)	2	11.33	3,318,248	Rut	62,033,639	Rut
Inverted	GT	Sha (1/2/4)	2	14	99,999,999	Rut	1,000,000	Rut
Inverted	Sha	Sha (1/2/4)	2	14	41,065,215	Rut	1,000,000	Rut
Inverted	GT	Papadopoulos (1/6/10)	1	17	1,000,000	Rut	1,000,000	Rut
Inverted	GT	LaGrange (1/2/2.67)	3	17	44,219,888	Fatigue	1,000,000	Rut
Inverted	Sha	LaGrange (1/2/2.67)	3	17	1,798,439	Fatigue	1,000,000	Rut
Inverted	Sha	Papadopoulos (1/6/10)	1	17	1,000,000	Fatigue	1,000,000	Rut
Conventional	Sha	PCASE LE Design	5	19.5	475,953	Rut	19,539,492	Rut
Inverted	GT	Sha (1/2/4)	3	21	54,272,187	Fatigue	1,000,000	Rut
Inverted	Sha	Sha (1/2/4)	3	21	1,927,0000	Fatigue	1,000,000	Rut
Conventional	PCASE Default	PCASE LE Design	5	23	410,782	Rut	15,499,919	Rut
Conventional	GT	PCASE LE Design	7.5	23	477,447	Rut	19,548,298	Rut

The first item of note in Table 4.5 is that the thinnest, and therefore most economical, section of IBP with acceptable performance used the most realistic material model for inverted pavement (GT). Furthermore, it is less than 60% the thickness of the thinnest acceptable conventional section. Additionally, the thinnest acceptable conventional section was modeled with unrealistic material parameters for conventional pavement (the Sha material model). A more realistic material model, the GT material model, produced a conventional pavement twice the thickness of the thinnest IBP.

Also notable is that many of the simulated inverted test sections had AC layers of two inches or less, corroborating the suggestion of Papadopoulos (2014) and Papadopoulos & Santamarina (2015) that the membrane-like behavior of thin AC layers is optimal for inverted pavement. In addition, most IBP failed in rutting, indicating that the structures protect the AC layer from fatigue. Another interesting pattern is that the

inverted sections far exceed the conventional in allowable C-17 passes, but the opposite is true for F-15E traffic (in most cases).

The high-temperature case considered only the best-performing test sections (those noted in Table 4.5). The results of the high-temperature modeling are shown in Table 4.6.

Table 4.6 Modeling high-temperature case results

Design	Material model	Dimension ratio	AC thickness (in)	Total thickness (in)	C-17 passes	C-17 failure mode	F-15E passes	F-15E failure mode
Inverted	GT	LaGrange (1/2/2.67)	2	11.33	1,802,728	Rut	26,674,406	Rut
Inverted	GT	Sha (1/2/4)	2	14	99,999,999	Rut	1,000,000	Rut
Inverted	Sha	Sha (1/2/4)	2	14	99,999,999	Rut	1,000,000	Rut
Inverted	GT	LaGrange (1/2/2.67)	3	17	99,999,999	Rut	1,000,000	Rut
Inverted	GT	Papadopoulos (1/6/10)	1	17	1,000,000	Rut	1,000,000	Rut
Inverted	Sha	LaGrange (1/2/2.67)	3	17	99,999,999	Rut	1,000,000	Rut
Inverted	Sha	Papadopoulos (1/6/10)	1	17	99,999,999	Rut	1,000,000	Rut
Conventional	Sha	PCASE LE Design	5	19.5	3,953	Rut	33,936	Rut
Inverted	GT	Sha (1/2/4)	3	21	99,999,999	Rut	1,000,000	Rut
Inverted	Sha	Sha (1/2/4)	3	21	99,999,999	Rut	1,000,000	Rut
Conventional	PCASE Default	PCASE LE Design	5	23	42,045	Rut	148,608	Rut
Conventional	GT	PCASE LE Design	7.5	23	12,680	Rut	148,608	Rut

All three conventional sections did not reach the amount of C-17 passes required by the traffic pattern in Table 4.3, and the one that used the Sha material model also failed to provide an acceptable number of F-15E passes. As in the base case, inverted test sections far exceeded the required number of passes. All simulated IBP sections fail in rutting, again indicating that the thin AC layer may not be the weak point of inverted pavements.

The low-temperature case also considered only the best-performing test sections. The results of the high-temperature modeling are shown in Table 4.7.

Table 4.7 Modeling low-temperature case results

Design	Material model	Dimension ratio	AC thickness (in)	Total thickness (in)	C-17 passes	C-17 failure mode	F-15E passes	F-15E failure mode
Inverted	GT	LaGrange (1/2/2.67)	2	11.33	3,309,166	Rut	61,800,165	Rut
Inverted	GT	Sha (1/2/4)	2	14	99,999,999	Rut	1,000,000	Rut
Inverted	Sha	Sha (1/2/4)	2	14	41,065,215	Rut	1,000,000	Rut
Inverted	GT	LaGrange (1/2/2.67)	3	17	99,999,999	Rut	1,000,000	Rut
Inverted	GT	Papadopoulos (1/6/10)	1	17	1,000,000	Rut	1,000,000	Rut
Inverted	Sha	LaGrange (1/2/2.67)	3	17	1,798,439	Fatigue	1,000,000	Rut
Inverted	Sha	Papadopoulos (1/6/10)	1	17	1,000,000	Fatigue	1,000,000	Rut
Conventional	Sha	PCASE LE Design	5	19.5	478,142	Rut	19,573,000	Rut
Inverted	GT	Sha (1/2/4)	3	21	54,257,368	Rut	1,000,000	Rut
Inverted	Sha	Sha (1/2/4)	3	21	1,927,000	Fatigue	1,000,000	Rut
Conventional	PCASE Default	PCASE LE Design	5	23	422,836	Rut	15,611,642	Rut
Conventional	GT	PCASE LE Design	7.5	23	490,553	Rut	19,683,036	Rut

All test sections modeled in the low-temperature case surpassed the required design life. Inverted sections again far exceeded the conventional sections in C-17 passes, and conventional test sections far exceeded all but one IBP section in F-15E passes. Additionally, all but three test sections failed in rutting. The three sections that failed due to fatigue were inverted sections with a Sha material model, where the AC modulus is exceptionally (unreasonably) high. A stiffer AC layer could lead to greater fatigue cracking in cold weather due to its rigidity and brittleness and inability to deform to relieve tensile stress.

These results indicate promising performance for inverted pavements in airfields. Not only did modeling predict that inverted pavements can provide the required design

life, but IBP with more economical cross sections can perform better than conventional pavement designed for the same loading. Total cross sections were thinner, indicating less material overall, and the best IBP test sections had 13% to 60% of the asphalt concrete of comparable conventional sections. Inverted pavements therefore may provide a cheaper and more sustainable solution for airfields. The model used in this research has its limitations: it depends on a linear elastic model without principal stress rotation, and it does not consider shear developed in AC by increased tension at the top of that layer. These results, however, provide significant justification for the pursuit of research with full-scale test sections to investigate the effect of those factors.

5. CONCLUSIONS AND RECOMMENDATIONS FOR FUTURE WORK

5.1 CONCLUSIONS

The first goal of this study was to investigate the long-term performance of inverted base pavements ("inverted pavement" or IBP) in the United States. Field evaluation was conducted on two test sections of inverted pavement in Georgia, consisting of falling weight deflectometer (FWD) measurements and a surface distress survey. At 21 years of age, the test section at Morgan County showed inverted designs had performed better than conventional pavements. The maximum deflections from FWD testing were greater for conventional pavement than the IBP, signifying that the inverted sections exhibited greater resistance to deformation over the life of the roadway. Analysis of the surface distress survey showed that the inverted sections had accumulated less distress than the conventional section, indicating superior holistic performance. The LaGrange test section confirmed these results. While there was no conventional section for comparison, the IBP in LaGrange, GA demonstrated similar structural stiffness with little degradation in stiffness or surface condition over time. Moduli backcalculated from FWD data provided useful parameters for the modeling effort conducted in this research.

The second goal of this study was to examine the performance of IBP under airplane traffic, as few field, lab, or modeling studies have explored this application. A modeling effort was therefore undertaken with a mechanistic-empirical pavement analysis software to compare inverted and conventional pavement under simulated aircraft loading. Simulated test sections were designed using material properties and

dimensions from literature, the field study in this thesis, and the layered elastic design module in the software. The layered elastic evaluation module was then used to compare the lifecycle performance of each test section with standard aircraft traffic loading. The software predicted inverted pavements would withstand a significantly greater amount of traffic in every climate tested, when compared to conventional sections designed for the same loading. Furthermore, many inverted designs outperformed conventional pavements despite having thinner cross sections and thinner asphalt concrete surface layers. This indicates that inverted pavements may provide a cheaper, more sustainable solution for airfield pavements with no drop in performance.

5.2 RECOMMENDATIONS FOR FUTURE WORK

This study and the body of work present in the literature have demonstrated that inverted designs can result in better performing, more economical, and more sustainable pavement than conventional designs. Significant gaps in knowledge, however, must be rectified for this technology to be put into practice in the United States. One notable area requiring further study is the effect of climate extremes on inverted pavements. Environmental effects from moisture and extreme temperatures (low and high) are a substantial source of distress and degradation for pavements. To date, most field sections of inverted pavement in the United States have been constructed in warm, wet climates, mostly in the southeastern part of the country (see Appendix A). A wider variety of climes would provide greater insight into the long-term behavior of IBP. Furthermore, concerns exist regarding the “sandwich” construction of inverted pavement and its effect on drainage within the structure. There is the potential for the two bound layers to trap

moisture in the unbound base layer, leading to various forms of damage. Further research, likely with full-size test sections, can provide greater understanding of the drainage behavior of inverted pavement systems.

Another limitation in the literature and this study is the lack of an accurate accounting of traffic on inverted pavement test sections. Modern roadway design uses equivalent single axle loads (ESALs) as a measure of a structure's exposure to loading. To date, inverted field test sections have made an estimate of this figure. A better understanding of IBP performance would require an accurate measurement.

One additional gap is the incongruence between the materials characterization methods used in inverted pavement literature versus those used in modern pavement design and evaluation, as recommended by the Mechanistic-Empirical Pavement Design Guide (MEPDG). Thus far, most inverted pavement literature has used measures to characterize materials (backcalculated modulus, relative compaction, California bearing ratio, and unconfined compressive strength) that are different from the "Level I" inputs recommended as most accurate by the MEPDG (e.g., dynamic modulus for asphalt concrete and resilient modulus for stabilized and unstabilized soil or aggregate) (AASHTO 2020). To properly evaluate IBP according to a modern framework, modern inputs are required.

Few inverted pavement studies have provided any cost accounting to justify the superior economy of IBP. Future studies should include a lifecycle cost analysis that compares the lifecycle costs of conventional and inverted pavements.

Numerical modeling and simulation have been a valuable tool in advancing knowledge of inverted pavements. Models used in literature and this study, however, are

limited by their assumptions. Many models have only considered a uniform vertical circular load, and many have assumed pavement materials as linear elastic. This removes the important considerations of principal stress rotation and stress-dependent stiffness, two characteristics that have significant relevance when considering how pavement structures respond to loading. The models in the literature that have used finite element techniques to account for these phenomena, however, have not used a mechanistic-empirical framework to accurately predict lifecycle performance with respect to fatigue and environmental effects.

Furthermore, some models have identified a potential for high shear in inverted pavement with thin asphalt concrete surfaces (Papadopoulos 2014). These models were finite element models, not mechanistic-empirical models considered to be state-of-the-art in predicting pavement performance. Modern mechanistic-empirical models should be improved to consider the effects of shear and tension at the top of the asphalt concrete surface of flexible pavements. This would allow for a more accurate prediction of the fatigue behavior of inverted pavements. Another method for further investigation of shear in thin-surfaced IBP might be instrumentation and forensic analysis of full-size inverted test sections. Additionally, the behavior of asphalt concrete is highly dependent on loading rate. The effects of loading frequency should be included in future studies of thin AC surfaces.

Finally, this study has provided justification for additional testing of inverted pavements under aircraft traffic. Whether using accelerated pavement testing techniques or field sections, future research should further explore this application of IBP. Tests should use modern materials characterization and instrumentation to explore the

possibility of maximizing the performance, economy, and sustainability of airfield pavements. The results of this thesis lend weight to the potential for inverted pavements to change the way roadway and airport pavements are designed, built, and maintained.

APPENDIX A: TEST SECTION CLIMATE DATA

Three climate metrics are reported here to illustrate the environmental exposure withstood by testing locations mentioned in this thesis. The three quantities are design air temperature, air freezing index, and annual precipitation. Design air temperature is the air temperature used by Pavement-Transportation Computer Assisted Structural Engineering (PCASE) software to evaluate the stiffness of asphalt concrete (AC) in the layered elastic evaluation of pavements (LEEP) module. The design air temperature is the average between the mean daily maximum temperature and the mean daily temperature of the hottest month at a given location (IIT Corp 2015). PCASE uses the design air temperature as the air temperature when calculating the temperature-dependent stiffness of AC. The design air temperatures reported here are from PCASE 7.0.1 (IIT Corp 2015). The design air temperatures here should be considered an indication of the effects of high temperatures on the pavements tested in each location. Elevated temperatures not only decrease AC stiffness, but also can affect the durability of the AC material.

Air freezing index is a measure of the severity of a freezing season used in foundation design. Air freezing index indicates both the magnitude (temperature) and duration of air temperatures below freezing in a given year. A higher air freezing index corresponds to a more severe freezing season. Cold temperatures can have several effects on pavements: first, AC behaves stiffer and less ductile in the cold, affecting durability. Furthermore, moisture can penetrate the pavement structure and expand as it freezes in voids, causing frost damage that weakens susceptible layers. The air freezing indices

reported here, from Bilotta et al. (2015), should therefore be considered a representation of the exposure of the relevant pavement to cold-weather damage.

Finally, the annual precipitation in inches from the year 2021 is reported from NCEI (2022) to indicate a site's exposure to moisture-related damage. When water infiltrates a flexible pavement structure, it can lead to many forms of damage: moisture can reduce the shear strength of unbound layers and cause rutting by increasing pore pressure and/or creating voids when fine particles are washed out. "Stripping" can occur where the bond between asphalt binder and aggregate in AC is damaged by water pressure. Frost heave can damage pavement structures if infiltrated moisture is allowed to cyclically freeze and thaw, creating a cyclic expansion and contraction than can rearrange soil fabric in a weakening manner. Finally, structures can swell or collapse if expansive or collapsible soils are present and moisture is introduced. The annual precipitation of a site therefore demonstrates the exposure of those pavements to these forms of distress.

Table A1 contains these three relevant climate metrics pertaining to the testing locations mentioned in this thesis.

Table A1 Test section climate data

Reference	Year built	Site name	State	Design air temp (ºF)	Air freezing index	2021 annual precipitation (in)
Johnson (1960)	1954	Tesuque-Pojoaque	NM	79	2059	12
Johnson (1960)	1954	Road Forks	NM	89	1294	13
McGhee (1971)	1958	Route 360 & Route 7360	VA	82	180	38
Grau (1973) & Costigan (1984)	Various	WES	MS	87	78	49
Rasoulian et al. (2000)	1991	LA 97	LA	87	8	68
Various	2001	Morgan County	GA	85	158	50
Various	2009	LaGrange	GA	85	223	55
Young (2022)	2012	Raton	NM	76	2113	16
Vaughan (2018)	2012	Bull Run	VA	82	88	35
Qamhia et al. (2018)	2018	ICT	IL	80	230	45
Vaughan (2018)	2015	Pineville	NC	85	222	37
Jiang et al. (2022)	2019	Knoxville	TN	83	253	53

APPENDIX B: SURFACE DISTRESS SURVEY RESULTS

Table B1 contains the results from the survey of surface distresses at the Morgan County test section in the inbound lane. Table B2 contains the results from the survey of surface distresses at the Morgan County test section in the outbound lane. Table B3 displays the results from the survey of surface distresses at the LaGrange test section in the westbound lane. Table B4 displays the results from the survey of surface distresses at the LaGrange test section in the eastbound lane. Crack severity levels are as defined by Tsai et al. (2021) in the PACES manual.

Table B1 Morgan County test section surface distresses, inbound lane

Segment	Avg left rut depth (in)	Avg right rut depth (in)	Load cracking extent (%), severity 1	Load cracking extent (%), severity 2	Load cracking extent (%), severity 3	Load cracking extent (%), severity 4	Block cracking extent (%), severity 1	Block cracking extent (%), severity 2	Block cracking extent (%), severity 3	PACES rating
0-100	0.121	0.187	0	33	67	0	0	0	0	28
100-200	0.008	0.028	0	0	83	17	0	0	0	14
200-300	0.000	0.126	33	17	17	0	33	0	0	39
300-400	0.000	0.024	0	0	0	0	0	100	0	69
400-500	0.000	0.000	17	0	0	0	0	83	0	62
500-600	0.000	0.020	0	0	0	0	17	17	67	68
600-700	0.000	0.012	0	0	33	0	0	17	50	40
700-800	0.000	0.001	17	17	0	0	17	50	0	60
800-900	0.011	0.001	0	0	0	0	33	50	17	83
900-1000	0.007	0.000	0	83	0	0	17	0	0	65
1000-1100	0.000	0.001	67	0	0	0	33	0	0	76
1100-1200	0.000	0.174	86	14	0	0	0	0	0	71
1200-1300	0.000	0.478	83	17	0	0	0	0	0	70
1300-1400	0.000	0.106	33	33	0	0	33	0	0	58
1400-1500	0.000	0.011	17	83	0	0	0	0	0	63
1500-1600	0.005	0.000	17	0	0	0	33	50	0	75
1600-1700	0.003	0.000	33	17	0	0	50	0	0	64
1700-1800	0.000	0.002	33	33	0	0	50	0	0	57

Table B2 Morgan County test section surface distresses, outbound lane

Segment	Avg left rut depth (in)	Avg right rut depth (in)	Load cracking extent (%), severity 1	Load cracking extent (%), severity 2	Load cracking extent (%), severity 3	Load cracking extent (%), severity 4	Block cracking extent (%), severity 1	Block cracking extent (%), severity 2	Block cracking extent (%), severity 3	PACES rating
0-100	0.232	0.293	0	0	100	0	0	0	0	50
100-200	0.072	0.211	0	0	100	0	0	0	0	50
200-300	0.000	0.022	0	50	50	0	0	0	0	20
300-400	0.000	0.042	0	50	50	0	0	0	0	20
400-500	0.003	0.087	0	0	100	0	0	0	0	50
500-600	0.021	0.277	0	0	100	0	0	0	0	50
600-700	0.000	0.147	0	0	100	0	0	0	0	50
700-800	0.000	0.230	0	0	100	0	0	0	0	50
800-900	0.001	0.046	0	0	100	0	0	0	0	50
900-1000	0.012	0.073	0	0	67	0	0	0	33	32
1000-1100	0.006	0.005	0	0	0	0	83	0	17	82
1100-1200	0.000	0.001	17	0	0	0	50	33	0	83
1200-1300	0.001	0.048	0	83	0	0	17	0	0	65
1300-1400	0.000	0.051	0	0	0	0	17	83	0	69
1400-1500	0.000	0.122	0	50	33	0	0	17	0	25
1500-1600	0.000	0.430	0	0	0	0	0	50	50	76
1600-1700	0.000	0.314	43	29	0	0	14	14	0	57
1700-1800	0.000	0.071	20	40	0	0	0	0	40	45

Table B3 LaGrange test section surface distresses, westbound lane

Segment	Avg left rut depth (in)	Avg right rut depth (in)	Load cracking extent (%), severity 1	Load cracking extent (%), severity 2	Load cracking extent (%), severity 3	Load cracking extent (%), severity 4	Block cracking extent (%), severity 1	Block cracking extent (%), severity 2	Block cracking extent (%), severity 3	PACES rating
0-100	0.106	0.003	22	0	0	0	33	0	0	84
100-200	0.034	0.002	88	0	0	0	13	0	0	80
200-300	0.031	0.094	100	0	0	0	67	0	0	72
300-400	0.169	0.000	83	0	0	0	17	0	0	80
400-500	0.133	0.012	100	0	0	0	33	0	0	78
500-600	0.141	0.000	86	0	0	0	14	0	0	79
600-700	0.166	0.000	33	0	0	0	33	0	0	82
700-800	0.074	0.025	50	0	0	0	17	0	0	80
800-900	0.012	0.130	33	0	0	0	33	0	0	82
900-1000	0.106	0.093	83	0	0	0	33	0	0	78
1000-1100	0.133	0.045	100	0	0	0	17	0	0	80
1100-1200	0.176	0.185	67	0	0	0	17	0	0	80
1200-1300	0.223	0.071	83	0	0	0	17	0	0	80
1300-1400	0.261	0.044	100	0	0	0	0	0	0	85
1400-1500	0.266	0.099	50	0	0	0	17	0	0	80
1500-1600	0.174	0.057	100	0	0	0	0	0	0	85
1600-1700	0.192	0.071	100	0	0	0	17	0	0	80
1700-1800	0.261	0.183	100	0	0	0	17	0	0	80
1800-1900	0.199	0.189	100	0	0	0	17	0	0	80
1900-2000	0.084	0.285	100	0	0	0	17	0	0	80
2000-2100	0.124	0.245	71	0	0	0	14	0	0	79
2100-2200	0.089	0.122	100	0	0	0	83	0	0	67
2200-2300	0.235	0.069	17	17	0	0	33	0	0	69
2300-2400	0.215	0.034	17	0	0	0	17	0	0	87
2400-2500	0.122	0.147	17	0	0	0	33	0	0	85
2500-2600	0.090	0.082	33	0	0	0	17	0	0	84
2600-2700	0.085	0.089	17	0	0	0	50	0	0	83
2700-2800	0.045	0.074	17	0	0	0	67	0	0	80
2800-2900	0.092	0.058	17	0	0	0	83	0	0	75
2900-3000	0.124	0.064	0	0	0	0	67	0	0	87
3000-3100	0.102	0.067	17	0	0	0	33	0	0	85
3100-3200	0.076	0.120	0	0	0	0	67	0	0	87
3200-3300	0.007	0.244	0	0	0	0	33	0	0	93
3300-3400	0.006	0.195	100	0	0	0	0	0	0	85

Table B4 LaGrange test section surface distresses, eastbound lane

Segment	Avg left rut depth (in)	Avg right rut depth (in)	Load cracking extent (%), severity 1	Load cracking extent (%), severity 2	Load cracking extent (%), severity 3	Load cracking extent (%), severity 4	Block cracking extent (%), severity 1	Block cracking extent (%), severity 2	Block cracking extent (%), severity 3	PACES rating
0-100	0.107	0.150	100	0	0	0	25	0	0	79
100-200	0.175	0.169	100	0	0	0	50	0	0	75
200-300	0.073	0.053	100	0	0	0	33	0	0	78
300-400	0.153	0.049	100	0	0	0	17	0	0	80
400-500	0.196	0.057	100	0	0	0	50	0	0	75
500-600	0.335	0.043	83	17	0	0	50	0	0	59
600-700	0.336	0.031	83	17	0	0	67	0	0	56
700-800	0.216	0.096	17	83	0	0	50	0	0	53
800-900	0.123	0.022	50	33	0	0	33	0	0	56
900-1000	0.213	0.047	50	0	0	0	50	0	0	75
1000-1100	0.152	0.088	100	0	0	0	63	0	0	73
1100-1200	0.137	0.094	67	33	0	0	33	0	0	56
1200-1300	0.070	0.089	100	0	0	0	33	0	0	78
1300-1400	0.072	0.111	100	0	0	0	50	0	0	75
1400-1500	0.108	0.106	0	100	0	0	33	0	0	63
1500-1600	0.062	0.050	40	60	0	0	60	0	0	46
1600-1700	0.162	0.090	100	0	0	0	80	0	0	67
1700-1800	0.140	0.101	43	57	0	0	43	0	0	47
1800-1900	0.115	0.081	83	17	0	0	50	0	0	59
1900-2000	0.121	0.043	50	50	0	0	67	0	0	42
2000-2100	0.091	0.043	67	33	0	0	67	0	0	72
2100-2200	0.111	0.065	100	0	0	0	50	0	0	75
2200-2300	0.170	0.084	38	63	0	0	50	0	0	48
2300-2400	0.085	0.055	83	17	0	0	83	0	0	51
2400-2500	0.034	0.013	33	67	0	0	50	0	0	49
2500-2600	0.155	0.041	67	33	0	0	100	0	0	45
2600-2700	0.255	0.014	67	33	0	0	17	0	0	58
2700-2800	0.207	0.000	100	0	0	0	67	0	0	72
2800-2900	0.237	0.007	100	0	0	0	80	0	0	67
2900-3000	0.088	0.017	71	29	0	0	43	0	0	56
3000-3100	0.273	0.004	100	0	0	0	80	0	0	67
3100-3200	0.136	0.058	100	0	0	0	50	0	0	75
3200-3300	0.090	0.023	83	17	0	0	67	17	0	56
3300-3400	0.073	0.010	71	29	0	0	0	0	0	65

APPENDIX C: MODELING DESIGNS AND RESULTS

Table C1 contains the designs and results from the base case modeling. Table C2 shows the designs and results from the high-temperature modeling case. Table C3 displays the designs and results from the low-temperature modeling case.

Table C1 Base case modeling designs and results

Design (inverted or conventional)	Material model	Dimension ratio	AC thickness (in)	Base thickness (in)	Subbase thickness (in)	Total thickness (in)	C-17 passes	C-17 failure mode	F-15E passes	F-15E failure mode
Inverted	GT	LaGrange	1	2	2.67	5.67	180	Rut	93	Rut
Inverted	Sha	LaGrange	1	2	2.67	5.67	79	Rut	24	
Inverted	GT	Sha	1	2	4	7	5,395	Rut	6,899	Rut
Inverted	Sha	Sha	1	2	4	7	760	Rut	509	
Inverted	GT	LaGrange	2	4	5.33	11.33	3,318,248	Rut	62,033,639	Rut
Inverted	Sha	LaGrange	2	4	5.33	11.33	258,163	Rut	2,499,645	
Inverted	GT	Sha	2	4	8	14	99,999,999	Rut	1,000,000	Rut
Inverted	Sha	Sha	2	4	8	14	41,065,215	Rut	1,000,000	Rut
Inverted	GT	Papadopoulos	1	6	10	17	1,000,000	Rut	1,000,000	Rut
Inverted	GT	LaGrange	3	6	8	17	44,219,888	Fatigue	1,000,000	Rut
Inverted	Sha	LaGrange	3	6	8	17	1,798,439	Fatigue	1,000,000	Rut
Inverted	Sha	Papadopoulos	1	6	10	17	1,000,000	Fatigue	1,000,000	Rut
Conventional	Sha	PCASE LE Design	5	14.5	0	19.5	475,953	Rut	19,539,492	Rut
Inverted	GT	Sha	3	6	12	21	54,272,187	Fatigue	1,000,000	Rut
Inverted	Sha	Sha	3	6	12	21	1,927,000	Fatigue	1,000,000	Rut
Conventional	PCASE default	PCASE LE Design	5	18	0	23	410,782	Rut	15,499,919	Rut
Conventional	GT	PCASE LE Design	7.5	15.5	0	23	477,447	Rut	19,548,298	Rut
Inverted	GT	LaGrange	5	10	13.33	28.33	3,716,088	Fatigue	1,000,000	Rut
Inverted	Sha	LaGrange	5	10	13.33	28.33	613,497	Fatigue	1,000,000	Rut
Inverted	GT	Papadopoulos	2	12	20	34	99,999,999	Rut	1,000,000	Rut
Inverted	Sha	Papadopoulos	2	12	20	34	2,155,517	Fatigue	1,000,000	Rut
Inverted	GT	Sha	5	10	20	35	4,746,071	Fatigue	1,000,000	Rut
Inverted	Sha	Sha	5	10	20	35	605,081	Fatigue	1,000,000	Rut
Inverted	GT	Papadopoulos	3	18	30	51	63,222,654	Fatigue	1,000,000	Rut
Inverted	Sha	Papadopoulos	3	18	30	51	356,449	Fatigue	1,000,000	Rut
Inverted	GT	Papadopoulos	5	30	50	85	14,426,690	Fatigue	1,000,000	Rut
Inverted	Sha	Papadopoulos	5	30	50	85	640,047	Fatigue	1,000,000	Rut

Table C2 High-temperature case modeling designs and results

Design (inverted or conventional)	Material model	Dimension ratio	AC thickness (in)	Base thickness (in)	Subbase thickness (in)	Total thickness (in)	C-17 passes	C-17 failure mode	F-15E passes	F-15E failure mode
Inverted	GT	LaGrange	2	4	5.33	11.33	1,802,728	Rut	26,674,406	Rut
Inverted	GT	Sha	2	4	8	14	99,999,999	Rut	1,000,000	Rut
Inverted	Sha	Sha	2	4	8	14	99,999,999	Rut	1,000,000	Rut
Inverted	GT	LaGrange	3	6	8	17	99,999,999	Rut	1,000,000	Rut
Inverted	GT	Papadopoulos	1	6	10	17	1,000,000	Rut	1,000,000	Rut
Inverted	Sha	LaGrange	3	6	8	17	99,999,999	Rut	1,000,000	Rut
Inverted	Sha	Papadopoulos	1	6	10	17	99,999,999	Rut	1,000,000	Rut
Conventional	Sha	PCASE LE Design	5	14.5	0	19.5	3,953	Rut	33,936	Rut
Inverted	GT	Sha	3	6	12	21	99,999,999	Rut	1,000,000	Rut
Inverted	Sha	Sha	3	6	12	21	99,999,999	Rut	1,000,000	Rut
Conventional	GT	PCASE LE Design	7.5	15.5	0	23	12,680	Rut	148,608	Rut
Conventional	PCASE default	PCASE LE Design	5	18	0	23	42,045	Rut	669,156	Rut
Inverted	GT	LaGrange	2	4	5.33	11.33	1,802,728	Rut	26,674,406	Rut
Inverted	GT	Sha	2	4	8	14	99,999,999	Rut	1,000,000	Rut
Inverted	Sha	Sha	2	4	8	14	99,999,999	Rut	1,000,000	Rut
Inverted	GT	LaGrange	3	6	8	17	99,999,999	Rut	1,000,000	Rut
Inverted	GT	Papadopoulos	1	6	10	17	1,000,000	Rut	1,000,000	Rut
Inverted	Sha	LaGrange	3	6	8	17	99,999,999	Rut	1,000,000	Rut
Inverted	Sha	Papadopoulos	1	6	10	17	99,999,999	Rut	1,000,000	Rut
Conventional	Sha	PCASE LE	5	14.5	0	19.5	3,953	Rut	33,936	Rut
Inverted	GT	Sha	3	6	12	21	99,999,999	Rut	1,000,000	Rut
Inverted	Sha	Sha	3	6	12	21	99,999,999	Rut	1,000,000	Rut
Conventional	GT	PCASE LE Design	7.5	15.5	0	23	12,680	Rut	148,608	Rut
Conventional	PCASE default	PCASE LE Design	5	18	0	23	42,045	Rut	669,156	Rut

Table C3 Low-temperature case modeling designs and results

Design (inverted or conventional)	Material model	Dimension ratio	AC thickness (in)	Base thickness (in)	Subbase thickness (in)	Total thickness (in)	C-17 passes	C-17 failure mode	F-15E passes	F-15E failure mode
Inverted	GT	LaGrange	2	4	5.33	11.33	3,309,166	Rut	61,800,165	Rut
Inverted	GT	Sha	2	4	8	14	99,999,999	Rut	1,000,000	Rut
Inverted	Sha	Sha	2	4	8	14	41,065,215	Rut	1,000,000	Rut
Inverted	GT	LaGrange	3	6	8	17	99,999,999	Rut	1,000,000	Rut
Inverted	GT	Papadopoulos	1	6	10	17	1,000,000	Rut	1,000,000	Rut
Inverted	Sha	LaGrange	3	6	8	17	1,798,439	Fatigue	1,000,000	Rut
Inverted	Sha	Papadopoulos	1	6	10	17	1,000,000	Fatigue	1,000,000	Rut
Conventional	Sha	PCASE LE Design	5	14.5	0	19.5	478,142	Rut	19,573,000	Rut
Inverted	GT	Sha	3	6	12	21	54,257,368	Rut	1,000,000	Rut
Inverted	Sha	Sha	3	6	12	21	1,927,000	Fatigue	1,000,000	Rut
Conventional	GT	PCASE LE Design	7.5	15.5	0	23	490,553	Rut	19,683,036	Rut
Conventional	PCASE default	PCASE LE Design	5	18	0	23	422,836	Rut	15,611,642	Rut
Inverted	GT	LaGrange	2	4	5.33	11.33	3,309,166	Rut	61,800,165	Rut
Inverted	GT	Sha	2	4	8	14	99,999,999	Rut	1,000,000	Rut
Inverted	Sha	Sha	2	4	8	14	41,065,215	Rut	1,000,000	Rut
Inverted	GT	LaGrange	3	6	8	17	99,999,999	Rut	1,000,000	Rut
Inverted	GT	Papadopoulos	1	6	10	17	1,000,000	Rut	1,000,000	Rut
Inverted	Sha	LaGrange	3	6	8	17	1,798,439	Fatigue	1,000,000	Rut
Inverted	Sha	Papadopoulos	1	6	10	17	1,000,000	Fatigue	1,000,000	Rut
Conventional	Sha	PCASE LE	5	14.5	0	19.5	478,142	Rut	19,573,000	Rut
Inverted	GT	Sha	3	6	12	21	54,257,368	Rut	1,000,000	Rut
Inverted	Sha	Sha	3	6	12	21	1,927,000	Fatigue	1,000,000	Rut
Conventional	GT	PCASE LE Design	7.5	15.5	0	23	490,553	Rut	19,683,036	Rut
Conventional	PCASE default	PCASE LE Design	5	18	0	23	422,836	Rut	15,611,642	Rut

REFERENCES

AASHTO. 2020. *Mechanistic-empirical pavement design guide*. Washington, DC: American Association of State Highway and Transportation Officials.

AASHTO. 1993. *Design of pavement structures*. Washington, DC: American Association of State Highway and Transportation Officials.

ASCE. 2021. "Roads." *Report card for America's infrastructure*. Accessed July 13, 2022. https://infrastructurereportcard.org/cat-item/roads-infrastructure/.

Barksdale, R.D. 1984. "Performance of crushed-stone base courses." *Transportation Research Record*. 954, 78-87.

Bilotta, R., J.E. Bell, E. Shepherd, and A. Arguez. 2015. "Calculation and evaluation of an air-freezing index for the 1981-2010 climate normal period in the coterminous United States." *Journal of Applied Meteorology and Climatology*. 54, 69-76.

Christopher, B.R., C. Schwartz, and R. Boudreau. 2006. *Geotechnical Aspects of Pavements*. Washington, DC: National Highway Institute.

Cortes, D.D. 2010. "Inverted base pavement structures." Ph.D. thesis, Atlanta, GA: Georgia Institute of Technology.

Costigan, R.R. 1984. "Response and performance of contingency airfield pavements containing stabilized material layers." Ph.D. thesis, Urbana, IL: University of Illinois at Urbana-Champaign.

DoD. 2001. *Pavement design for airfields*. Washington, DC: Department of the Army.

DoD. 2001. *Airfield pavement evaluation*. Washington, DC: Department of Defense.

DoD. 2016. *Pavement design for roads and parking*. Washington, DC: Department of Defense.

Dynatest. 2019. *Elmod 6 quick start manual*. Ballerup, Denmark: Dynatest International A/S.

FHWA. 2017. *Using falling weight deflectometer data with mechanistic-empirical design and analysis, volume I: final report*. McLean, VA: Federal Highway Administration.

FHWA. 2017. *Using falling weight deflectometer data with mechanistic-empirical design and analysis, volume III: guidelines for deflection testing, analysis, and interpretation*. McLean, VA: Federal Highway Administration.

FHWA. 2019. “Miles by type of surface and ownership/functional system national summary.” *Highway Statistics.* Accessed July 13, 2022. https://www.fhwa.dot.gov/policyinformation/statistics/2019/hm12.cfm.

FHWA. 2020. “Miles by measured pavement roughness/present serviceability rating.” *Highway Statistics*. Accessed July 13, 2022. https://www.fhwa.dot.gov/policyinformation/statistics/2020/hm63.cfm.

FHWA. 2020. “Miles by measured pavement roughness - rural.” *Highway Statistics*. Accessed July 13, 2022. https://www.fhwa.dot.gov/policyinformation/statistics/2020/hm47.cfm.

FHWA. 2020. “Miles by measured pavement rutting (inches) - rural.” *Highway Statistics*. Accessed July 13, 2022. https://www.fhwa.dot.gov/policyinformation/statistics/2020/hm47.cfm

Frost, J.D. 2017. *Long-term performance of granular bases including the effect of wet-dry cycles on inverted base pavement performance*. Forest Park, GA: Georgia Department of Transportation.

GDOT. 2022. *Pavement design manual*. Atlanta, GA: Georgia Department of Transportation.

GDOT. 2022. “Traffic data.” *Traffic analysis and data application*. Accessed August 16, 2022. https://gdottrafficdata.drakewell.com/publicmultinodemap.asp.

Google. (n.d.a). [Google map of Martin Marietta Quarry Morgan County, GA]. Accessed August 15, 2022. https://www.google.com/maps/place/Martin+Marietta+-+Morgan+Quarry/@33.5460489,-83.3606654,17z/data=!4m5!3m4!1s0x14e3db6ae8390bb3:0x352a083b46859550!8m2!3d33.5460489!4d-83.3584767.

Google. (n.d.b). [Google map of Pegasus Parkway, GA]. Accessed August 15, 2022. https://www.google.com/maps/place/Pegasus+Parkway,+LaGrange,+GA+30240/@32.9896843,-85.0631105,17z/data=!4m5!3m4!1s0x888b57c9ccc82fad:0x5e883959807b84a0!8m2!3d32.9896798!4d-85.0609218.

Grau, R.W. 1973. *Evaluation of structural layers in flexible pavement*. Vicksburg, MS: US Army Engineer Waterways Experiment Station.

Horne, D., G. Belancio, S. Gaj, N. Jackson, D. Lucas, S.A. Carradine, J. Hallin, C. Jordan, and R. Zink. 1997. *FHWA study of South African pavement and other highway technologies and practices*. Federal Highway Administration.

IIT Corp. 2015. “Pavement-transportation computer assisted structural engineering” [computer software].

Jiang, X., J. Gabrielson, H. Titi, B. Huang, Y. Bai, P. Polacyzk, W. Hu, M. Zhang, and R. Xiao. 2022. “Field investigation and numerical analysis of an inverted pavement system in Tennessee, USA.” *Transportation Geotechnics*. 35, 100759.

Johnson, C.W. 1960. “Comparative studies of combinations of treated and untreated bases and subbases for flexible pavements.” *Highway Research Board Bulletin*. 289, 44-61.

Jooste, F., E. Sadzik, and L. Sampson. 2005. “Direct economic benefits arising from technology development work on G1 base pavements.” In. *Proc., 24th South African Transport Conference*, Pretoria, South Africa: SATC.

Lewis, D.E., K. Ledford, T. Georges, and D.M. Jared. *Construction and performance of inverted pavements in Georgia*. Forest Park, GA: GDOT.

McGhee, K.H. 1971. *Pavement design and performance studies final report on phase C experimental flexible pavements.”* Charlottesville, VA: Virginia Highway Research Council.

NCEI. 2022. “County precipitation.” *Climate at a Glance*. Accessed August 30, 2022. https://www.ncei.noaa.gov/access/monitoring/climate-at-a-glance/county/mapping/110/pcp/202112/12/value.

Papadopoulos, E. and J.C. Santamarina. 2014. “Optimization of inverted base pavement designs with thin asphalt surfacing.” In *Proc., Geo-Congress 2014 Technical Papers*, Reston, VA: ASCE, 2996-3004.

Papadopoulos, E. and J.C. Santamarina. 2015. “Analysis of inverted base pavements with thin-asphalt layers.” *International Journal of Pavement Engineering*. 17 (7), 590-601.

Papadopoulos, E. 2014. “Performance of unbound aggregate bases and implications for inverted base pavements.” Ph.D. thesis, Atlanta, GA: Georgia Institute of Technology.

Pavemetrics Systems. 2022. “LcmsRoadInspect” [computer software].

Qamhia, I., E. Tutumluer, and H. Ozer. 2018. *Field performance evaluation of sustainable aggregate by-product applications*. Urbana, IL: Illinois Center for Transportation.

Rasoulian, M., B. Becnel, and G. Keel. 2000. “Stone interlayer pavement design.” *Transportation Research Record*. 1709, 60-68.

Rasoulian, M, H. Titi, M. Martinez, B. Becnel, G. Keel. 2001. *Long term performance of stone interlayer pavement*. Baton Rouge, LA: Louisiana Transportation Research Center.

Seo, J., Y. Kim, J. Cho, and S. Jeong. 2013. "Estimation of in situ dynamic modulus by using MEPDG dynamic modulus and FWD data at different temperatures." *International Journal of Pavement Engineering*. 14 (4), 343-353.

Sha, A., Z. Han, L. Jiao, L. Hu, and H. Li. 2020. "Optimal structure combination for inverted asphalt pavement incorporating cracks in cement-treated subbase." *Transportation Research Record*. 2674 (1), 68-78.

Terrell, R. G. 2002. "Measuring directional stiffnesses in pavement base material." M.S. thesis, Austin, TX: University of Texas at Austin.

Tsai, Y., C. Jiang, and Z. Wang. 2012. "Pavement crack detection using high-resolution 3D line laser imaging technology." In *Proc., 7th RILEM International Conference on Cracking in Pavements*, Delft, Netherlands: RILEM, 169-178.

Tsai, Y., Z. Wang, X. Zhang, and Z. Yang. 2021. *An enhanced GDOT pavement preservation guide with optimal timing of pavement preservation*. Atlanta, GA: GDOT.

Tutumluer, E. and R.D. Barksdale. 1995. "Inverted flexible pavement response and performance." *Transportation Research Record*. 1482, 102-110.

Tutumluer, E. 2013. *Practices for unbound aggregate pavement layers*. Washington, DC: Transportation Research Board.

USDOT. 2021. *National transportation statistics 2021*. US Department of Transportation.

Van Steenburg, G. 2021. "PCASE." *PCASE Workshop*, lecture.

Vaughan, K.M. 2018. "Inverted pavement." lecture.

Wang, H. and X. Dong. 2020. "Analysis of the mechanical response of asphalt pavement with different types of base." *Advances in Environmental Vibration and Transportation Geodynamics*. 849-865